

**STUDY ON COHERENT SOFT X-RAY GENERATION
FROM CAPILLARY DISCHARGE PLASMAS**

By

SHREEKANT BARNWAL

PHYS 03 2010 04 003

Raja Ramanna Centre for Advanced Technology, Indore

*A thesis submitted to the
Board of Studies in Physical Sciences*

*In partial fulfillment of requirements
for the Degree of*

DOCTOR OF PHILOSOPHY

of

HOMI BHABHA NATIONAL INSTITUTE

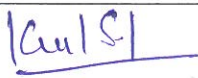
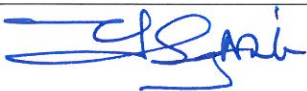
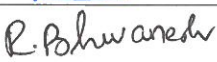

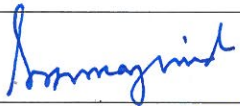

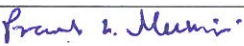




August, 2017

Homi Bhabha National Institute¹

Recommendations of the Viva Voce Committee

As members of the Viva Voce Committee, we certify that we have read the dissertation prepared by Shreekant Barnwal entitled "Study on coherent soft X-ray generation from capillary discharge plasmas" and recommend that it may be accepted as fulfilling the thesis requirement for the award of Degree of Doctor of Philosophy.

Chairman - Prof. K. S. Bindra		Date: 20/2/18
Guide / Convener - Prof. P. A. Naik		Date: 20/2/18
Examiner - Prof. Bhuvanesh Ramakrishna		Date: 20/2/18
Member 1- Prof. S. R. Mishra		Date: 20-2-2018
Member 2- Prof. S. K. Majumder		Date: 20/2/18
Member 3- Prof. A. Moorti		Date: 20/2/18
Member 4- Prof. P. K. Mukhopadhyay		Date: 20/2/18
Member 5- Prof. C. Mukherjee		Date: 20/2/18
Member 6- Prof. T. C. Kaushik		Date: 20/2/18

Final approval and acceptance of this thesis is contingent upon the candidate's submission of the final copies of the thesis to HBNI.

I/We hereby certify that I/we have read this thesis prepared under my/our direction and recommend that it may be accepted as fulfilling the thesis requirement.

Date: 20-Feb-2018

Place: RRCAT, Indore



<Signature>

Guide

¹ This page is to be included only for final submission after successful completion of viva voce.

STATEMENT BY AUTHOR

This dissertation has been submitted in partial fulfillment of requirements for an advanced degree at Homi Bhabha National Institute (HBNI) and is deposited in the Library to be made available to borrowers under rules of the HBNI.

Brief quotations from this dissertation are allowable without special permission, provided that accurate acknowledgement of source is made. Requests for permission for extended quotation from or reproduction of this manuscript in whole or in part may be granted by the Competent Authority of HBNI when in his or her judgment the proposed use of the material is in the interests of scholarship. In all other instances, however, permission must be obtained from the author.

Shreekant Barnwal

SHREEKANT BARNWAL

DECLARATION

I, hereby declare that the investigation presented in the thesis has been carried out by me.
The work is original and has not been submitted earlier as a whole or in part for a degree /
diploma at this or any other Institution / University.

Shreekant Barnwal

SHREEKANT BARNWAL

List of Publications arising from the thesis

Journal

1. “Exploring X-ray lasing in nitrogen pinch plasma at very high and fast discharge current excitation”, **S. Barnwal**, S. Nigam, K. Aneesh, Y. B. S. R. Prasad, M. L. Sharma, P. K. Tripathi, A. S. Joshi, P. A. Naik, H. S. Vora and P. D. Gupta, *Applied Physics B:Lasers and Optics*, **2017**, Vol. 123, p.178 (9 pages)
2. “Impact of discharge current profile on the lasing efficiency of 46.9 nm capillary discharge soft X- ray laser”, **S. Barnwal**, S. Nigam, K. Aneesh, Y.B.S.R. Prasad, A. S. Joshi and P. A. Naik, *Laser Physics*, **2017**, Vol. 27, p. 055003 (5 pages)
3. “Effect of the rate of rise in discharge current on the output of a 46.9 nm soft X-ray laser based on capillary discharge”, **S. Barnwal**, S. Nigam, K. Aneesh, Y.B.S.R. Prasad, P.A. Naik, C.P. Navathe and P.D. Gupta, *Applied Physics B : Lasers and Optics*, **2016**, Vol. 122, p. 169 (6 pages)
4. “Characterization of the 46.9-nm soft X-ray laser beam from a capillary discharge”, **S. Barnwal**, Y.B.S.R. Prasad, S. Nigam, K. Aneesh, M.L. Sharma, R.P. Kushwaha, P.K. Tripathi, P.A. Naik, J.A. Chakera, C.P. Navathe, and P.D. Gupta, *Applied Physics B : Lasers and Optics*, **2014**, Vol. 117, p. 131-139
5. “Generation of intense soft x-rays from capillary discharge plasmas”, Y.B.S.R. Prasad, S. Nigam, K. Aneesh, **S. Barnwal**, P. K. Tripathi, P. A. Naik, C. P. Navathe and P. D. Gupta, *Sadhana*, **2011**, Vol. 36, p. 349-355

Conferences

1. “Gain optimization studies of 46.9 nm soft X-ray laser from discharge driven plasma”, **S. Barnwal**, Y.B.S.R. Prasad, S. Nigam, K. Aneesh, A.S. Joshi and P.A. Naik, *DAE - BRNS National Laser Symposium (NLS-25)*, Odisha, Dec. 20-23, 2016

2. "Spectroscopic study of nitrogen Z-pinch plasma towards X-ray lasing from fast capillary discharge", **S. Barnwal**, Y.B.S.R. Prasad, S. Nigam, K. Aneesh, A. S. Joshi, P. A. Naik, C. P. Navathe and P. D. Gupta, *30th National Symposium on Plasma Science & Technology, Kolkata, Dec. 1-4, 2015*
3. "Effect Of Rate Of Rise Of Discharge Current On The Gain-Coefficient Of 46.9 nm Soft X-ray Laser From Fast Capillary Discharge", **S. Barnwal**, S. Nigam, K. Aneesh, Y. B. S. R. Prasad, M. L. Sharma, A. S. Joshi, P. A. Naik, C. P. Navathe and P. D. Gupta, *30th National Symposium on Plasma Science & Technology, Kolkata, Dec. 1-4, 2015*
4. "Measurement of gain-coefficient of 46.9 nm capillary discharge soft x-ray laser", **S. Barnwal**, Y. B. S. R. Prasad, S. Nigam, K. Aneesh, P. A. Naik, C. P. Navathe, and P. D. Gupta, *29th National Symposium on Plasma Science & Technology, Kottayam, Dec. 8-11, 2014*
Received "Best poster award of the Plasma Science Society of India"
5. "Study on nitrogen Z-pinch plasma for x-ray lasing", **S. Barnwal**, S. Nigam, K. Aneesh, Y. B. S. R. Prasad, P. K. Tripathi, P. A. Naik, C. P. Navathe, and P. D. Gupta, *29th National Symposium on Plasma Science & Technology, Kottayam, Dec. 8-11, 2014*
6. "Capillary discharge X-ray laser: Effect of discharge current rise-time on laser output energy", **S. Barnwal**, Y.B.S.R. Prasad, S. Nigam, K. Aneesh, J.A. Chakera, P. A. Naik, C. P. Navathe and P.D. Gupta, *22nd DAE-BRNS National Laser Symposium, MIT, Manipal University, Karnataka, Jan. 8-11, 2014*
7. "Development of a compact capillary discharge pumped soft x-ray laser at 46.9 nm wavelength", S. Nigam, K. Aneesh, **S. Barnwal**, Y. B. S. R. Prasad, P. K. Tripathi, J. A. Chakera, C. P. Navathe, P. A. Naik and P. D. Gupta, *22nd DAE-BRNS National Laser Symposium, MIT, Manipal University, Karnataka, Jan. 8-11, 2014*
8. "Energy measurement of soft x-ray laser produced from capillary discharge plasma", **S. Barnwal**, Y.B.S.R. Prasad, K. Aneesh, S. Nigam, J.A. Chakera, P.A. Naik, C.P. Navathe and P.D. Gupta, *21st National Laser Symposium, BARC Mumbai, Feb. 6-9, 2013*

9. "Measurement of the Coherence of a Soft X-ray Laser by Interferometry", **S. Barnwal**, Y.B.S.R. Prasad, S. Nigam, K. Aneesh, P.A. Naik, J.A. Chakera, M.L. Sharma, C.P. Navathe, and P.D. Gupta, *27th National symposium on Plasma Science and Technology (PLASMA-2012), Pondicherry, Dec. 10-13, 2012*
10. "Demonstration of lasing action in Ar in capillary discharge plasmas", **S. Barnwal**, Y.B.S.R. Prasad, S. Nigam, K. Aneesh, P.A. Naik, J.A. Chakera, M.L. Sharma, C.P. Navathe, and P.D. Gupta, *National Laser Symposium (NLS-20), Anna University, Chennai, Jan. 9-12, 2012*
11. "Alignment system using a bi-planar quadrant detector for the soft x-ray laser at 46.9 nm wavelength", S. Nigam, K. Aneesh, **S. Barnwal**, Y.B.S.R. Prasad, M.L. Sharma, J.A. Chakera, C.P. Navathe, P.A. Naik, and P.D. Gupta, *National Laser Symposium (NLS-20), Anna University, Chennai, Jan. 9-12, 2012*
12. "Soft x-ray lasing at 46.9 nm from Capillary Discharge Argon Plasma", **S. Barnwal**, Y.B.S.R. Prasad, S. Nigam, K. Aneesh, P.A. Naik, J.A. Chakera, M.L. Sharma, C.P. Navathe, and P.D. Gupta, *26th National Symposium on Plasma Science & Technology (PLASMA-2011), Patna, Dec 20-23, 2011*
13. "Dynamics of capillary discharge plasma", **S. Barnwal**, Y. B. S. R. Prasad, S. Nigam, K. Aneesh, J. A. Chakera, P. A. Naik, C. P. Navathe, and P. D. Gupta, *25th National Symposium on Plasma Science & Technology (PLASMA-2010), Guwahati, Dec. 8-11, 2010*

Shreekant Barnwal.

SHREEKANT BARNWAL

DEDICATIONS

I

dedicate this thesis

to my parents

and

wife “SHWETA”

who have been

quite instrumental

in realizing my dreams

ACKNOWLEDGEMENTS

First of all, I thank my all-time companion, the almighty supreme authority “Shiv Baba”, for providing me the required strength and wisdom to carry out and complete this research work. The present thesis work would have not been possible without the guidance, support, encouragement and help received from several persons. It is high time and also my greatest pleasure to acknowledge their contributions in successful completion of this research work.

First and foremost, I owe deep sense of gratitude to my thesis guide *Prof. P. A. Naik*, Director RRCAT, for his constant guidance, support and encouragement throughout the research work. He has been a constant source of inspiration as well as the driving force for the research work all these years. I am also highly obliged to him for receiving his invaluable time and efforts whenever required at various stages of the research work in spite of his busy schedule.

I am extremely thankful to Prof. P. D. Gupta, former Director, RRCAT for his continuous support and encouragement from the very early beginning of the research work. His active support and guidance was instrumental in the success of Capillary Discharge X-ray Laser program.

I am greatly indebted to *Shri Y. B. S. R. Prasad* for his continuous guidance, useful discussions and encouragement during planning and execution of the experiments. His guidance played pivotal role in the analysis of the various results. I am also thankful to him for his invaluable time and efforts spent in thesis preparation and finalization.

I am profoundly thankful to *Dr. J. A. Chakera* and *Shri A. S. Joshi* for their valuable advises, support and encouragement during the research work. I am highly indebted to *Dr. J. A. Chakera* also for his fruitful advises and efforts in thesis preparation and finalization.

I am very fortunate to have extremely vibrant and energetic team members from engineering side *Shri S. Nigam*, *Shri K. Aneesh* and *Shri M. L. Sharma* in the laboratory who have quite efficiently taken care of the challenges required in the pulse-power systems without which it would have not been possible to carry out the research activity.

Their constant support, encouragement and help has been quite instrumental in all these years.

I am highly thankful to *Shri P. K. tripathi* and *Shri R. P. Kushwaha* for all the required mechanical engineering support they have provided timely and promptly whenever there was a need for it.

I also acknowledge and give my sincere thanks to *all my colleagues* of Laser Plasma Section for all the fruitful discussions held from time to time which has helped me directly or indirectly in my research work.

I am extremely thankful to my wife *Mrs. Shweta* for her unconditional love, constant support and untiring efforts in taking care and managing the things quite efficiently at home during my research work. Without her support, it would have not been possible to complete the thesis work in time. The encouragement and motivation increased manifold since the entry of a little angel '*Anwita*', my daughter, in my life last year which has added a beautiful dimension to the life.

Finally, I owe deep sense of gratitude to the seed of my life, i.e. my parents, for all the love and affection which I have received from them and their unmatched sacrifices without which I would not have reached to this stage of my life.

CONTENTS

	Page No.
SYNOPSIS	i
LIST OF FIGURES	xii
LIST OF TABLES	xv
CHAPTER 1 INTRODUCTION	1-39
1.1 Motivation	1
1.2 Various applications of coherent X-ray sources	1
1.3 Various methods to generate coherent X-ray light	5
1.3.1 Free electron X-ray lasers	7
1.3.2 High order harmonic generation	10
1.3.3 Plasma based X-ray lasers	12
1.3.3.1 Basics of plasma-based X-ray lasers	13
1.3.3.2 Population inversion mechanisms in plasma	22
1.3.3.3 X-ray lasers based on laser produced plasma	29
1.3.3.4 X-ray lasers based on discharge produced plasma	34
1.4 Scope of the present thesis work	37
CHAPTER 2 CAPILLARY DISCHARGE BASED X-RAY LASER	40-58
2.1 Fast capillary discharge for X-ray laser	40
2.2 Capillary discharge X-ray Laser system	42
2.3 Various sub-systems and measurement devices	47
2.3.1 Marx-bank	47
2.3.2 Tesla-transformer	49
2.3.3 High voltage spark gaps	51
2.3.4 Pulsed high voltage measurements	52
2.3.5 Pulsed high current measurements	55
CHAPTER 3 DEMONSTRATION OF DISCHARGE DRIVEN SOFT X-RAY LASING AT 46.9 NANOMETER AND ITS CHARACTERIZATION	59-75
3.1 Experimental details	60
3.2 Results and discussion	61

3.2.1	Temporal study of capillary discharge emission	62
3.2.2	Study of the divergence	65
3.2.3	Spectral measurement of capillary discharge emission	65
3.2.4	Coherence measurement of the soft X-ray laser	70
3.3	Studies towards development of compact and repetitive soft X-ray laser at 46.9 nm	74
CHAPTER 4	ROLE OF DISCHARGE CURRENT PROFILE ON THE ENERGY AND GAIN OF SOFT X-RAY LASER AT 46.9 NANOMETER	76-94
4.1	Introduction	76
4.2	Experiments for changing the rate of rise (dI/dt) of the discharge current	78
4.3	X-ray laser pulse energy measurement	80
4.4	Effect of dI/dt on the X-ray laser pulse energy	83
4.5	Gain-coefficient measurement of the X-ray laser	87
4.6	Effect of current pulse duration on the gain-coefficient	89
4.7	Effect of current amplitude on the gain-coefficient	91
CHAPTER 5	EXPLORING X-RAY LASING AT SHORTER WAVELENGTH	95-116
5.1	Introduction	95
5.2	Up-gradation of capillary discharge system	97
5.3	Exploring X-ray lasing in Nitrogen Z-pinch plasma	100
5.3.1	Experimental details	1000
5.3.2	Results and discussion	101
5.4	Exploring X-ray lasing in Carbon Z-pinch plasma	110
5.4.1	Initial experiments in C ₂ H ₂ filled capillary and results	110
5.5	Exploring X-ray lasing in Krypton Z-pinch plasma	113
5.5.1	Initial experiments in Kr filled capillary and results	113
CHAPTER 6	SUMMARY AND FUTURE OUTLOOK	117-121
6.1	Summary of the important results	117
6.2	Future outlook	120
	REFERENCES	122

SYNOPSIS

Since the time of invention of laser in 1960, there has always been a keen interest in the scientific laser community to extend the lasing towards shorter wavelength region, especially in X-ray region, of the electromagnetic spectrum. This interest increased manifold with the realization of compact table-top X-ray laser sources. The motivation behind the development of compact table-top X-ray laser sources lies in the fact that as the laser technology advances towards shorter wavelength e.g. X-ray region, several applications begin to arise in diverse and newer areas of science and technology. Today, even when the development of X-ray laser is not in its mature stage, it finds potential applications in the areas like nano-imaging, 3-dimensional molecular imaging, dense plasma diagnostics, lithography, holography, study of radiation-induced damage in bio-molecules etc [1-7]. There is no doubt that if its development reaches to a stage where intense X-ray laser sources become easily available in a compact table-top form in the laboratories at various wavelengths and affordable to a large user community, several new applications may come up in future [8].

Towards this objective, research and development in the area of Capillary Discharge X-ray Laser is quite promising. Such X-ray lasers based on fast capillary discharge scheme have great potential to provide coherent X-ray light sources of relatively compact size compared to big facilities like X-FEL or those driven by high power laser systems. This is due to involvement of pulse power systems as driver which can be made very compact. On the other hand, the capillary discharge based techniques have advantage of very high coupling of electrical energy with the plasma. This makes

the scheme very efficient in generating multiply-ionized, hot and dense plasma column having large aspect ratio with high uniformity which is ideal for providing larger gain-volume [8]. As a result, much higher photon flux can be achieved in the lasing wavelength. The research in this area gained momentum after the first demonstration of soft X-ray lasing in $3s^1P_1 - 3p^1S_0$ transition of Ne-like Ar ion (Ar^{8+}) at 46.9 nm by Rocca et al in 1994 [9]. Achieving lasing through fast capillary discharge scheme was not an easy task due to various complexities involved therein. This was clearly reflected from the fact that even after the first demonstration of soft X-ray lasing at 46.9 nm, no other group could reproduce these results for next 6 to 7 years. Later on, groups from Israel [10], Japan [11-14], Italy [15-18], Malaysia [19, 20], China [21, 22] and Czech-Republic [23] were successful in realizing this lasing and contributed significantly in various aspects of this area of research. The scheme was extremely successful in making highly powerful X-ray laser in \sim mW level at a wavelength of 46.9 nm with the average power comparable to that of the third generation synchrotron facility. However, extending the lasing wavelength below 46 nm still remains a big challenge in this scheme and investigations are being carried out in this direction [24-27].

The work presented in this thesis describes the various experimental studies carried out on X-ray lasing in discharge driven plasmas. Here, the objective is to achieve X-ray lasing in different gas media subjected to large and fast discharge excitations and study the role of experimental parameters on the laser output. In this direction, soft X-ray emission was first obtained from argon pinch plasma generated by fast capillary discharge excitations and later on, lasing was also successfully achieved at 46.9 nm during the present research work [28, 29]. This X-ray lasing depends on several

experimental parameters like gas pressure, pre-pulse conditions, capillary dimensions as well as discharge current profile i.e. its amplitude and duration. Among these, the profile of the discharge current especially its pulse duration is one of the most important parameter. At the same time, it is the most difficult parameter to be changed as it is directly related to the geometry of the capillary discharge system. Changing the geometry of a capillary discharge system is quite a difficult task due to the various complexities involved therein and that is why, there are not many experimental studies in literature emphasizing the role of current profile on the laser output. This problem has been attempted in the present study where the effect of discharge current pulse duration on the gain-coefficient of the 46.9 nm soft X-ray laser has been investigated [30]. It was experimentally demonstrated for the first time that the gain-coefficient increases significantly if the argon plasma is excited by faster discharge current. The effect of current amplitude on the lasing efficiency was also studied and some interesting observations were recorded [30]. The present research work also established that the rate of rise of discharge current i.e. dI/dt has much important role to play rather than the peak value of the current to achieve higher energy in the laser pulse [31]. It was shown experimentally that similar laser energy can be achieved at a much smaller peak current if the dI/dt value remains same. This study may have important implications in future endeavours to build X-ray laser at shorter wavelengths e.g. 13.4 nm using nitrogen plasma where peak current requirements, predicted by simulations, are very high [32].

Another research problem taken up in the present thesis work is to explore the feasibility of extending this X-ray lasing to even shorter wavelength region (below ~ 46 nm) using fast capillary discharge scheme. There has been significant interest worldwide

in achieving this goal but no success has been achieved till date. Extensive studies have been carried out under the present thesis work to explore X-ray lasing at 13.4 nm in H-like N ions based on collisional recombination scheme [33]. The experimental studies have been done using the recently upgraded capillary discharge system in our laboratory which is able to deliver a high discharge current of ~ 95 kA with ~ 46 ns quarter period. These current parameters are very promising and no other group had previously attempted studies for X-ray lasing in N_2 at such a high and fast discharge current excitations. Although, the final goal of X-ray lasing at 13.4 nm has still not achieved, but some important observations as well as conclusions were drawn which would be quite useful for future work in this direction. Similarly, C_2H_2 and Kr plasma were also explored for possible lasing at 18.2 nm in H-like C ion and 32.8 nm in Ni-like Kr ion respectively. These studies also provide important inputs for extending the fast capillary discharge scheme for X-ray lasing towards shorter wavelength. A chapter-wise brief description of the present thesis is detailed below.

Chapter 1 of the thesis begins with a discussion on the motivation behind the research and development of X-ray laser. The chapter briefly discuss the various applications of X-ray laser which has been the main guiding force throughout this study. As discussed above, there are different methods to generate coherent light in the X-ray region of the spectrum. Therefore, it becomes natural that a brief discussion on the salient features of these methods finds its place in chapter 1. The chapter also describes the basic fundamentals of plasma based X-ray laser in contrast to conventional laser sources. Unlike conventional laser sources, the population inversion is not easier to obtain when lasing is to be achieved in X-ray region. Therefore, part of the first chapter is devoted on

discussing the different mechanisms of generation of population inversion in X-ray wavelength. It is worth mentioning here that this later part of the chapter is equally applicable to X-ray laser generated from laser produced plasma or discharge driven plasma although the thesis is mainly focussed on discharge driven X-ray lasers.

Chapter 2 describes the capillary discharge scheme for generation of coherent radiation in X-ray wavelength in detail. It also includes a general description of the various components of a Capillary Discharge X-ray Laser (CDXL) system. The pulse power system is the heart of CDXL system which delivers the required current profile for excitation of the plasma inside the capillary. Since, the system involves high voltages up to a few hundreds of kilo-volts (e.g 400 kV) and discharge current amplitudes up to a few tens of kilo-amperes (e.g. 40 kA) to be delivered in a few tens of nanoseconds (e.g. ~45 ns), it demands a challenging geometry. Similarly when the laser comes out of the capillary, it is subjected to specially designed geometry of the system to address critical issues involved therein. All these issues have been part of the discussion in this chapter. Beside this, a general description of the various diagnostics and detectors, which have been used in the research work, is also included in this chapter of the thesis.

Chapter 3 discusses in detail the experiments carried out for demonstration of soft X-ray lasing at 46.9 nm from argon plasma. The pulse power system was used to drive high discharge current through pre-ionized argon gas column inside long alumina capillary having 15 cm length and 2.8 mm inner diameter (ID). This created a hot and dense argon plasma column after strong magnetic compression at the capillary axis. By optimizing the various experimental parameters, intense lasing pulse of 1.2 ns (FWHM) was obtained in vacuum diode signal. Various diagnostics were used to characterize this

X-ray laser by studying its temporal, spatial and spectral profiles. The divergence of the laser was measured to be ~ 3.5 mrad establishing its good directional behaviour compared to the incoherent plasma emission from the capillary. The spectrum recorded with a transmission grating spectrograph indicated intense lasing line at 46.9 nm along with its various diffraction orders which could be recorded up to as high as 10th order. The chapter also explains the interesting results of young's double slit experiment done with this X-ray laser with a purpose to confirm its coherent nature. These experimental studies have been reported in Applied Physics B [29] and Sadhana [28]. The chapter also briefly discusses the results of the experiment done to find out the lowest current at which the soft X-ray lasing at 46.9 nm is still possible. This particular study has led to develop an ultra-compact and portable version of this laser operating at significantly smaller voltages and delivering XUV pulses at repetition rate of 6 pulses per minute.

Among the various experimental parameters, rate of rise of current (dI/dt) is an important parameter of Capillary Discharge X-ray Laser. **Chapter 4** covers the experimental details and the obtained results in which the effect of this parameter on the energy of 46.9 nm soft X-ray laser has been studied. In this direction, the geometry of the capillary discharge system was modified to minimize the inductance in the discharge path with an aim to make the current faster. It was found that if the duration of the discharge current is made shorter, the same 2 μ J energy in the X-ray laser pulse is obtained at a much smaller peak discharge current of ~ 25 kA which was initially required to be ~ 40 kA. The value of dI/dt in these two cases were comparable. When dI/dt value was further enhanced by increasing the current amplitude from ~ 25 kA to ~ 44 kA keeping the duration of current fixed, the energy of the X-ray laser beam was significantly increased

from 2 μJ to 4 μJ . Another interesting fact revealed was that if the dI/dt value is fixed, mere increase in the peak discharge current does not enhance the laser energy. The chapter also deals with the gain measurement studies conducted with the 46.9 nm soft X-ray laser. The study was aimed at maximizing the gain of this laser and emphasized the important role played by the discharge current profile on the lasing efficiency of this laser. The discharge current profile was changed either by making the current faster with a fixed value of its amplitude or by changing its amplitude while keeping the duration fixed. During the study, it was observed that the gain-coefficient of the laser was increased substantially from 0.69 cm^{-1} to 1.02 cm^{-1} when the current pulse duration was made shorter. The gain-coefficient was also measured at varying amplitudes of the discharge current while keeping its duration fixed. It was found that there exists an optimum value of the current amplitude where the gain-coefficient becomes maximum. Exploiting this fact, the gain-coefficient of the X-ray laser was further enhanced to 1.33 cm^{-1} . These studies have been published in Laser Physics [30] and Applied Physics B [31].

Chapter 5 covers the detailed experimental efforts and their outcome directed at exploring possibilities for realization of recombination X-ray lasing at 13.4 nm in nitrogen pinch plasma. The study has been published in the journal Applied Physics B [33]. The first theoretical proposal in this direction was given by Vrba et al in 2005 for possible lasing in Balmer- α transition in H-like N ion using fast capillary discharge scheme. Since then, efforts were made in this direction by various groups worldwide. But, the success has not been achieved as yet due to very stringent conditions required for this lasing. These conditions include requirement of large pumping power to nitrogen plasma achieving high density and high temperature to generate fully ionized nitrogen ions,

subsequent rapid cooling to achieve high density and low temperature plasma for faster 3-body recombination to form H-like N ion. In order to meet these criteria, the capillary discharge system in our laboratory was upgraded to deliver a higher discharge current of ~ 95 kA with a quarter period of ~ 46 ns. The possibilities for the aforesaid lasing was explored with this electrical driver and reported for the first time by any group working in this area on such fast and high current regimes. He- α emission at 2.8 nm and Ly- α emission at 2.4 nm were observed under optimized conditions indicating formation of N⁵⁺ and N⁶⁺ charge states of nitrogen. Although lasing could not be achieved but some important conclusions were drawn which provide important inputs for future experiments in this direction. In these studies, favorable role of pre-pulse in achieving higher charge states of nitrogen has also been established. The Chapter also discusses the experimental efforts made in the direction of investigating Carbon and Krypton plasmas for possible shorter wavelength X-ray lasing with the upgraded fast and high current capillary discharge system. Acetylene (C₂H₂) is well suited for possible recombination pumped X-ray lasing at 18.2 nm in H-like C ion where carbon, being low-Z ion than nitrogen, requires lesser pump power to become fully ionized. Kr on the other side is promising for X-ray lasing at 32.8 nm in Ni-like Kr ion based on collisional excitation pumping and requires smaller pump power to achieve Ni-like closed shell configuration. Initial experiments were conducted with these gas mediums and the outcomes have been very encouraging.

Chapter 6 gives a brief summary of the research work. It also includes a brief discussion on the future direction for these experiments with an aim to achieve X-ray lasing at shorter wavelength region. It was felt that even much higher as well as faster

electrical driver has to be employed for achieving recombination based X-ray lasing. Role of inner diameter of capillary has to be studied in greater detail along with the powerful electrical driver. Smaller ID capillary with faster current pulse seems to be a good relaxation for high peak current requirements of such X-ray lasers.

References

1. C. A. Brewer, F. Brizuela, P. Wachulak, D. H. Martz, W. Chao, E. H. Anderson, D. T. Attwood, A. V. Vinogradov, I. A. Artyukov, A. G. Ponomareko, V. V. Kondratenko, M. C. Marconi, J. J. Rocca, and C. S. Menoni, *Opt. Lett.* **33**, 518 (2008)
2. M. Purvis, J. Grava, J. Filevich, M. C. Marconi, J. Dunn, S. J. Moon, V. N. Shlyaptsev, E. Jankowska, and J. J. Rocca, *Phys. Rev. E* **76**, 046402 (2007)
3. M. C. Marconi and P. W. Wachulak, *Prog. in Quant. Elect.* **34**, 173 (2010)
4. P. W. Wachulak, M. C. Marconi, R. A. Bartels, C. S. Menoni, and J. J. Rocca, *J. Opt. Soc. Am. B* **25**, 1811 (2008)
5. I. Kuznetsov, J. Filevich, F. Dong, M. Woolston, W. Chao, E. H. Anderson, E. R. Bernstein, D. C. Crick, J. J. Rocca and C. S. Menoni, *Nat. Commun.* **6**, 6944 (2015)
6. E. Novakova, L. Vysin, T. Burian, L. Juha, M. Davidkova, V. Mucka, V. Cuba, M. E. Grisham, S. Heinbuch, and J. J. Rocca, *Phys. Rev. E* **91**, 042718 (2015)
7. L. Urbanski, A. Isoyan, A. Stein, J. J. Rocca, C. S. Menoni and M. C. Marconi, *Opt. Lett.* **37**, 3633 (2012)
8. J. J. Rocca, *Rev. Sci. Instrum.* **70**, 3799 (1999)
9. J. J. Rocca, V. Shlyaptsev, F. G. Tomasel, O. D. Cortazar, D. Hartshorn and J. L. A. Chilla, *Phys. Rev. Lett.* **73**, 2192 (1994)
10. A. Ben-Kish, M. Shuker, R. A. Nemirovsky, A. Fisher, A. Ron and J. L. Schwob, *Phys. Rev. Lett.* **87**, 015002 (2001)
11. Y. Hayashi, H. Ghomi, Y. Zhao, Y. Cheng, Y. Sakai, M. Watanabe, A. Okino, K. Horioka and E. Hotta, *Jap. J. Appl. Phys.* **47**, 977 (2008)
12. N. Sakamoto, M. Masnavi, M. Nakajima, T. Kawamura and K. Horioka, *Jap. J. Appl. Phys.* **47**, 2250 (2008)
13. Y. Hayashi, Y. Xiao, N. Sakamoto, H. Miyahara, G. Niimi, M. Watanabe, A. Okino, K. Horioka, and E. Hotta, *Jap. J. Appl. Phys.* **42**, 5285 (2003)
14. Y. Hayashi, H. Taniguchi, H. Ghomi, P. Chalise, N. Sakamoto, M. Watanabe, A. Okino, M. Nakajima, K. Horioka and E. Hotta, *Jap. J. Appl. Phys.* **43**, 5564 (2004)

15. G. Tomassetti, A. Ritucci, A. Reale, L. Palladino, L. Reale, S.V. Kukhlevsky, F. Flora, L. Mezi, J. Kaiser, A. Faenov and T. Pikuz, *Eur. Phys. J. D.* **19**, 73 (2002)
16. G. Tomassetti, A. Ritucci, A. Reale, L. Palladino, L. Reale, S.V. Kukhlevsky, F. Flora, L. Mezi, A. Faenov, T. Pikuz, A. Gaudieri, *Opt. Commun.* **231**, 403 (2004)
17. A. Ritucci, G. Tomassetti, A. Reale, F. Flora and L. Mezi, *Phys. Rev. A* **70**, 023818 (2004)
18. A. Ritucci, G. Tomassetti, A. Reale and L. Reale, *Appl. Phys. Lett.* **86**, 101106 (2005)
19. C. A. Tan and K. H. Kwek, *J. Phys. D* **40**, 4787 (2007)
20. C. A. Tan and K. H. Kwek, *Phys. Rev. A* **75**, 043808 (2007)
21. Y. Zhao, Y. Cheng, B. Luan, Y. Wu and Q. Wang, *J. Phys. D* **39**, 342 (2006)
22. Y. P. Zhao, S. Jiang, Y. Xie and Q. Wang, *Appl. Phys. B* **99**, 535 (2010)
23. K. Kolacek, J. Schmidt, V. Bohacek, M. Ripa, O. Frolov, P. Vrba, J. Straus, V. Prukner, A. A. Rupasov and A. S. Shikanov, *Plasma Phys. Rep.* **34**, 162 (2008)
24. K. Kolacek, J. Schmidt, V. Prukner, O. Frolov and J. Straus, *Laser and Particle Beams* **26**, 167 (2008)
25. N. S. Kampel, A. Rikanati, I. Be'ery, A. Ben-Kish, A. Fisher, and A. Ron, *Phys. Rev. E* **78**, 056404 (2008)
26. I. Gissis, A. Rikanati, I. Be'ery, A. Fisher and E. Behar, *J. Quant. Spectrosc. Radiat. Transfer* **127**, 176 (2013)
27. Y. Sakai, S. Takahashi, T. Hosokai, M. Watanabe, G. H. Kim and E. Hotta, *J. Appl. Phys.* **107**, 083303 (2010)
28. Y. B. S. R. Prasad, S. Nigam, K. Aneesh, S. Barnwal, P. K. Tripathi, P. A. Naik, C. P. Navathe and P. D. Gupta, *Sadhana* **36**, 349 (2011)
29. S. Barnwal, Y. B. S. R. Prasad, S. Nigam, K. Aneesh, M. L. Sharma, R. P. Kushwaha, P. K. Tripathi, P. A. Naik, J. A. Chakera, C. P. Navathe and P. D. Gupta, *Applied Physics B: Lasers and Optics* **117**, 131 (2014)
30. S. Barnwal, S. Nigam, K. Aneesh, Y. B. S. R. Prasad, A. S. Joshi and P. A. Naik, *Laser Physics* **27**, 055003 (2017)
31. S. Barnwal, S. Nigam, K. Aneesh, Y. B. S. R. Prasad, P. A. Naik, C. P. Navathe and P. D. Gupta, *Applied Physics B: Lasers and Optics* **122**, 169 (2016)
32. P. Vrba, M. Vrbova, N. A. Bobrova, P. V. Sasorov, *Central European Journal of Physics* **3**, 564 (2005)

33. S. Barnwal, S. Nigam, K. Aneesh, Y. B. S. R. Prasad, M. L. Sharma, P. K. Tripathi, A. S. Joshi, P. A. Naik, H. S. Vora and P. D. Gupta, *Applied Physics B: Lasers and Optics* **123**, 178 (2017)

LIST OF FIGURES

Figure No.	Figure Caption	Page No.
Fig.1.1 :	Energy levels of an atom showing stimulated emissions	13
Fig.1.2 :	General Scheme of a laser.....	14
Fig.1.3 :	Energy level diagram explaining the conditions for non-equilibrium plasma....	19
Fig.1.4 :	Divergence of an X-ray laser in the plasma.....	21
Fig.1.5 :	Refraction of X-ray laser beam due to density gradient in plasma.....	22
Fig.1.6 :	Energy level diagram of Ne-like Ar soft X-ray laser.....	24
Fig.1.7 :	Energy level diagram of H-like C for recombination pumping.....	26
Fig.1.8 :	Scheme for resonant photo-excitation.....	28
Fig.1.9 :	Pumping scheme for resonant photo-excitation.....	29
Fig.2.10 :	Principle of fast capillary discharge technique for generation of X-ray laser...	40
Fig.2.11 :	Photograph of the Capillary discharge system for X-ray laser.....	43
Fig.2.12 :	Schematic layout of the Capillary discharge system for X-ray laser.....	44
Fig.2.13 :	Typical circuit diagram of Marx-bank for generation of high voltage.....	48
Fig.2.14 :	Typical circuit diagram of Tesla transformer for generation of high voltage....	50
Fig.2.15 :	High voltage switching action of spark gap.....	52
Fig.2.16 :	Resistive voltage divider.....	54
Fig.2.17 :	Capacitive voltage divider.....	55
Fig.2.18 :	A photograph of the Rogowski coil.....	57
Fig.2.19 :	Current transformer coil	58
Fig.3.20 :	Typical voltage and current signal from capillary discharge system.....	61
Fig.3.21 :	Vacuum diode signals a) showing the two types of X-ray emissions at a distance of 83 cm from the source, and b) same signal at a larger distance (1.7m) , showing the dominance of the lasing signal.....	64
Fig.3.22 :	Spatial profile recorded on MCP a) with pre-pulse and b) without pre-pulse...	66
Fig.3.23 :	Laser pulse recorded in equal amplitude in all four quadrants of Quadrant vacuum photodiode.....	67
Fig.3.24 :	Transmission grating spectrum along with its binned intensity profile a) with pre-pulse and b) without pre-pulse; showing lasing line at 46.9 nm along with its various diffraction orders.....	68

Fig.3.25 : Diffraction orders recorded up to (a) 10 th order in the spectrum and disappear (b) in absence of pre-pulse.....	70
Fig.3.26 : Schematic diagram of experimental layout for Young's double slit experiment.....	71
Fig.3.27 : Good contrast Interference fringe pattern shown in (a). Also, shown is the transverse line-out (b) of these fringes.....	72
Fig.3.28 : A very compact capillary discharge X-ray laser operating at repetition rate of 0.1 Hz.....	75
Fig.3.29 : Discharge current and the laser pulse from compact capillary discharge X-ray laser operating at repetition rate of 0.1 Hz.....	75
Fig.4.30 : Photograph of the upgraded system (Version 2) in comparison to the old system (Version 1).....	79
Fig.4.31 : Clean X-ray laser pulse recorded with vacuum diode placed at 2.6 m from the source.....	81
Fig.4.32 : Discharge current profiles from old system (black solid curve) and the new system (red dashed curve) showing different rate of rise.....	84
Fig.4.33 : Graph showing the dependence of X-ray laser energy on dI/dt value of the current.....	87
Fig.4.34 : Semi-log plot of gain vs plasma length for slower (30 cm long capillary; triangular datapoints) and faster currents (15 cm long capillary; circular datapoints). Solid curves are the curve fitting of the initial exponentially varying part with Linford's formula ¹⁵⁴	89
Fig.4.35 : Discharge current profiles for 30 cm long capillary (black curve) and 15 cm long capillary (red curve).....	90
Fig.4.36 : Semi-log plots of laser-gain vs plasma length for different discharge current amplitudes 41 kA, 36 kA, 31 kA and 26 kA. Exponentially varying portion of each plot has been fitted (shown as solid curve) with Linford's formula ¹⁵⁴ to estimate gain-coefficient.....	92
Fig.4.37 : Dependence of gain-coefficient on the discharge current amplitude showing optimum behaviour.....	93
Fig.5.38 : Energy level diagram of H-like N ion for recombination pumping.....	95

Fig.5.39 : Schematic diagram of upgraded capillary discharge system ‘Version 3’	97
Fig.5.40 : Typical voltage and current waveforms delivered by upgraded capillary discharge system ‘Version 3’ with peak current at 105 kA. Also, shown is the simultaneously obtained argon X-ray laser pulse at 46.9 nm.....	99
Fig.5.41 : Schematic diagram of experimental setup for transmission grating spectrograph.....	100
Fig.5.42 : Temporal profile of the emission from nitrogen Z-pinch plasma as recorded by quadrant diode at different gas pressure: a) 2.5 mbar, b) 7.0 mbar, c) 9.0 mbar and d) 3.0 mbar (on expanded time-scale). Also, shown is the discharge current profile at each gas pressure.....	102
Fig.5.43 : Transmission grating spectrum recorded with 95 kA peak current and 8.5 mbar gas pressure in presence of prepulse. The intensity profile of spectrum is shown in the lower portion.....	104
Fig.5.44 : Transmission grating spectrum at 95 kA peak current and 8.5 mbar gas pressure in absence of pre-pulse. The intensity profile of spectrum is shown in the lower portion.....	106
Fig.5.45 : Transmission grating spectrum at 95 kA peak current and 2.0 mbar gas pressure in presence of pre-pulse. The intensity profile of spectrum is shown in the lower figure.....	108
Fig.5.46 : Temporal profile of emission from carbon Z-pinch plasma in presence of prepulse.....	111
Fig.5.47 : Temporal profile of emission from carbon Z-pinch plasma in absence of prepulse.....	112
Fig.5.48 : Transmission grating spectrum of carbon Z-pinch plasma at ~ 90 kA peak discharge current and gas pressure of 5.0 mbar (a) in presence of prepulse and, (b) in absence of prepulse.....	113
Fig.5.49 : Temporal profile of Krypton Z-pinch plasma at ~ 53 kA peak current and gas pressure of 0.13 mbar.....	114
Fig.5.50 : Spectrum of Krypton Z-pinch plasma at ~ 53 kA peak current and gas pressure of 0.13 mbar.....	115

LIST OF TABLES

Table No.	Table Caption	Page No.
4.1	Increase in laser energy as the dI/dt value of discharge current increases.....	85

CHAPTER 1: INTRODUCTION

1.1 Motivation

Development of coherent light sources in shorter wavelength region of the electromagnetic spectrum, especially in X-ray region, has always been in the forefront of the interest shown by the scientific community engaged in the development of lasers. As the laser technology advances towards shorter to shorter wavelength, it opens up plethora of newer areas of science and technology to be explored which may have tremendous potential for the benefits of society in the long run. The research and development in this field is quickly approaching towards developing compact table-top X-ray lasers which can be easily accessible to larger user community for carrying out numerous experiments in a small scale laboratory setup. Potential applications of X-ray lasers are enormous but are yet in their nascent stage. Nano-imaging¹ including 3-dimensional molecular imaging², dense plasma diagnostics³, nano-patterning⁴, lithography⁵, holography⁶, study of radiation-induced damage in bio-molecules⁷ are some of the applications where X-ray lasers have shown great potential. There is no doubt that many more applications will appear in near future with the availability of practical table top X-ray lasers in a range of wavelengths. It would be worth to cover some of these applications here before proceeding further.

1.2 Various applications of coherent X-ray sources

A. Nano-imaging

Significant and rapid progress in nanotechnology and nanoscience has generated the need for new and efficient practical imaging tools which can resolve nanometer sized

features. The resolution in optical imaging techniques are limited by the wavelength of the illuminating light due to diffraction phenomena. However, lasers in the X-ray region provides excellent opportunities to develop imaging systems with the highest resolution i.e. comparable with the X-ray wavelength ranging from few nanometer to few tens of nanometers. Nano-scale microscopy requires light with short wavelength, good directionality, short pulse and high photon flux which is readily available with the some of state-of-art X-ray lasers available today from large facilities to compact desktop systems. For imaging applications, higher spatial coherence is not required as it gives fringes or speckles in the image which affect the quality of the image. The field was actively pursued by the scientific community to develop compact and widely accessible optical microscopes based on high-harmonic light sources^{8,9}, plasma sources¹⁰ and Extreme Ultra-violet (EUV) and soft X-ray laser sources¹¹⁻¹⁴ where resolution could be obtained few times the wavelength of light used. Very compact EUV microscope capable of imaging with a resolution approaching the wavelength of illumination i.e. 46.9 nm was also developed using capillary discharge X-ray laser¹. Images of 50 nm carbon nanotubes could be recorded using this microscope. High resolution imaging of bio-specimens e.g. living bacterial cells is an area where use of X-ray lasers was initially found not very suitable due to severe problem of radiation damage. However, the problem was overcome by the emergence of Free electron X-ray lasers (X-ray FEL) capable to deliver ultra-short femtosecond duration X-ray laser pulses with unprecedented brightness. Such sources made it possible to image in a single snap-shot biological samples close to their natural state without being damaged by laser radiation¹⁵.

B. Interferometric lithography

The advancement of nanoscience is dependent upon capability to fabricate structures with sizes below 100 nanometer. Fabrication of periodic nanostructures in the form of gratings or arrays of pillars or holes are of particular interest to fabricate UV polarizers¹⁶, plasmonic structures¹⁸⁻²⁰, photonic crystals and nanophotonics materials^{21,22}, high density magnetic memories^{23,24}, miniaturized RF oscillators²⁵, printing of nanometer period gratings etc. Interferometric lithography (IL) has emerged as a very attractive maskless alternative to print arrays of nanoscale periodic structures in a simpler way. This technique generates interference pattern from two or more mutually coherent light beams which is then used to activate a light-sensitive medium e.g. photoresist to print periodic lines with a period given by $p = \lambda/2 \sin(\theta)$, where λ is the wavelength of illumination and θ is the incidence angle. This clearly indicates that use of X-ray wavelength is essential for realizing interference patterns having dimensions below tens of nanometers. Also, high degree of spatial as well as temporal coherence is required to achieve a good contrast in the interference fringes over large areas. These characteristics have been the main motivation for using X-ray lasers for this application. Using the configuration of Lloyd's mirror interferometer with a very compact table-top soft X-ray laser, printing of gratings and arrays of nanodots have been demonstrated^{26,27}. Amplitude division interferometer configuration has also been utilized to serve the similar purpose²⁸. In such interferometric setup, it was possible to print large area or regular lines with periods below 100 nm in a single exposure.

C. Holographic projection and imaging

The interferometric lithography described in the previous section is useful to generate periodic patterns. Since, it is based on interference process, its output is limited to generate periodic structures. This technique can be extended further towards creating arbitrary patterns which is termed as Holographic lithography. In this approach, a hologram is reconstructed by coherent illumination on the surface of the sample and in this way arbitrary motifs can be printed on the surface of the photoresist²⁹⁻³². The approach has the advantage of having a very simple setup which consists of a single diffractive element, a holographic binary mask designed as a computer generated hologram (CGH) and a coherent light beam. The CGH is designed by calculating the interference pattern produced between the diffracted wave of selected hologram motif and the reference beam. Holographic lithography requires an illumination with a larger degree of spatial and temporal coherence as compared to interferometric lithography. Table-top soft X-ray lasers were used successfully to demonstrate holographic projection technique³³. Such table-top setups have also been used successfully for taking holographic images of nanostructures with a very good spatial resolution of 46 ± 2 nm by Wachulak et al⁶. This was the first demonstration of soft X-ray holography with wavelength resolution.

D. Probing of high density plasmas

With the progress in laser technology, there has been significant interest in probing of high dense region ($> 10^{21}$ cm⁻³) of large variety of plasmas using laser as probe. However, free-free absorption and refraction of the probe beam at such high densities severely limit

the use of conventional optical lasers to extract useful information like maximum electron density, plasma size, plasma density gradient etc. The development of high flux X-ray lasers has opened up the possibilities of extending the laser interferometry to a significantly broader range of plasma parameters. With their high brightness and short wavelength, they have become quite effective probe for investigating high density plasmas^{34,35}. Two dimensional diagnosis of plasma electron density with picosecond (ps) time resolution have been carried out with very high precision using soft X-ray laser interferometry³⁶. It has shown great potential in extending the scheme to probe dense plasmas of significant importance such as in inertial confinement fusion. In 1995, first soft X-ray plasma interferometry experiment was performed using 15.5 nm Neon-like Yttrium soft X-ray laser pumped by world's most powerful laser "Nova laser"^{34, 37}. First demonstration of soft X-ray interferometry of plasma with a table-top laser was shown in 1999 by Rocca et al³⁸ and Moreno et al³⁹. Lloyd's mirror interferometer was used in combination of 46.9 nm capillary discharge pumped soft x-ray laser. Using this configuration, regions of electron density as high as $n_e \sim 5 \times 10^{23} \text{ cm}^{-3}$ of a pinch plasma could be probed successfully. A novel soft X-ray amplitude-division interferometer was proposed by Filevich et al⁴⁰ in which specially constructed diffraction gratings were used as beam splitter. With the advent of X-ray FEL capable to deliver highly intense laser radiation ($> 10^{17} \text{ watts / cm}^2$), it has now become possible to explore matter close to solid densities which are relevant to stellar interiors and core of giant planets⁴¹.

1.3 Various methods to generate coherent X-ray light

In view of the immense potential applications of coherent X-ray light sources in diverse areas of science and technology as briefed above, efforts are constantly being

made worldwide to achieve newer heights in the X-ray laser technology. There are different approaches in which coherent X-ray light can be generated. All these approaches are complimentary to each other as they have their own advantages and limitations. One such technique is X-ray FEL which is capable to deliver the brightest X-ray laser light with broad tunability of lasing wavelength⁴². However, it is quite large (~ few km long), expensive and complex setup and requires multi-nation collaboration and therefore limited to small user community. The other technique is through high-order harmonic up-conversions of ultra-short ultra-intense Ti:Sa laser pulses from its non-linear interactions with plasma⁴³. This scheme provides coherent X-ray pulses with high peak power but is limited by its low efficiency of harmonic up-conversion and small average power. Plasma based X-ray laser provides efficient alternative method for developing compact coherent X-ray sources with good average power. Unlike conventional laser sources in infra-red, visible or ultra-violet wavelength, the gain medium in such X-ray laser is in plasma state. As the lasing wavelength is in X-ray region, the spontaneous emission from upper laser level of an atom dominates over the stimulated emission demanding much powerful pumping to achieve population inversion. This pump power requirement is so high that it naturally converts any medium into plasma state. Such a plasma state is highly suitable for achieving population inversion in the inner shell of the highly ionized species and acts as an efficient amplifier for the lasing wavelength in X-ray region. Plasma as a gain medium for X-ray lasing can be generated either by using ultra-short Ti:Sa laser beam focussed to ultra-high intensity⁴⁴⁻⁴⁸ or by using fast and high discharge current through gas medium in a capillary^{49,50}. The X-ray laser based on the first method is known as laser produced plasma based X-ray laser whereas the second

method is called Capillary discharge X-ray laser. The laser plasma based X-ray lasers can have extremely short duration (picosecond to hundreds of femtosecond) lasing realized in various wavelengths down to few nanometers using the most powerful optical lasers such as Nova laser³⁴. However, the conversion efficiency of optical laser energy to plasma is quite poor and also the gain-volume is quite small. Due to requirement of powerful lasers for shorter wavelength lasing, the size of the system is large. On the other hand, the capillary discharge based techniques have advantage of very high energy coupling of electrical driver with the plasma. This makes the scheme very efficient in generating multiply-ionized, hot and dense plasma column having large aspect ratio with high uniformity which is ideal for providing larger gain-volume^{51,52}. As a result, much higher photon flux can be achieved in the lasing wavelength. Also, this technique has great potential in making X-ray lasers of relatively compact size compared to big facilities like X-FEL or high power laser systems. This is due to involvement of pulse power systems as driver which can be made very compact. A brief overview of these approaches is given in the next section.

1.3.1 Free-Electron X-ray Laser

Free electron X-ray lasers, also called as X-ray FEL, are the most powerful and brightest source of coherent radiation in X-ray region available to date. These lasers have remarkable tunability over a broad range of wavelength varying from extreme ultra-violet to hard X-ray region⁵³ and able to deliver ultra-short duration (few fs to 100 fs) pulses. Such unique capabilities make these lasers quite suitable for variety of applications⁵⁴. X-ray FEL makes use of a simple and elegant gain medium which is a relativistic free electron in a magnetic field. So, this is a new kind of laser in which electrons are not

bound in atomic or molecular systems. Source of these highly energetic and relativistic free electrons are electron accelerator, such as a linac or synchrotron. It is thus a classical rather than a quantum-mechanical laser. The free energetic electrons are forced to oscillate in transverse direction by propagating it along the axis of a periodic lattice of alternating magnetic dipolar fields, known as ‘undulator’. An Undulator is an array of magnets which are assembled in a very specific way with their poles alternating so that the magnetic field alters its direction every few centimeters. The transverse undulation of electron beam by the magnetic field generates electromagnetic radiation. This radiation is emitted in the forward direction in a narrow cone with cone angle $1/\gamma$ where γ is the relativistic Lorentz factor of electrons (typically several thousand for X-ray emission). The fundamental wavelength emitted is proportional to λ_u/γ^2 , where λ_u is the undulation period, typically a few centimeters. The concept of free-electron laser (FEL) was first proposed in 1971 describing a small gain process in a relativistic electron beam with undulator system and hypothesized to generate coherent X-ray radiation⁵⁵. It was probably this potential that ignited significant interest in the FEL for the scientific community. Few years later, the first amplification and lasing from FEL was demonstrated in a small-gain infrared FEL oscillator system^{56,57}. In FEL, the undulator, which wiggles the high-energy relativistic electron beam, amplifies the power of the light dramatically by means of light-matter interaction under the periodic magnetic field. If the FEL has to run as an oscillator, there has to be a resonator cavity to provide positive feedback. This is usually provided by a Fabry-Perot resonator with mirrors at both ends. Radiation is typically coupled out through a hole in one of the mirrors or sometime by using a partially reflecting mirror. When the FEL is to be operated as an amplifier, the

resonator cavity is not there, but a seed radiation is required to be provided. In the 1980s, a new exciting scheme called as self-amplified spontaneous emission (SASE) was introduced which enabled FEL to work in cavity-free, single-pass operation but yet able to generate high power coherent radiation. SASE-FELs are the most promising candidates for X-ray lasers. In SASE-FEL, a long undulator is used to amplify the initial spontaneous radiation originated from the shot-noise fluctuation of the electron beam. The most significant characteristic of this scheme is its wavelength scalability which means that light properties can be easily varied over the entire wavelength region only by controlling the parameters of electron beam and the undulator. Here, the wavelength λ of light is given by

$$\lambda = \lambda_u \left(1 + K^2/2\right) / 2n\gamma^2 \quad \dots(1)$$

where n is the harmonic order and K is the magnetic deflection parameter given as,

$$K = eB_u \lambda_u / 2\pi mc \quad \dots(2)$$

where B_u is the strength of the magnetic field

Light amplification is a result of resonant coupling between the ultra-relativistic electron beam guided by the static and periodic magnetic field of long undulator and a co-propagating electromagnetic wave originated by spontaneous incoherent electron emission. As a result of the interaction between the electrons and the electromagnetic field, the electron beam is modulated in energy, with the period of modulation being equal to the wavelength λ of the electromagnetic wave. When this beam travels sufficient distance by propagating further inside the undulator, its energy modulation naturally transforms into the spatial modulation of electron density at the fundamental wavelength λ . This leads to micro-bunching of the electron beam which emits in phase, generating

coherent emission at the fundamental wavelength. Since bunching can have strong harmonic components, such coherent emission can also be produced at the harmonics of the resonant wavelength i.e. λ/n , where $n > 1$ is an integer.

Equation (1) clearly signifies the fact that an increase in the electron beam energy is quite effective for shortening the wavelength of the emitted radiation. This interesting fact guided the researchers to build X-ray FEL facilities using large-scale accelerators, such as Linac Coherent Light Source (LCLS)⁵⁸ at SLAC National Accelerator Laboratory and the European X-FEL⁵⁹ at Hamburg where electron beam energies higher than 10 GeV have been utilized. Equation (1) also indicates that it is possible to shorten the wavelength with less electron beam energy but with a smaller value of λ_u i.e. using a short period undulator. This concept, combining a compact-scaled accelerator with a short-period undulator, led to the development of an X-FEL facility in Japan, the Spring-8 Angstrom Compact free-electron Laser (SACLA)⁶⁰ which operates at sub-angstrom wavelength. Two soft X-ray FELs, FLASH⁶¹ and FERMI⁶² are also in operation at DESY, in Germany, and Sincrotrone Trieste, in Italy. LCLS is being upgraded to LCLS-II⁶³ which will cover both the soft and hard X-ray regions, from 10 nm to less than 1 Å.

1.3.2 High order harmonic generation

High harmonic generation (HHG) is an extremely non-linear optical process in which a large number of low energy photons are converted into a single soft X-ray photon. This happens when ultra-short laser pulse interacts with the matter and generates coherent radiation at multiples of the laser frequency. It is not possible to explain the generation process of these high harmonics in terms of perturbation expansion of the polarization of the atom or molecule as is normally done in conventional non-linear harmonic

up-conversion. The process can be understood in a simpler semi-classical approach (3-step model) although it is much more complex. The intense laser field distorts and lowers the coulomb barrier of the atom or molecule to facilitate tunneling of least bound electron. As the electron is tunneled out, it is accelerated in the laser field in half cycle and in next half cycle, it is recollided with the parent atom. Upon re-collisions, it can recombine with the ion and release its kinetic energy gained in the laser field as one high-energy photon which is seen as a high harmonic photon emission. The entire process is coherently driven by the oscillations of the laser electric field and lasts for a very short time which is fraction of the optical cycle. The laser field must be strong enough so that electron may efficiently tunnel out and gain enough energy in the laser field before being recombined with the atom. But, the laser photon energy must be much smaller than the ionization potential of the atom or molecule in order to facilitate tunneling ionization. Ultra-short (femtosecond) Ti:Sa laser pulse focused with intensity of 10^{15} W/cm² is fairly good for HHG.

Today's HHG based X-ray sources are capable to deliver laser-like pulses with excellent spatial and temporal coherence properties⁶⁴⁻⁶⁸. The photon energy can easily reach into soft X-ray region^{69,70} and the pulse durations from several 100's of femtosecond down to 100 attosecond⁷¹. Such remarkable properties make HHG-based X-ray sources ideal to probe several ultrafast electronic processes with ultra-high precisions. These sources have also formed a very commendable foundation of attosecond science.

The HHG process was discovered in 1987 when a group of researchers focused a picosecond laser pulse into a gas target and observed a plateau of weak, odd order

harmonics extended up to XUV region^{72,73}. The physical mechanism behind the process was understood with 3-step simple model as explained above. It was soon realized that this process can go ahead with the generation of attosecond pulses^{74,75}. However, the complexity of the experiments led to almost a decade to finally demonstrate the generation of attosecond pulse trains⁷⁶ and isolated attosecond pulses⁷⁷. As major breakthrough for HHG source development, photon energy cutoff was extended into the keV regime^{69,78} and a frequency comb was demonstrated for the first time in the VUV region enabled by HHG inside a cavity^{79,80}. The first high-order harmonics and/or attosecond pulses were generated in simple gas targets. Later on, other novel methods have also been explored which includes HHG in gas-filled capillaries⁸¹ as well as from plasma surfaces⁸² and solids⁸³.

1.3.3 Plasma based X-ray laser

Generation of plasma based X-ray laser is itself a quite challenging task. Unlike conventional laser sources in infra-red to ultra-violet wavelength, the gain medium in such X-ray laser is in plasma state and the population inversion has to take place in the inner shell of highly ionized species. In X-ray region, the spontaneous emission from upper laser level dominates over the stimulated emission demanding higher pump power to achieve population inversion. This pump power requirement is so high that the gain medium will be naturally converted into plasma state. Therefore, plasma acts as an inherent and efficient gain medium for X-ray laser. Before discussing into the various aspects of plasma-based X-ray lasers, it is worth to discuss in detail the basic fundamentals of these lasers for better understanding of this field of research.

1.3.3.1 Basics of plasma-based X-ray laser

There exists a gap of nearly two decades between conception and experimental realization of plasma-based soft X-ray lasers which clearly reflects the level of difficulty and challenges in achieving the X-ray lasers. This difficulty is a direct consequence of the basic physics underlying the lasing action. Considering a two-level system of atoms shown in Fig. 1.1 which are in thermal equilibrium with the radiation field, the processes of spontaneous emission and stimulated emission can be related to each other. Rate of spontaneous emission is equal to $A_{21}N_2$ and that of stimulated emission is equal to $B_{21} u(\nu) N_2$. Here, N_1 and N_2 are the population in the lower and upper energy level respectively. A_{21} and B_{21} are the Einstein coefficients for the spontaneous emission and stimulated emission respectively. Spectral energy density of the radiation field at the frequency of transition (ν) is denoted as $u(\nu)$.

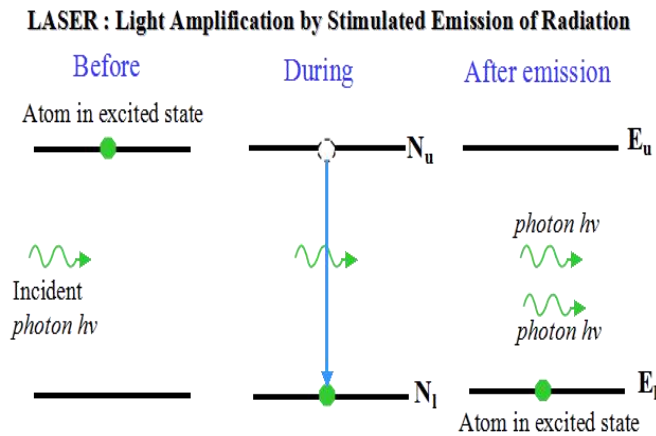


Fig.1.1: Energy levels of an atom showing stimulated emissions

The ratio of the rates of spontaneous emission to the stimulated emission is given as:

$$\frac{\text{Rate of spontaneous emission}}{\text{Rate of stimulated emission}} = \frac{A_{21}}{B_{21}u(\nu)} = \exp(h\nu/kT) - 1 \quad \dots(1)$$

$$\approx \exp(h\nu/kT) \gg 1 ; \text{ for X - ray region at room temperature} \\ \text{as } h\nu \gg kT$$

This clearly indicates that losses due to spontaneous emission are much higher at shorter wavelengths. As a result, the population in the upper level is transferred rapidly to the lower level by the high rate of spontaneous emission making it more difficult to sustain the population inversion at shorter wavelength. That is why, obtaining lasing at shorter wavelength e.g. in X-ray region, is inherently more difficult.

As for laser, creation of population inversion is a pre-requisite for stimulated emission to take place in a laser. A laser basically consists of three parts:

1. Gain medium \longrightarrow to sustain population inversion between suitable energy levels
2. Pump source \longrightarrow to create population inversion in the gain medium
3. Resonator \longrightarrow to confine the light of suitable transition for multiple transits and amplification through the gain medium

In a classical laser system as depicted in Fig. 1.2, the light photons at the lasing

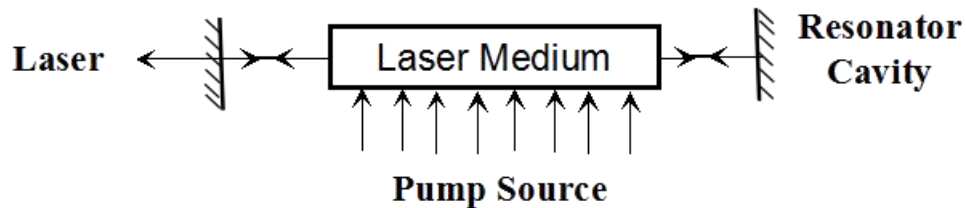


Fig.1.2: General Scheme of a laser

wavelength makes several passes through a gain-medium placed in a resonance cavity or called as 'resonator' before being amplified and become laser. The resonator is formed by

two mirrors placed at the end which facilitates the required several passes of the beam. When the beam is amplified to high enough value to lase, it transmits through one of the mirrors that is semi transparent. However, in the XUV region, this simpler picture becomes difficult to realize. A brief description of this picture has been explained below.

A. Pump source for X-ray laser

Population inversion of a medium is essential for amplification of any light through that medium. It means upper electronic level has to be populated more than the lower one. In case of X-ray lasers, the gap between the two energy levels involved in the lasing transition remains very large. So, a strong pump source is required to create the population inversion between the two highly separated energy levels in order to generate X-ray laser. Beside this, the rate of spontaneous emission predominates manifold over the stimulated emission when the lasing has to take place in X-ray region as seen earlier. So, the pump source has to compensate for the power loss by the spontaneous emission. The power loss by spontaneous emission (P_{sp}) has following relation with the wavelength (λ) of transition,

$$P_{sp} = \left[\frac{1.5 \times 10^{21}}{\lambda^4 \left(\frac{\text{\AA}}{\text{\AA}} \right)} \right] \alpha L \frac{\Delta\lambda}{\lambda} \text{ W/cm}^2 \quad \dots(2)$$

; where αL is the gain-length product

It is noted here that the power loss and hence the pump power requirement scales as inverse fifth power of the wavelength. It means that if one wishes to make a laser at 10 nm, the pump power required for this will be more than 10^8 times the power required for

making a laser at visible wavelength. This factor becomes more than 10^{13} to have a laser at 1 nm. This large pump power requirements can be fulfilled by short duration laser pulses (from ns to fs duration with suitable energy) or by powerful electrical discharges. In both these cases, the pump intensity or energy density is so high that the gain medium will naturally convert into plasma.

B. Gain medium for X-ray laser

Due to large pump power requirements for population inversion in X-ray region, hot plasma becomes the inherent gain medium for X-ray lasers. Such a hot plasma consists of highly ionized atoms where the transitions between the excited states correspond to X-ray region. These hot plasmas are usually generated by fast heating process through either lasers or electric discharges. In order to create population inversion, ion species with relatively stable closed shell configurations are chosen and the reason is explained here. In general, multiply charged ions are not stable like atoms. They have lost multiple electrons by ionization and might contain excess energy which makes them unstable. Such ions may not be suitable for population inversion. However, ions which have closed electronic shell configuration, are relatively stable and thus they are the most suitable candidate for creating population inversion leading to generation of X-ray laser. Therefore, lasing ions are mostly H-like, He-like, Ne-like, Ni-like, Pd-like. These are referred as iso-electronic sequence of the elements having same number of residual electrons. In such highly ionized plasma as gain medium, the temporal changes in the populations of ion levels are influenced by ionization, recombination, collisional excitation, de-excitation and radiative decay. All these processes must be taken into

account while trying to model the population inversion in plasma.

C. Resonator for X-ray laser

At visible wavelengths, mirrors are easily available with reflectance more than 99.99%. It means that it is possible to construct a resonator which can have gain-length (αL) product per pass very small as little as 0.01 but still possible to lase after several passes through the gain medium. However, in the soft X-ray region, the best mirrors available have a reflectance of ~ 20 -50%. Also, the life-time of the population in the excited states of highly ionized species is very small i.e. few picoseconds (ps) to tens of ps which provides very short time-scale for amplification of soft X-ray photons. During 1 ps, the photon moves only 300 micron (μm) distance. This makes it necessary to use either a very small resonator or else the photons would have almost no time to bounce back and forth within the resonator cavity for many passes. Furthermore, if one tries to use a very small resonator, mirrors have to be kept very close to the gain medium which happens to be hot plasma in the present case and the mirrors will soon get damaged. Therefore, resonators are in general impractical for X-ray lasers. They are mostly operated without mirrors as single pass devices or sometimes with one mirror that produces a half cavity. The gain-coefficient for X-ray laser requires to be higher compared to conventional lasers due to their single pass amplification configuration.

D. Population inversion in plasma for X-ray laser

Plasma as a gain medium with its highly ionized atoms is not stable in time. Therefore, only those ions, having closed shell configuration with iso-electronic

sequences, remains in sufficient abundance and participate in creating population inversion for soft X-ray lasing. Population inversion is typically realized in a three-level system embedded in a reservoir of energy levels of closed shell ions e.g. Ne-like or Ni-like ions. The upper laser level is directly populated by collisions with electrons from ground state but the direct transition from the upper state to the ground state is forbidden, thus creating a metastable state. The lower laser level is rapidly de-populated by either radiative or collisional processes. These processes facilitate building of population inversion between the two lasing levels.

The gain, represented as the small-signal gain coefficient $g(\nu)$, is a measure of the amplification in the system without consideration of its origin. It is given as the product of the stimulated emission cross section (σ) and the density of the population inversion $\Delta N = (N_u - N_l g_u / g_l)$, where N_u, g_u are the population and degeneracy of the upper level and N_l, g_l are the same for lower level respectively.

$$g(\nu) = \sigma \times \Delta N = A_{ul} \lambda^2 / 8\pi \Delta \nu \times (N_u - N_l g_u / g_l) \quad \dots(3)$$

Here, the Einstein coefficient for spontaneous emission, $A_{ul} \propto \lambda^2$, and the line width $\Delta \nu \propto A_{ul}^{-1}$. Hence, the gain coefficient, $g(\nu) \propto \Delta N \lambda^2 \propto N_u \lambda^2$...(4)

Here, the gain increases with the plasma electron density n_e , but is restricted by the electron collisions which can thermalize the populations in excited energy levels thereby destroying the population inversion. Having populations inversion means rate of stimulated emission is more than the rate of absorption, i.e.

$$N_u B_{u,l} > N_l B_{l,u} \Rightarrow N_u / g_u > N_l / g_l \quad [\text{as } B_{u,l} / B_{l,u} = g_l / g_u] \quad \dots(5)$$

If the system is in thermal equilibrium, populations in different energy levels will be

governed by the Boltzmann distribution, i.e.

$$N_u = N_l (g_u / g_l) \exp\{-(E_u - E_l) / kT\} \quad \dots(6)$$

$\Rightarrow N_u / g_u < N_l / g_l$ is true always, i.e. No inversion in thermal equilibrium

It clearly signifies an important fact that plasma has to be in a state of non-thermal equilibrium to have population inversion. Also, collisional excitation and de-excitation bring the system towards thermal equilibrium whereas the radiative processes can push the system to a highly non-equilibrium state, if the emitted photon is able to escape from the system. If ΔE is the separation of energy level, the collisional excitation rate (R_{col}) is inversely proportional to ΔE i.e. $R_{col} \propto 1/\Delta E$ and radiative transition rate (R_{rad}) is proportional to square of ΔE i.e. $R_{rad} \propto \Delta E^2$. In a typical energy level diagram of an ion as shown in Fig. 1.3, the upper energy levels have smaller separation (small value of ΔE) which increases gradually towards lower energy levels. Hence, collisional processes will

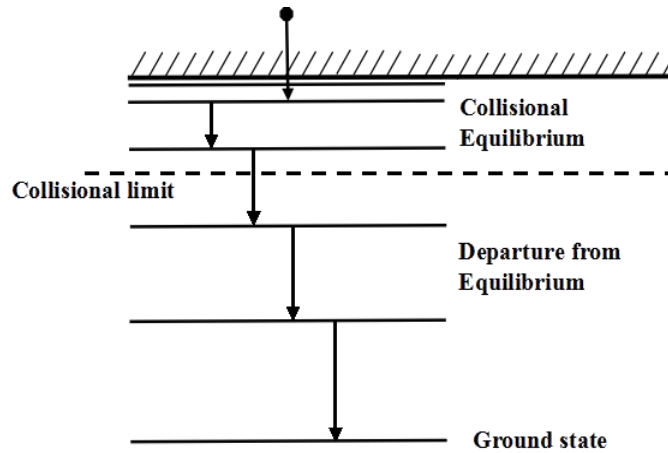


Fig.1.3: Energy level diagram explaining the conditions for non-equilibrium plasma

be more dominant in the closely spaced upper energy levels whereas the widely separated lower levels will be largely governed by the radiative processes. As a result, there will be

collisional equilibrium among the upper levels but the lower levels will depart from the equilibrium provided the emitted photons are allowed to escape from the plasma which needs to be optically thin for such photons. In fact, there exists a level above which levels are in collisional equilibrium and below which they are not in equilibrium. This particular level is called Collisional Limit. Collisional limit has a dependence on plasma parameters i.e. density and temperature and also on the energy level parameters. In general, levels near the collisional limit actively participate in generation of population inversion.

The high pump power density required for X-ray laser can be realized with small volume of gain medium (plasma). Also, this gain medium must have longer length for sufficient amplification in a single pass as well as it must have small optical thickness in the transverse direction which allows the escape of photons emitted from radiative transition from lower lasing level. These requirements impose conditions on the geometry of the gain medium for X-ray laser. It is found that plasma in a cylindrical geometry is best suited as a gain medium for such lasers as shown in Fig. 1.4. Plasma column with diameter varying from 10 - 200 μm and length varying from few millimeter to few centimeters, the aspect ratio of the gain medium comes close to 1:1000. Such a large aspect ratio is important as it also determines the divergence of the soft X-ray laser beam generated from the gain medium. The maximal divergence of the output laser beam lies in the range of 1 - 10 mrad. This value strongly depends on the input pump power and often limits the effective gain-length of the active medium due to refraction effects. However, in general, it is quite desirable to have maximum possible aspect ratio as it increases the gain-length, improves the transverse spatial coherence and facilitates to operate the X-ray laser in saturated regime. The soft X-ray laser beam is required to

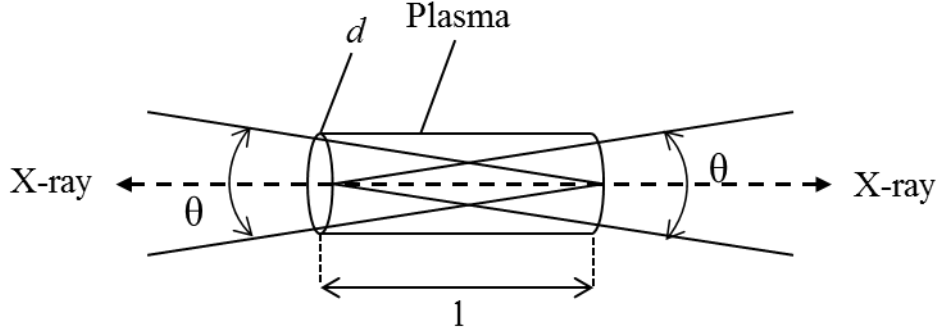


Fig.1.4: Divergence of an X-ray laser in the plasma

propagate sufficient distance in the gain volume along the axis for a high output and reasonable collimation at a preferably high plasma density. However, this laser beam is deflected by the refractive index gradients ∇n arising out of the plasma density gradient ∇n_e as shown in Fig. 1.5. These two are related by,

$$\nabla n = -\frac{1}{n} \frac{\nabla n_e}{2n_c} \quad \dots(7)$$

Here, the refractive index of plasma is given by, $n = \sqrt{1 - \left(\frac{n_e}{n_c}\right)}$... (8)

where, n_e is the electron density and $n_c = \frac{\pi m_e c^2}{e^2 \lambda^2}$ is the critical density of plasma

Since, the high gain region in the plasma has a very narrow transverse spatial extent (several tens of μm), the X-ray laser beam is easily refracted out of the gain volume and thus limiting the total accessible gain length. The typical distance in the direction of amplification in which the laser beam stays within the lasing medium before bending out is defined as the characteristic refraction length l_{ref} which is given by,

$$l_{ref} = l_x \left(\frac{n_c}{n_{oe}}\right)^{1/2} \quad \dots(9)$$

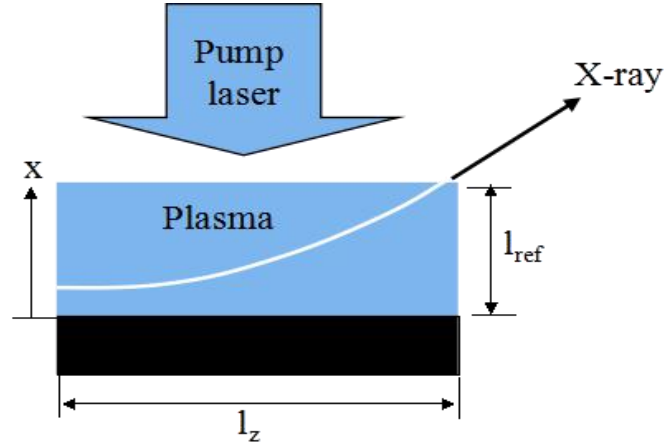


Fig.1.5: Refraction of X-ray laser beam due to density gradient in plasma

where, $l_x \Rightarrow$ transverse extension of gain medium ; $n_{oe} \Rightarrow$ maximum electron density

The corresponding refraction angle (θ_{ref}) is expressed as,

$$\theta_{ref} = (n_c / n_{oe})^{1/2} \quad \dots(10)$$

In one dimensional case, the refraction reduces the gain by $1/l_{ref}$. For a large plasma length $l > l_{ref}$, the effective gain coefficient (g_{eff}) is reduced to

$$g_{eff} = g - \frac{1}{l_{ref}} \quad \dots(11)$$

Refraction effects can be minimized to certain extent by using pre-ionization of gain medium in order to suppress the inhomogeneity and sharp density gradient in plasma.

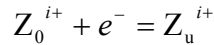
1.3.3.2 Population inversion mechanisms in plasma

There are various schemes of achieving population inversion. In most of the schemes, ions having closed shell configuration are chosen as the lasing species. This is because such ions are available in much higher fractional abundance due to a larger energy gap between the closed shell and the next higher shell. The major schemes for attaining

population inversion have been described as below.

A. Collisional electron excitation

The collisional excitation is the most robust and popularly applied pumping mechanism for generating population inversion in plasma. This excitation process can be expressed as



Here, the ground state (0) of Z^{i+} ion, having closed shell configuration, is excited to the upper state (u) by electron collisions. During the collisions, the energetic free electrons transfer their energy to the ion by populating both the lower as well as upper lasing levels. However, the two lasing levels exist such that the radiative decay from the lower lasing level is predominant over that from the upper lasing level. This leads to generation of population inversion between the two levels. Transitions in Ne-like and Ni-like iso-electronic sequences are the most preferred one for this mechanism. The lasing transition in Ne-like scheme takes place among following energy levels :



Fig. 1.6 shows the energy level diagram for Ne-like Ar which indicates that the $2p^5 3s$ state is rapidly de-populated to ground state ($2p^6$) by fast radiative decay whereas transition from $2p^5 3p$ state to ground state is a forbidden transition. This creates population inversion between $2p^5 3p$ and $2p^5 3s$ states leading to soft X-ray lasing. Using such Ne-like scheme, first x-ray laser was successfully demonstrated in 1985⁸⁴. The lasing was in Ne-like Se^{24+} ions at 20.63 nm and 20.96 nm. Subsequently, lasing action has been demonstrated in various elements e.g. Ne-like strontium ($Z=38$),

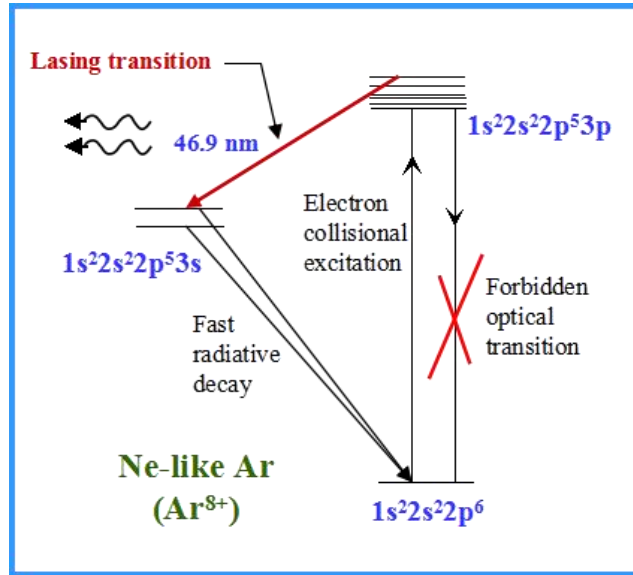


Fig.1.6: Energy level diagram of Ne-like Ar soft X-ray laser

molybdenum ($Z=42$), silver ($Z=47$) etc. Another common configuration is Ni-like scheme in which lasing transition takes place in following energy levels,



4d level is in a metastable state with respect to the radiative decay to the ground state $3d^{10}$ whereas the $3d^9 4p$ level has rapid radiative decay to the ground state. This creates the required population inversion between the two lasing levels. The main advantage of Ni-like sequence is that it is more favorable for achieving shorter wavelength lasing as compared to Ne-like sequence.

There are certain requirements which need to be fulfilled for making this collisional excitation pumping more efficient. The gain medium must have sufficient abundance of lasing ions (either Ne-like or Ni-like). Plasma electron density should be high enough to provide higher rate of collisional pumping but should not be too high to de-populate the upper lasing level. Electron temperature should be suitable enough to efficiently pump the upper lasing level. The opacity of the plasma should be low enough to facilitate

depopulation from the lower lasing level. Also, the density gradients should be kept low in order to avoid strong refraction effects.

The collisional electron excitation scheme described above is in fact a quasi-steady state scheme in which lasing takes place as long as the plasma conditions, essential for population inversion, are maintained. There exists a slightly advanced version of this scheme, also called as, transient collisional excitation scheme, which makes use of the fact that much larger (1-2 order) population inversion can be achieved under rapid transient excitation. The scheme uses the difference between the population inversion lifetime – a few tens of picoseconds – and the ionization time of hundreds of picoseconds. With the use of ultra-fast high power lasers, the plasma can be heated at a rate much faster than the ionization as well as the relaxation rate of the excited states. The time-scale involved here can be typically sub-picoseconds to tens of picoseconds. Such rapid transient heating of plasma can give rise to transient gains in excess of 100 cm^{-1} . The pump power requirement in such scheme goes down significantly. Also, the lasing can be achieved even with the ground state directly.

B. Recombination scheme

The recombination scheme is based on 3-body recombination of an additional free electron to fully ionized ions or ions having closed shell configuration, e.g. fully ionized to H-like ion, He-like to Li-like, Ne-like to Na like etc. A schematic energy level diagram explaining the recombination mechanism in H-like C ion is shown in Fig. 1.7. This was the very first demonstration of X-ray lasing through recombination pumping. Here, fully ionized carbon ion undergoes 3-body recombination to acquire one free electron to

become H-like C ion. The electron enters the energy level which is within energy of the order of kT_e from the ionization limit where T_e is the plasma temperature. If kT_e is within few tens of eV, the electron recombines into the outer high n energy levels lying much above the collisional limit which are also known as Rydberg levels. Collisional recombination rates are highest into the Rydberg levels of an ion and these highly excited ions then cascade down to ground state via radiative decay. Since, the lower levels are

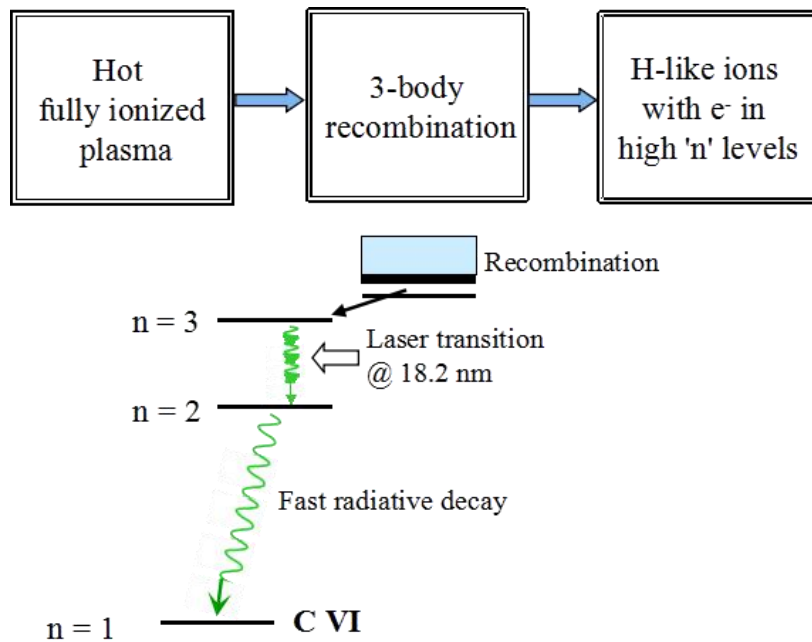


Fig.1.7: Energy level diagram of H-like C for recombination pumping

already empty, a population inversion is naturally created here. However, if the recombination scheme has to work with ions having closed shell configuration instead of being fully ionized, such cascading is followed by the fast radiative decay from the lower levels below the collisional limit and create population inversion in the recombined ion. The recombination rate is given by,

$$R_{3br} = n^4 n_e^2 T_e^{-9/2} \quad \dots(12)$$

This clearly signifies very important fact that the recombination rate is dominant for cold dense plasma. It means that highly ionized hot plasma must be cooled to allow 3-body recombination of a cold electron into the ion. However, the cooling must be faster than the recombination rates in order to avoid thermalization of populations as well as further recombination of lasing species. Several approaches have been applied to rapidly cool the plasma e.g. cooling through expansion of plasma or cooling through conduction by introducing some cold surface to plasma etc.

The recombination scheme for population inversion has been demonstrated on several soft X-ray transitions at various laboratories. Using this scheme, lasing has been observed in H-like Carbon⁸⁵, Fluorine, Sodium etc. Lasing on Balmer- α line of Carbon at 18.2 nm was demonstrated at the same time as the collisionally pumped selenium laser in 1985. Also, lasing has been observed in several ions e.g. in Li-like ions (He-like recombining to Li-like ions) in plasma of aluminum ($Z=13$), titanium ($Z=22$) etc.

C. Photo-ionization and resonant photo-excitation pumping

These two population inversion mechanisms for X-ray amplification make use of two cylindrical plasmas generated side by side. One of the two plasmas called as ‘Pump plasma’ generates high energy X-ray photons which either excites the upper level population in the suitable lasing species in the other plasma (called as ‘Lasant plasma’) to drive photo-excitation pumping or creates highly excited ions by inner-shell ionization to drive photo-ionization pumping. Both the processes can lead to generation of large population inversion. The schematic of the scheme is shown in Fig. 1.8. In

photo-ionization pumping, if the energy of generated X-ray photons is just above the threshold for inner-shell photo-ionization, its cross-section is an order of magnitude higher for inner-shell electrons as compared to outer-shell electrons. This creates larger number of inner-shell vacancies which are highly suitable for population inversion. The incoherent X-ray photons, which pump the laser media, are normally generated by a nearby plasma created by heating a high-Z (e.g. Au) target with an intense ultra-short

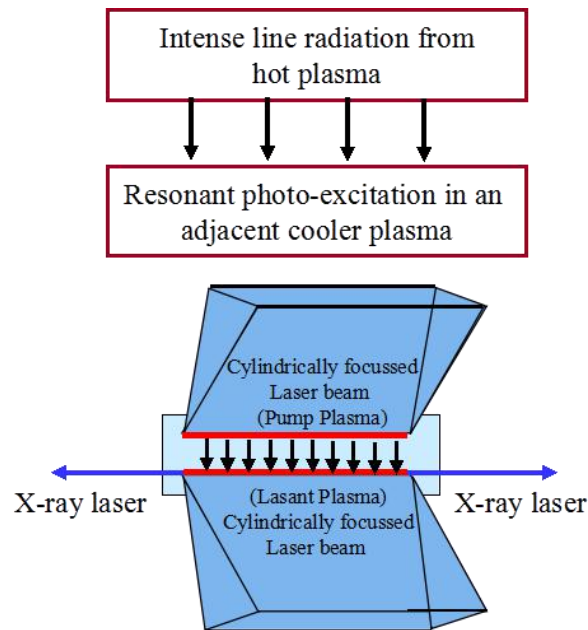


Fig.1.8: Scheme for resonant photo-excitation

laser pulse. Photons with energy smaller than the inner-shell binding energy are removed with an appropriate filter in order to avoid pumping of the laser lower level. Since, photo-ionization cross sections are quite broad, one can use a broadband X-ray source to produce specific excited state of the atom.

In the resonant photo-excitation pumping, intense line-emission from laser-driven hot plasma is utilized for resonantly photo-excite the adjacent colder plasma as shown in Fig. 1.8. In contrast to the photo-ionization scheme, resonant photo-pumping relies on very

intense line-emission rather than a broadband X-ray source to pump the laser upper level. Hence, this scheme requires a very precise wavelength coincidence between the pump lines and the lines which can populate the upper laser level by resonance absorption from a highly populated state, typically a ground state. Many such resonances have been identified in H, Ne, Li and F-like ions to be working as pump-lasant pairs. One such pair which has drawn most attention is the Na-Ne pair as illustrated in Fig. 1.9. Resonance line emission Na X 2 ¹P – 1 ¹S at 1.1003 nm from Na plasma can resonantly photo-excite a transition in Ne IX 4 ¹P – 1 ¹S at 1.0000 nm. Sufficient strong pumping on this transition can lead to an inversion of the 4-3 line at 23 nm and 4-2 transition at 5.8 nm.

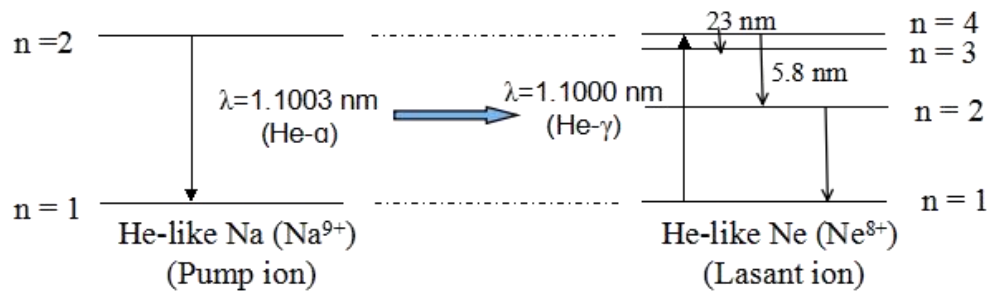


Fig.1.9: Pumping scheme for resonant photo-excitation

1.3.3.3 X-ray lasers based on laser produced plasma

A hot and highly ionized plasma, created by the interaction of an intense laser pulse with a solid or a gas target, acts as a very efficient gain medium for generation of soft X-ray lasers. The intense laser pulse is cylindrically focused to achieve hot and dense plasma with sufficient length enough for amplification to take place. As discussed earlier, population inversion in the plasma can be mostly achieved by pumping through either

electron collisional excitations or through recombination scheme. Mostly, till date, it is the electron collisional excitation pumping which is successfully driving all soft X-ray lasers operating in gain saturation regime based on laser-driven approach. A common type of such laser system is based on population inversion generated in Ne-like and Ni-like plasmas produced with short pulse lasers, in the range of nanoseconds to picoseconds, on solid targets. Although, the recombination pumping has also been used to demonstrate several soft X-ray lasing, it has still not attained saturation. Coherent X-ray emissions have been achieved in the range below 40 nm and down to 4 nm in laser-driven X-ray laser systems⁸⁶.

Large gain-length products were demonstrated in soft X-ray region for the first time in laser produced plasmas using collisional⁸⁴ and recombination schemes⁸⁵ almost simultaneously. The method of creating population inversion through recombination scheme was proposed much earlier⁸⁷⁻⁸⁹. However, observations of weak amplified emission at 11.7 nm in a laser-produced Li-like Al ions⁹⁰ and at 18.2 nm in H-like C^{91,92} ion finally opened up the path to development of recombination soft X-ray lasers. Independent proposals were also presented for electron impact collisional excitation pumping to develop soft X-ray lasers based on Ne-like ions⁹³⁻⁹⁶. The scheme was conceptualized while trying to extend Ne-like ion lasers, already working in the visible or near-UV spectrum, to vacuum UV region. The initial collisional scheme was based on the lasing transition of $2p^53p - 2p^53s$ in Ne-like ions later replaced by more efficient one in Ni-like ions having lasing transitions in $3d^94d - 3d^94p$. Collisional schemes have provided so far much better results in terms of generating laser beams with good quality as well as their applications. The recombination scheme is mostly based on H-like ions although

He-like and Li-like ions have also been studied for short wavelength lasing. The recombination scheme for lasing action finds their importance due to their wavelength scaling as a function of ion charge (Z). It was found that scaling for recombination scheme converges much faster to the shorter wavelength regions even for quite moderate Z as compared to collisional scheme. Interestingly, the scaling for 2-1 transition in recombination scheme reaches attractive wavelength ~ 1 nm for H-like Ne ion.

Initial work on development of soft X-ray lasers had been carried out on large size facility. But it was realized that the soft X-ray lasers have to be much more compact in order to be more useful for wide range of applications. In this direction, relatively compact lasers having sufficiently high intensity for entering into the very exciting area of optical field ionization (OFI) were used to generate gain in recombination scheme. Here, gain was achieved for the first time in the transition to ground state (2-1 transition) of H-like Li ion at 13.5 nm⁹⁷. The pump laser pulse had very short duration ~ 500 fs with only ~ 50 mJ energy, but high intensity $\sim 10^{17}$ W/cm². Although a gain of 20 cm⁻¹ was achieved, the maximum gain-length product, GL could not exceed 4. Even after raising the intensity several times (200 mJ, 250 fs), no improvement was seen in the gain-length⁹⁸. Nevertheless, population inversions were obtained between levels 3 and 2, 4 and 2 and even 5 and 2. It was also realized that pumping intensity does not remain uniform along the laser beam propagation and it falls off rapidly after short distance of propagation⁹⁸. It became crucial to find some way to increase the length of gain-medium beyond 2 mm. Some improvements were found in terms of gain-length (GL $\sim 6 - 7$) when a preformed plasma inside a hollow LiF micro-capillary (inner diameter 250 - 300 μ m and length \sim several mm) was used⁹⁹ as a waveguiding for the sub-picosecond (250 fs)

laser pump pulse as well as for the generated soft X-ray laser beam. However, such schemes were limited by the large gain fluctuations from shot-to-shot. The OFI method was also applied for the first time to collisional scheme in a compact system which utilized circularly polarized high intensity laser pulses of ~ 70 mJ in 30 fs at 10 Hz repetition rate¹⁰⁰. Circularly polarized light pulse instead of linearly polarized one was used to provide higher energy to electrons which is crucial for collisional excitation pumping. Here, large gain-length, $GL \sim 12$, was obtained by longitudinal pumping of Pb-like Xe ion at a wavelength of ~ 41.8 nm. A considerable progress was achieved with the introduction of low intensity pre-pulse preceding the main pulse which reduces the steepness of plasma density gradient and allows deeper penetration of pump radiation in plasma¹⁰¹⁻¹⁰³. This pre-pulse technique together with transient collisional excitation scheme of pumping led to development of more efficient soft X-ray lasers.

Another significant modification in the collisional scheme came into picture when grazing incidence pumping (GRIP) was proposed by Shlyaptsev et al¹⁰⁴ in 2003. This was experimentally demonstrated in 2005 for the first time¹⁰⁵. In GRIP, a laser pre-pulse is used to create initial plasma and then, after a specified delay, the main laser pump pulse is allowed to incident on the target in grazing incidence geometry with an optimum angle of incidence chosen such that the refraction effects are minimized on generation of gain-length. Here, the pump beam is redirected along a region of selected high electron density near target where the maximum amplification of soft X-ray laser can take place. In comparison to the earlier transverse pumping, this geometry provides near longitudinal pumping making it more efficient. GRIP enables the generation of large gain-length product in 10-30 nm wavelength region using pump energy of fraction of a joule to few

joules at high repetition rate. The first experimental demonstration of GRIP¹⁰⁵ achieved a large gain-length product $GL \sim 14$ in Ni-like Mo at 18.9 nm with only 150 mJ energy per pulse at repetition rate of 10 Hz in 4 mm long plasma. Strong gain saturations were achieved using ~ 1 J pumping energy per pulse at 5 Hz in several Ni-like ions in 4p – 4d transitions e.g. 16.5 nm in Ru, 14.7 nm in Pb, 13.9 nm in Ag, 13.2 nm in Cd, 11.9 nm in Sn, 11.4 nm in Sb and 10.9 nm in Te^{106,107}. In another major breakthrough experiment, such highly energetic soft X-ray laser plasma amplifier was seeded with high quality coherent beam available from high-harmonic laser sources. As a result, compact soft X-ray picosecond laser (32.8 nm in Ni-like Kr) operating at 10 Hz and exhibiting full saturation, high energy, high coherence and full polarization was achieved¹⁰⁸. Here, the seed beam (25th harmonic of the Ti:Sa laser) was obtained by focusing a 20 mJ, 30 fs infra-red laser beam in gas cell filled with argon. It utilized 1J, 30 fs as the pump pulse for longitudinal pumping of OFI plasma. In another exciting experiment¹⁰⁹, the 32.6 nm Ne-like Ti soft X-ray laser amplifier based on GRIP and operating at 5 Hz, was seeded by 25th harmonic of Ti:Sa femtosecond laser. This system also reached full spatial coherence in saturated amplification with a very high peak spectral brightness estimated to be 2×10^{26} photons / (s mm² mrad² in 0.1% bandwidth). Fully coherent soft X-ray lasing at even much shorter wavelengths, i.e. 18.9 nm in Ni-like Mo and 13.9 nm in Ni-like Ag were obtained in similar experiments¹¹⁰ with high harmonic seeded GRIP soft X-ray amplifier. The dramatic increase in the efficiency of the collisional scheme with such seeded amplifiers has raised greater hope in bringing the lasing wavelength down to water window region (2.3 – 4.4 nm) in future.

1.3.3.4 X-ray lasers based on discharge produced plasma

Fast capillary discharge is one of the most promising techniques for generation of compact table-top X-ray laser systems. The scheme utilizes compact pulse power driver to drive high electric discharge current (few tens of kA) in a short span of time (few tens of nano-seconds) to generate plasma column of suitable medium inside an insulating capillary tube. The high magnetic field generated by such large electric current exerts huge magnetic pressure on the plasma column to compress it radially inward to form what is known as ‘Z-pinch’ which has sufficiently high density and temperature for generation of population inversion in inner shell of highly ionized species. This technique has several advantages over the other techniques for generation of X-ray laser such as high efficiency for creating highly ionized hot and dense plasma column with a large aspect ratio (1000:1) with high uniformity, capability to deliver higher photon flux in the lasing wavelength and relatively compact sizes compared to large facilities like FEL or high power laser driven X-ray laser systems. The capillary discharge technique was utilized for the first time to observe soft X-ray amplification at 18.2 nm in Balmer- α transition of H-like C (C^{5+}) atom based on recombination pumping¹¹¹. Here population inversion builds up for Balmer- α transition by recombining one electron into fully ionized C atom (C^{6+}) to form H-like C atom. However, this was a slow discharge called as ablative discharge where the current interacts with the wall of the evacuated capillary (made of carbon containing material) for sufficient time to create carbon plasma by ablation from the wall. In such ablative discharges, the laser had very small gain-length product due to limitations in terms of poor control over the plasma density as well as non-uniformity of plasma beyond few millimeters.

However, a major breakthrough was achieved in 1994 by Rocca et al⁴⁹ with the first experimental demonstration of soft X-ray lasing at 46.9 nm in Ne-like Ar (Ar⁸⁺) ion based on collisional electron excitation pumping. Here, population inversion is required to build up between 3s and 3p energy level of Ne-like Ar ion by electron collisional excitation of its ground state. Argon gas was filled inside the capillary which was subjected to fast electric discharge to generate and control the required lasing species. The axial uniformity up to a longer plasma length (few tens of centimeters) can be ensured here by creating pre-plasma in the capillary before passing the main discharge current. As a result, it was possible to get a higher gain-length product for this soft X-ray laser. Very soon, this laser was shown to be operated in saturation regime^{112,113}. Further progress was made by the same group in building compact version of this soft X-ray laser system running at few hertz repetitive mode^{114,115}. However, achieving soft X-ray lasing through fast capillary discharge was not an easy task and has several complexities involved therein. This is quite evident from the fact that even after the first successful demonstration of the soft X-ray lasing at 46.9 nm by Rocca et al⁴⁹, no other group around the world could demonstrate the same for next 6-7 years. It was only after so many years that groups from Israel¹¹⁶, Japan¹¹⁷⁻¹¹⁹, Italy¹²⁰⁻¹²³, Malaysia^{124,125}, China¹²⁶⁻¹²⁹ and Prague¹³⁰ were successful in achieving this milestone. Significant contributions have been made by these groups in various aspects of this soft X-ray lasing. Fast capillary discharge scheme has been successfully utilized to demonstrate soft X-ray lasing in some other elements also like Ne-like S at 60.8 nm¹³¹ and Ne-like Cl at 52.9 nm¹³².

Presently, significant efforts are being made worldwide to further reduce the wavelength of X-ray laser generated by fast capillary discharge. Balmer- α transition at

13.4 nm in H-like N is the most promising candidate in this direction which is based on recombination pumping. Here, population inversion builds up for Balmer- α transition by recombination of an electron in the fully ionized N ion (N^{7+}). Fully stripped nitrogen ion is formed by rapid ionization at the pinch formation whereas the recombination takes place when the rapid cooling occurs at the time of pinch expansion. This lasing was first proposed in 2005 by Vrba et al¹³³ through 1-D MHD simulations which predicted a gain of 1.0 cm^{-1} for a discharge current of $\sim 50 \text{ kA}$ with quarter period $\sim 40 \text{ ns}$, capillary diameter of 3 mm and argon gas pressure of 5 mbar. The first experimental effort was made by Kolacek et al¹³⁴ with a discharge current of $\sim 56 \text{ kA}$ having quarter period $\sim 100 \text{ ns}$ exciting nitrogen filled alumina capillary of 3 mm inner diameter. In their study, some line emissions of N^{5+} ion were recorded but the most important emission of He- α was absent. Kampel et al¹³⁵ utilized a more powerful pulse power driver delivering 60 kA current with $\sim 70 \text{ ns}$ quarter period to generate nitrogen Z-pinch in a 9 cm long capillary of inner diameter $\sim 5 \text{ mm}$. With this system, he was able to demonstrate formation of only 10% of N^{7+} ions against the required abundance of $\sim 50\%$. Gissis et al¹³⁶ investigated the X-ray spectra generated from similar current profile and showed the presence of He- α as well as Ly- α emissions from N^{5+} and N^{6+} charge states respectively. Based on these observations, need for further upgradation of the electrical driver was felt in order to achieve higher ionization degree for 13.4 nm X-ray lasing. In another study¹³⁷, triangular pulse shaping was also tried with peak current of $\sim 50 \text{ kA}$ and pulse width $\sim 50 \text{ ns}$ in a nitrogen filled capillary of $\sim 3 \text{ mm}$ diameter and 7.5 cm length. But, plasma density and temperature were found to be insufficient to achieve the X-ray lasing in nitrogen. Although this X-ray lasing has not been achieved as yet using fast capillary discharge

scheme, all these experimental efforts have undoubtedly pointed out and stressed on the need of much higher pulse power driver to pump the plasma. In the experiments done in our laboratory on 46.9 nm X-ray laser, it was found that if faster current is used to drive the plasma, then the requirement of high peak current can be relaxed by substantial amount to achieve similar energy in the laser pulse. In view of these studies, it seems to be of great interest to investigate the nitrogen discharge plasma with a high as well as fast discharge current to explore X-ray lasing at 13.4 nm.

1.4 Scope of the present thesis work

The present thesis work is mainly focused on the experimental studies done in the area of X-ray lasing from plasmas driven by fast capillary discharge method. The main objective here is to achieve X-ray lasing using different gas media which are subjected to large and fast discharge current excitations and study the role of some important experimental parameters on the laser output. Towards this objective, soft X-ray lasing in argon plasma at a wavelength of 46.9 nm has been successfully realized and has been well characterized for its various properties¹³⁸. Such an X-ray lasing achieved through fast capillary discharge technique is dependent on several experimental parameters like gas pressure, pre-pulse conditions, capillary dimensions, discharge current profile etc. Among these, discharge current profile especially its pulse duration is one of the most important parameter affecting the lasing process. However, this happens to be the most difficult parameter to be changed in a capillary discharge setup. This is because of the fact that it has a direct correlation with the geometry of the discharge setup (i.e. size of the capillary discharge X-ray laser) which can not be changed easily due to its quite complex nature and high voltages involved. That is why, there are not enough studies available in

the literature emphasizing the role of current profile on the laser output. This problem has been attempted in the present study where the effect of pulse duration of the discharge current on the gain-coefficient of 46.9 nm soft X-ray laser has been investigated¹³⁹. It was experimentally demonstrated for the first time that the excitation of argon plasma by a faster discharge current significantly increases the gain-coefficient of the soft X-ray laser. Beside it, the study of the effect of current amplitude on the lasing efficiency also led to some important observations¹³⁹. The present research work also establishes well that a discharge current with a higher rate of rise i.e. dI/dt is more favorable rather than mere higher amplitude to deliver higher energy in the X-ray laser pulse¹⁴⁰. This study finds its important implications in ongoing endeavors worldwide of building discharge pumped X-ray lasers at shorter wavelengths, e.g. at 13.4 nm using nitrogen pinch plasma where peak current requirements are very high as predicted by simulations¹³³. This has not been realized till date despite significant interest worldwide in achieving the goal. This has been taken up as another research problem in the present thesis work to explore experimental feasibility for shorter wavelength (below 46 nm) X-ray lasing. Extensive studies were carried out in this direction using the recently upgraded capillary discharge system in our laboratory which is capable to deliver a high discharge current of ~95 kA with ~46 ns quarter period¹⁴¹. These current parameters are quite promising for 13.4 nm X-ray lasing in N₂ which has not been attempted by any other group at such a high and fast discharge current excitations. We have reported the first temporal and spectroscopic study of nitrogen Z-pinch plasma with such a powerful electrical driver. We have also reported the first experimental evidence of the effect of pre-pulse on the spectrum of the highly ionized nitrogen Z-pinch plasma, confirming the very important role of the

pre-pulse in attaining higher charge states of nitrogen. Although, the final goal of X-ray lasing at 13.4 nm is yet to achieve, but some important observations as well as conclusions were drawn which would be quite useful for future work in this direction. Similarly, C₂H₂ and Kr plasma were also explored for possible X-ray lasing at 18.2 nm in H-like C ion and 32.8 nm in Ni-like Kr ion respectively. These studies also provide important inputs for extending the fast capillary discharge scheme for X-ray lasing towards shorter wavelength.

CHAPTER 2: CAPILLARY DISCHARGE BASED X-RAY LASER

2.1 Fast capillary discharge for X-ray laser

Fast capillary discharge is an efficient method for creating highly ionized, hot and dense plasma column with conditions suitable for generation of soft X-ray laser. The technique is capable of generating a long plasma column and to deliver higher photon flux in the lasing wavelength due to efficient coupling of electrical energy into plasma. In this technique, a high and fast rising electric current (I), having ~ few tens of kiloampere (kA) amplitude in few tens of nanosecond (ns) duration with dI/dt exceeding 10^{11} A/s, is allowed to pass through a pre-ionized cold plasma inside an insulating (ceramic) capillary. A schematic diagram of the principle is shown in Fig. 2.10. Since, the presence of pre-plasma minimizes the development of plasma instabilities, a pre-ionized cold plasma (of temperature 1-2 eV) of suitable gas is formed inside the capillary by applying a small pre-discharge current of few ampere (A) and duration of few tens of microseconds (μ s). This pre-discharge current is applied few μ s before the main discharge current. As the

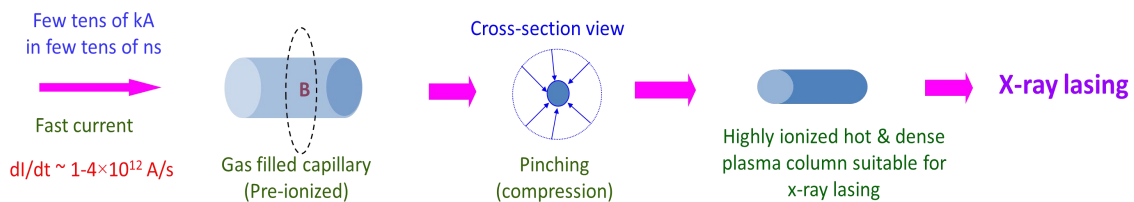


Fig.2.10: Principle of fast capillary discharge technique for generation of X-ray laser

pre-formed plasma acts like a conductor, the main discharge current starts flowing through the outer surface of this plasma and not through its bulk volume. During its flow, the main discharge current creates strong magnetic field in the azimuthal direction on the

outer cylindrical surface which interacts with the current itself. This magnetic field generates a strong Lorentz force acting radially inwards on the outer sheath of the plasma. As a result, the plasma column gets detached from the wall of the capillary and a fast compression of the entire length of plasma column takes place. This leads to formation of a hot and dense plasma column axially with diameter almost 10 times smaller than the capillary inner diameter. Such a compressed plasma column is also termed as Z-pinch. In a Z-pinch plasma, highly ionized species are formed as a result of strong shock implosion towards the axis. The pinch plasma takes up a finite diameter under the Bennet's equilibrium¹⁴²⁻¹⁴⁴ between the kinetic pressure of the plasma acting radially outward and the magnetic pressure acting radially inward. The pinch plasma lasts for a short duration and soon it expands outwards when the kinetic pressure overcomes the magnetic pressure during the falling phase of the current pulse. If the electrical driver is strong enough, it can lead to formation of closed shell ions e.g. Ne-like or Ni-like ions which are quite suitable for generation of X-ray laser through electron collisional pumping scheme. If the capillary is filled with argon gas, this process can create Ne-like Ar ion i.e. Ar⁸⁺ in abundance at the pinch formation. Under suitable conditions of density and temperature, the bound electrons in the ground state (2p⁶) of Ar⁸⁺ can be further excited by electron collisional excitations to the two upper energy levels 2p⁵3s and 2p⁵3p [see Fig. 1.6]. This can lead to formation of population inversion between 3p and 3s energy levels as discussed in section 1.3.3.2A in chapter 1 and can generate soft X-ray laser at 46.9 nm. Single pass amplification at this Soft X-ray lasing wavelength takes place along the capillary axis if uniform conditions are maintained along the length of the plasma column at the time of pinch formation. This is essential for achieving sufficient intensity in the

laser pulse and can be achieved by uniform compression along the plasma length. The pre-pulse used for creating pre-plasma before the main discharge play a very important role in this direction. It not only avoids the growth of instabilities in the plasma at the very early stage of compression but also ensures that main discharge current begins to flow from the outer surface uniformly and not in random filamentary paths through the bulk. The uniform initiation of compression finally leads to a pinch plasma formation which has uniform plasma condition along its length and helps to achieve higher gain-length in soft X-ray amplification. Wall ablation of capillary at the initial phase of compression should be minimized in order to restrict the wall impurities from going into plasma. A discharge current with higher dI/dt can do this to a greater extent. Also, efficient pinching of plasma column is required to get higher amplification. The efficient pinch formation is highly dependent on pre-plasma conditions, discharge current, gas pressures in the capillary etc. It is seen that optimum conditions of electron density $\sim 10^{18-19} \text{ cm}^{-3}$ and plasma temperatures in the range 60 - 80 eV are needed along with small transverse dimension of plasma column for higher abundance of Ar^{8+} ion and strong amplification at 46.9 nm lasing wavelength^{145,146}.

2.2 Capillary discharge X-ray Laser system

Capillary discharge system developed at RRCAT is shown in Fig. 2.11. The system was developed with an aim to explore X-ray lasing in Ar gas filled capillary by using fast discharge scheme. Later on, compact versions of this system were developed in due course to obtain faster and higher capillary currents to explore the lasing at shorter

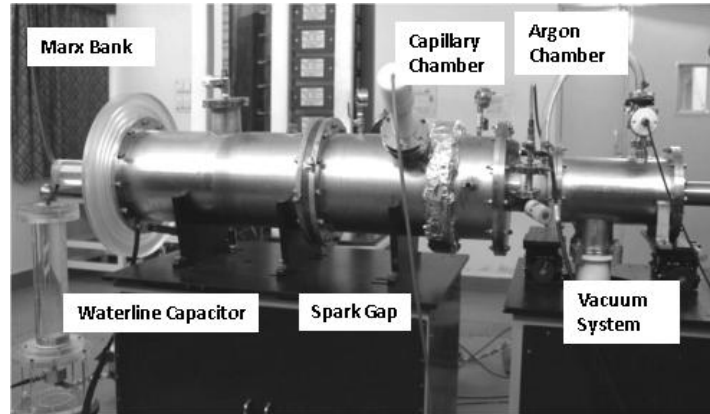


Fig.2.11: Photograph of the Capillary discharge system for X-ray laser

wavelengths in other gas media. Fig. 2.12 shows a schematic diagram of the system. The system uses a 450-kV, 10-stage Marx Bank to charge a pulse forming line (PFL). The PFL is based on a co-axial waterline capacitor ($C = 6 \text{ nF}$, $L = 70 \text{ nH}$ and $Z = 3.3 \Omega$) charged up to a voltage of $\sim 400 \text{ kV}$. The waterline capacitor consists of two co-axial 60 cm long cylinders. The inner radius of the outer cylinder was 26.6 cm and the outer radius of the inner cylinder was 16.8 cm. The gap between the two cylinders is filled with de-ionized water (with conductivity $< 2 \mu\text{S}$) acting as a dielectric medium which can sustain pulsed voltages up to few hundreds of kilo-volts due to its high dielectric constant (~ 80). This capacitor is connected axially to the gas-filled capillary through a self-triggered spark-gap switch which was pressurized with SF_6 gas. This switch is closed rapidly as soon as the capacitor is charged beyond a pre-set voltage depending upon the gap-separation and gas pressure in the spark-gap switch. This provides the required fast discharge current through the gas-field capillary. If this main discharge current is allowed to pass directly through the gas-filled capillary, it is seen experimentally that instabilities develop along the plasma length during z-pinch compression leading to improper

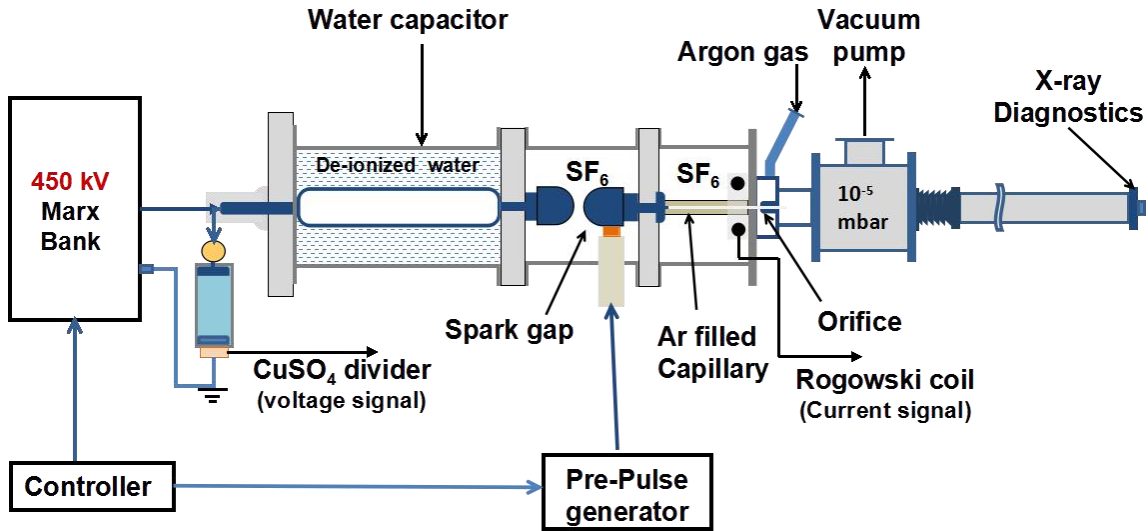


Fig.2.12: Schematic layout of the Capillary discharge system for X-ray laser

compression along the capillary length and not creating the required lasing condition. Therefore, it was essential to pre-ionize the gas by low current pulses before the main discharge current passes through it. The pre-ionization is achieved few microseconds ($5-10 \mu\text{s}$) before the main current pulse by passing a long duration (tens of μs) small pre-pulse current ($15 - 40 \text{ A}$) from a pre-pulse generator through a CuSO_4 solution based resistor. The pre-pulse current can be altered by varying the concentration of the CuSO_4 solution. The amplitude of the main discharge current can be controlled by the erected voltage on the PFL and the pressure of the SF_6 gas in the spark gap. An alumina capillary of 2.8 mm inner diameter and 15 cm length filled with Ar gas at different pressures was used in the present setup. The one end of the capillary has high voltage electrode from PFL side whereas the other end has an orifice (dia. - 1 mm) made of tungsten at a distance of $2-3 \text{ mm}$. This orifice acts as ground electrode as well as plays important role in maintaining the required differential vacuum between the capillary and the diagnostic side. The argon gas is fed inside the capillary through a small ($\sim 40 \text{ cm}^3$) 'argon chamber'

placed between the capillary and the orifice as shown in Fig. 2.12. The argon chamber is designed so as to keep the separation of capillary and the orifice not more than 2-3 mm. This reduces the cold argon region between the capillary and the orifice which can otherwise strongly attenuate the soft X-ray laser coming out of the capillary. A fine gas dosing and regulating valve (Pfeiffer EVN-116) is used to control the gas flow into the argon chamber. Appropriate measures are taken in order to minimize pressure gradients inside the long capillary. For example, after firing of each shot, the argon chamber and the capillary are evacuated up to 10^{-3} mbar pressure by closing the dosing valve in the gas input path. Argon gas is then allowed to fill to the required pressure in 1-2 minutes giving enough time to stabilize the distribution of the gas along the length of the capillary. A turbo-molecular pump (TMP) backed by a rotary pump is used to achieve the required vacuum ($< 10^{-4}$ mbar) on the other side of the orifice (diagnostic side). The argon gas pressure in the capillary is controlled precisely by the gas-dosing valve in the range of 0.1 to 0.7 mbar depending on the requirement. On the measurement side, a calibrated Rogowski coil is used to monitor the discharge current flowing through the gas filled capillary. The high voltage generated at the output of Marx bank is measured using a CuSO_4 voltage divider. The temporal profile of the emissions from the plasma is recorded using an in-house developed vacuum photodiode and quadrant vacuum photodiode. These signals are monitored on a digital oscilloscope (Lecroy: WR104MXi, 1 GHz, 10 GS/s). For spectral study, a transmission grating spectrograph is used which consists of a transmission grating (700 lines per mm) followed by micro-channel plate (MCP) and phosphor screen. The phosphor screen is imaged on to a CCD camera. Since the MCP requires a good vacuum better than 10^{-5} mbar, another TMP based vacuum system is used

close to MCP. It was found during the experiments that significant Electro-magnetic Interference (EMI) is generated during laser firing in every shot. The EMI strongly affects the operation of discharge control system, various diagnostics and measuring equipments and found to be responsible for their malfunctioning. Hence, all the measuring equipments and control systems are placed inside a Faraday cage to shield EMI. Signals from the detector placed on the system are carried out in special doubly shielded cables up to the Faraday cage in order to reduce the EMI coupling. Pulse power systems and control systems are grounded separately in order to avoid any electrical pick up through ground line. Wherever it is required to isolate the instruments from electrical noise through line, isolation transformers are used. Also, the control signals are carried out through optical fibers wherever possible in order to reduce the EMI coupling.

This system was upgraded in due course of time into different versions to obtain faster and higher capillary currents as per the requirements. The description given above is mostly for the first version of the system, termed as version 1, which was used in the initial experiments for demonstration of soft X-ray lasing at 46.9 nm in argon described in chapter 3. Later on, the system was improved to version 2 to deliver faster discharge current by significantly reduce the inductance of the discharge circuit. Here, the main spark-gap chamber and argon chamber were modified to very compact geometry to improve the inductance. The waterline capacitor was also modified in terms of its capacitance. As a result, the size of the system also reduced making it compact. This system was used in experiments which have been described in chapter 4. The quantitative changes in the system parameters are also discussed there. In order to investigate shorter wavelength X-ray lasing, system was subjected to further modifications where

Marx-bank was replaced by indigenously developed tesla-transformer based high voltage generator. The capillary chamber was reduced to accommodate smaller length capillary in order to further reduce the inductance of the discharge circuit. These changes led to shaping of a very powerful capillary discharge system, termed as ‘version 3’, which was capable to deliver ~ 100 kA current with ~ 46 ns quarter period. Experiments were performed on this system to explore shorter wavelength X-ray lasing which have been discussed in detail in chapter 5. In due course of time, the capillary discharge X-ray laser system in our laboratory evolved into more powerful versions capable to deliver much higher and faster discharge current in single shot mode. At the same time, another interesting evolution took place towards developing very compact table-top X-ray laser system operating at smaller voltages and smaller currents and yet capable to deliver soft X-ray lasing pulses at repetitive mode. This system, termed as ‘version 4’ is discussed briefly in the last section of chapter 3.

2.3 Various sub-systems and measurement devices

2.3.1 Marx-bank

It is a high-voltage impulse generator capable to generate voltages of few hundreds of kV to even MV and is a good solution to the limitations of a single capacitor which can not be used for voltages beyond 100 – 200 kV. Marx-bank uses a bank of capacitors which are charged in parallel and discharged in series for generating very high voltages¹⁴⁷,¹⁴⁸. It is extensively used to simulate the effects due to lightening on the aviation equipment. In addition to this, it is used in numerous other applications where high voltages of the order of few hundreds of kV or MV are required¹⁴⁸. For example, Sandia

National Laboratory uses a bank of 36 Marx generators to generate X-rays in their Z-Machine. Ignition switch for thermonuclear devices is another potential area where such systems can be used effectively. Fig. 2.13 shows a typical circuit diagram of Marx-bank generator to explain its working. In the diagram, C is the capacitance of each capacitor, R_s is the resistance of each charging resistors, G represent the spark-gap switches, R_1 and R_2 are the two wave-shaping resistors and T is the test load across which high voltage is required to be applied. At first, all the energy storage capacitors are charged in parallel to a voltage, say V , by a DC source. Then, a high voltage trigger pulse of short duration is applied to break down the first spark gap.

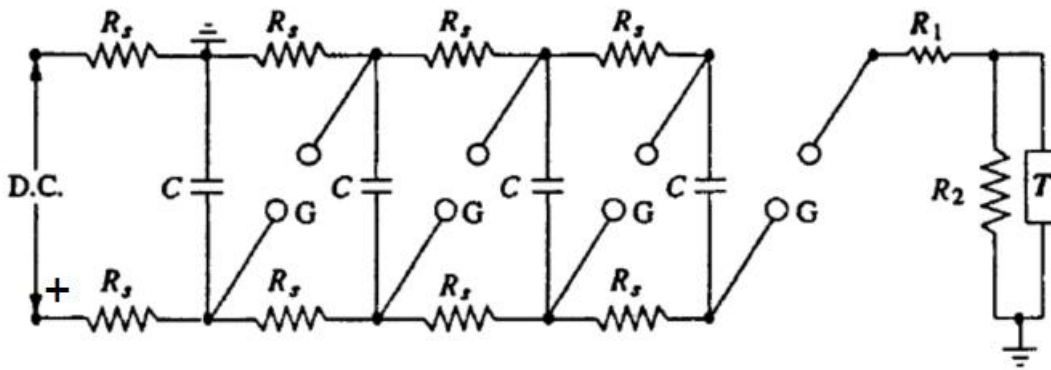


Fig.2.13: Typical circuit diagram of Marx-bank for generation of high voltage

This connects the lower end of first capacitor to the upper end of second capacitor (see Fig. 2.13). The voltage at the other end of the second capacitor gets doubled in order to maintain the same potential drop across itself. This voltage is becomes much higher compared to the breakdown voltage set for the second spark gap and therefore the second spark gap also breaks down. This time, the lower end of the second capacitor is connected in a similar fashion to the upper end of the capacitor of next stage as was done in the previous stage. The chain continues and the voltage keeps on adding in higher stages. If

there exists N stages of capacitor, the last capacitor is charged to a voltage of “NV” which appears across the external load. The gap spacing in the spark gaps are crucial and adjusted to initiate simultaneous breakdowns in higher stages. Otherwise, mismatch in simultaneous firing of spark gaps will cause appearance of multiple steps in the output waveform. The last spark gap is introduced in order to avoid any leakage of the charging current through the external load and to sharpen the rise time of the output waveform if the load is resistive. The performance of Marx generator is largely affected by the series inductance which introduces undesired oscillations and increases the rise-time of the output waveform if the load is resistive. The surge current capability of the Marx-bank is also reduced by the higher series inductance. Charging resistances R_s 's are non-inductive high value resistors of about 10 – 100 k Ω with high value rating between 50 to 100 kV which are used to limit the charging current. The discharge time constant CR_1/N (for N stage) remains very small typically in μ s compared to the charging time constant CR_s which is of few seconds. The capacitors used in Marx bank are generally meant for fast discharge energy storage. Hence, they have lower inductance and higher current rating. Marx generators are normally rated by the total voltage (nominal), the number of stages used and the gross energy stored. The nominal output voltage is given by NV and the nominal energy stored is given by $\frac{1}{2} C_{eq} V_T^2$; where $C_{eq} = C/N$ is the equivalent discharge capacitance.

2.3.2 Tesla-transformer

Tesla transformer is an air-core pulse transformer which is normally used for MV pulse generation with higher rep rate. There exists significant difference between a Tesla-coil transformer and the conventional transformer. Winding in a conventional

transformer are tightly coupled and its voltage gain depends largely on the ratio of the number of turns in the winding. Whereas in Tesla transformer, energy is transferred from one oscillating resonant circuit (the primary) to the other (the secondary) through coupled coils over a number of RF cycles¹⁴⁹. During this energy transfer, the secondary output voltage keeps on increasing until all of the available primary energy is transferred to the secondary. A well-designed Tesla-coil is able to transfer over 85% of energy stored initially in the primary capacitor to the secondary even if there are significant losses through spark gap. Such a doubly tuned resonant circuit is shown in Fig. 2.14. The voltage rating for the secondary can be as high as 2 order higher than the primary circuit. The primary coil is driven by AC or DC voltage source through a capacitor C_1 . A spark gap G connected across the primary can be triggered at the desired voltage V_1 across C_1 which induces a large self-excitation in the secondary. The spark gap remains open during the charging of C_1 and is short-circuited when C_1 discharges through L_1 in an oscillatory

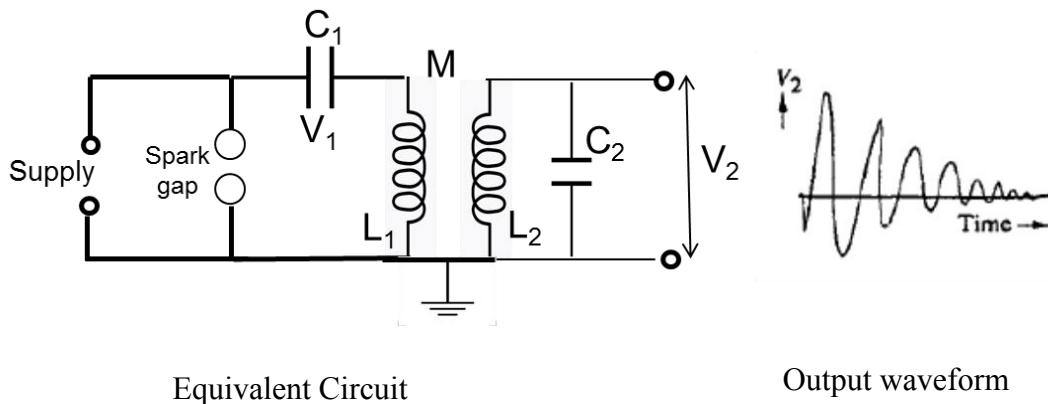


Fig.2.14: Typical circuit diagram of Tesla transformer for generation of high voltage

fashion. In this way, the primary capacitor transfers its electrical energy to the primary

inductor L_1 mostly having single turn. The secondary circuit consists of a large air-core multi-turn helical or spiral inductor (L_2) and a terminal which acts like a virtual capacitor. This arrangement together behaves as a resonant circuit which needs to be oscillating at frequency same to the primary circuit. In this way, RF electrical energy is inductively coupled from primary to secondary circuit and oscillates which results into development of extremely high RF voltages across the terminals. However, In pulsed applications, HVDC charged capacitor is used as a primary driver which gets discharged into the primary coil of the Tesla transformer through a spark gap switch kept in series with the coil. The output of the secondary coil is then delivered to another capacitor of pulse forming line (PFL) before load.

2.3.3 High voltage spark gaps

Spark gaps are fast switches which are used extensively for switching of high voltages. A spark gap consists of two electrodes separated by a dielectric medium which can be a pressurized inert gas. For a fixed gap, if the voltage across the two electrodes is increased gradually, the spark gap suddenly breaks down above a certain threshold voltage which means that the dielectric medium suddenly changes from non-conducting to conducting state. When this happens, it is like closing a fast switch to transfer the energy from input source to the load. This action of the spark gap is depicted in Fig. 2.15a and 2.15b.

There exists two broad categories of spark gaps:

- A) Self-triggered spark gap: Such a spark gap breaks down on its own without the help of any external agent when the applied voltage across it reaches the breakdown limit of the spark-gap¹⁴⁸.

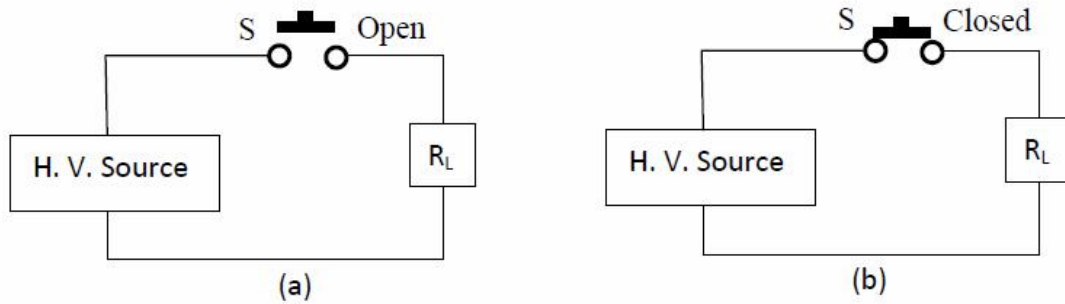


Fig.2.15: High voltage switching action of spark gap

B) Triggered spark gap: This type of spark gap is forced to breakdown much below its self-breakdown limit by an external agency which can be either an electron beam, a laser beam or by just increasing the electric field on some portion of the gap¹⁴⁸. Triggered spark gap have various advantages over the self-triggered spark gap which are operability over a wide range of voltage, short delay time leading to superior switching characteristics, short formative time, small jitter and increased reliability. A triggered spark gap is often characterized by its various parameters which are breakdown voltage, switching range, shot life, switching time lag, rise time, and jitter.

2.3.4 Pulsed high voltage measurements

Voltages in pulse power systems typically vary from kV to few MV which are needed to be measured in μs , ns and sub-ns time scale. Such pulsed high voltages are normally measured using spark gaps or voltage dividers.

A) Spark gaps

Spark gap measurement is the simplest method of measuring peak voltage to an approximate value. It is not an accurate method. It works on the working principle of

spark gap which says that if the voltage across the spark gap becomes equal to or larger than the breakdown voltage, the gap breaks down which can be perceived through optical emissions. In order to measure the high voltage, a sphere gap is formed by two adjacent metal sphere (polished) of equal sizes separated by a finite distance. For precise measurement of the peak voltage, highly polished surface of the spheres are preferred and the diameter of the sphere is needed to be much larger than the gap separation. Such sphere gaps can be irradiated by strong UV or ionizing radiation for transient measurements. In order to estimate the approximate value of peak voltage, it uses the fact that a spark over voltage of ~ 30 kV (peak) with a gap of 1cm in air at 20°C at atmospheric pressure occurs for a sphere gap or any uniform field gap.

B. Voltage dividers

Voltage dividers are used to scale down the high voltages, normally exceeding few hundreds of kV, to manageable level of few volts so that it can be safely recorded using conventional recording techniques. While dealing with pulsed voltages, it must have high bandwidth also. Voltage dividers can be categorized into three types viz. resistive, capacitive or combination of both.

Resistive dividers : Resistive dividers consists of two parts, one of high resistance R_1 and the other of low resistance R_2 as shown in Fig. 2.16.

In general, any resistance normally has series inductance (L_s) and parallel shunting capacitance (C_g) with respect to ground which is typically 10 - 20 pF. Thus, the performance of a voltage divider will not be affected till a desired frequency (ω),

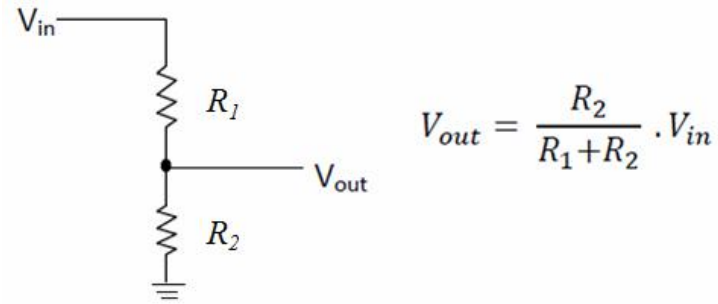


Fig.2.16: Resistive voltage divider

$$\text{if } R_1 \ll \frac{1}{\omega C_{g1}}; \quad R_1 \gg \omega L_{s1}$$

$$\text{and, } R_2 \ll \frac{1}{\omega C_{g2}}; \quad R_2 \gg \omega L_{s2}$$

In order to have fast rise times of ns order, R_1 has to be restricted to few $k\Omega$ in order to satisfy the condition of its shunting capacitance. However, the condition of inductance in R_1 is easily satisfied. At the same time, value of R_2 can not be higher than few tens of Ω . Hence, it is seen that condition of shunting capacitance for R_2 is easily met. But, the condition on its series inductance limits the inductance value to few nano-henry (nH). In addition, the higher resistance R_1 must have high wattage and higher voltage rating. Although, ceramic resistances can be used but electrolytic resistors are most popularly used such as copper sulphate solution with copper electrodes. Since R_2 should have low inductance, normally several low inductance resistors are joined in parallel and enclosed in a metal cylinder to achieve this. With proper designing, It is possible to make voltage dividers with rise time of few hundred ps.

Capacitive dividers : An equivalent circuit of a capacitive voltage divider is shown in Fig. 2.17. This can be used in high frequency applications. Such capacitive dividers are prone

to pickups and parasitic oscillation. Their performance can be improved if they are made as integral part of the pulse power system.

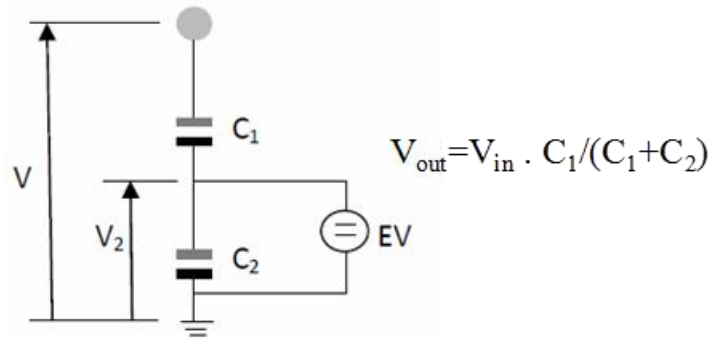


Fig.2.17: Capacitive voltage divider

Mixed (R-C) voltage dividers : Mixed voltage dividers make use of both resistances and capacitors in series or parallel. They offer high input impedance as compared to resistive dividers. In one such configuration, capacitor is connected in parallel with each resistor. Another improved version is to make an R-C series elements connection. Here, the high frequency component of the signal is handled by the capacitors while relatively smaller frequency component is handled by the resistors.

2.3.5 Pulsed high current measurements

Pulse power systems involve discharge current magnitude ranging from kA to MA. Such high currents are required to be measured precisely in different time scale as per requirements e.g. in μs , ns and sub-ns time scale. Techniques which are frequently used for such measurements are described below:

A) Current Viewing Resistor (CVR)

It is the simplest method for measuring high pulsed current in which a low ohmic pure resistive shunt is introduced in the path of the current. The current passing through the resistor develops a voltage which is measured to estimate the value of the current. The resistance of CVR is very small in the range from $10 \mu\Omega$ to few $m\Omega$ and voltage drop of few volts is generated across the resistor. The dimension (area) of the resistor is usually large in order to get small value of resistance. However, such large dimension causes stray inductance and capacitance to become dominant in fast pulse measurements. Hence, these shunt resistances require special geometry to suppress stray effects. Also, it requires to break the circuit to apply CVR in a pulse power system which is generally not advisable and sometimes not even possible. Due to these reasons, CVR are not preferred current probes.

B) Rogowski coil

Rogowski coil is basically a current probe which acts like an efficient transformer. It has an air-cored toroidal multi-turn coil which acts like the secondary of the transformer¹⁵⁰. This coil is placed around the current carrying conductor which acts as primary. A photograph of the coil is shown in Fig. 2.18. If 'M' is the mutual inductance between the primary and the secondary and $I(t)$ is the current to be measured and flowing through the conductor, then the voltage signal induced in the coil will be given as

$$V(t) = M \frac{dI(t)}{dt}$$

The induced voltage can be written as, $V(t) = \frac{AN\mu_0}{l} \frac{dI(t)}{dt}$; where $A = \pi a^2$ is the area

of each turn of the coil, N is the number of turns and $l = 2\pi R$ is the perimeter of the toroid, R and a are the major and minor radius of the toroid. Here, turns are assumed to be evenly spaced and their radius is assumed to be small relative to the radius of the

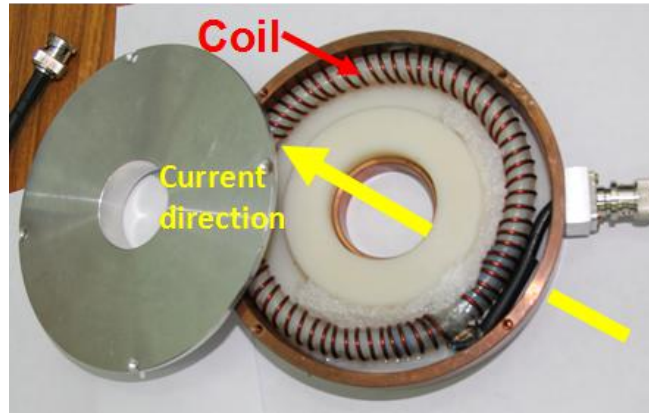


Fig.2.18: A photograph of the Rogowski coil

toroid (coil). Generally, the number of turns N is kept large to get higher induced signal. The formula shows that the output voltage is proportional to dI/dt . Hence, it requires an integrating circuit to get the output which is proportional to the current. Since, it uses air core, there is no saturation effects like in ferrite cores and the probe is suitable to measure higher currents.

C) Current transformer (CT)

Current transformer (CT) is a current step down probe which consists of a multi-turn coil with magnetized core placed around the current which is to be measured as shown in Fig. 2.19. The current to be measured acts like a single turn primary circuit while the CT multi-turn coil acts like secondary. When the secondary is connected to a low resistance load, the secondary current is given by the general formula of a transformer action, i.e.

$$\frac{\text{Secondary current}}{\text{Primary current}} = \frac{\text{Turns in Primary(one)}}{\text{Turns in Secondary}}$$

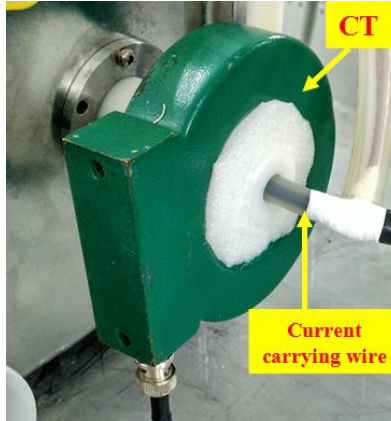


Fig.2.19: Current transformer coil

The cores of these CT's are of ferrite which enables the high frequency (bandwidth) operations. The disadvantage is that their use is restricted to limited regime of current-duration product.

CHAPTER 3: DEMONSTRATION OF DISCHARGE DRIVEN SOFT X-RAY LASING AT 46.9 NANOMETER AND ITS CHARACTERIZATION

The research in the area of X-ray laser driven by fast capillary discharge scheme received a big boost in 1994 when the soft X-ray lasing was observed for the first time at 46.9 nm in $3s^1P_1 - 3p^1S_0$ transition of Ne-like Ar (Ar^{8+}) ion by Rocca *et al*⁴⁹. Very soon, this laser was also operated in the saturation regime¹¹². The population inversion in this soft X-ray lasing is achieved via electron collisional excitation of Ne-like Ar ion produced by fast electric discharge inside a gas-filled capillary tube. Such an X-ray lasing through fast capillary discharge is a difficult task due to involvement of various complexities in the generation scheme as well as in the geometry of the pulse power systems and various sub-systems. This is reflected from the fact that no other group worldwide could achieve this soft X-ray lasing even six to seven years after its first demonstration. It was only after Ben-kish *et al*¹¹⁶ from Israel established the important role of pre-pulse in the lasing, few groups worldwide from Japan, Italy, Malaysia, China and Czech Republic were able to achieve this milestone under different experimental configurations¹¹⁷⁻¹³⁰. The activity on capillary discharge X-ray laser was also initiated¹⁵¹ a few years ago in our laboratory at Raja Ramanna Centre for Advanced Technology (RRCAT), Indore, India with an aim to build an X-ray laser for the first time in the country. After facing initial difficulties, the X-ray laser in Ne-like Ar (Ar^{8+}) was achieved and later it was also made operational even in saturated regime. Extensive studies were carried out to confirm the lasing action by measuring the temporal, spatial and spectral properties of the emission from the discharge plasma as well as the spatial coherence of

the laser. The details of these studies have been discussed in the following sections of this chapter. The chapter discusses the experimental setup for different measurements and optimization of the various experimental conditions leading to observation of lasing. In the spectral measurements, intense lasing line of 46.9 nm has been observed using a transmission grating spectrograph (TGS). Various higher diffraction orders as high as 10th order of the lasing line has been observed which is not reported in the literature so far. Normally, such higher diffraction orders are difficult to be detected due to small energy coupled into them. However, recording up to 10th diffraction order indicates that the intensity of the laser is sufficiently high. Further, these high orders also confirms on the spectral purity and monochromaticity of the X-ray laser.

3.1 Experimental details

Experiments described in this chapter were conducted on the first version of the system which has been described in detail in section 2.2. A photograph of the actual system and its schematic diagram are shown in Fig. 2.11 and Fig. 2.12 respectively. A detailed description of the system is already given in section 2.2 of chapter 2. A calibrated Rogowski coil was used to measure the discharge current flowing through the gas filled capillary. The high voltage generated at the output of Marx bank was measured using CuSO₄ voltage divider. In-house developed vacuum diode and quadrant vacuum diode were used to measure the temporal profile of the emissions from the plasma. These signals were monitored on a digital oscilloscope (Lecroy: WR104MXi, 1 GHz, 10 GS/s). The spectral study was carried out using a transmission grating spectrograph which consists of a transmission grating (700 lines per mm) followed by micro-channel plate (MCP) and phosphor screen. The phosphor screen was imaged on to a CCD camera.

3.2 Results and discussion

Soft X-ray lasing through fast capillary discharge method has dependence on several experimental parameters e.g. discharge current amplitude, its quarter period ($T_{1/4}$), pre-pulse amplitude, delay between the pre-pulse and the main pulse, argon gas pressure in capillary etc. The temperature, density and dimensions of the pinched plasma column is decided by these parameters which finally leads to the soft X-ray lasing. At first, a small pre-pulse current was applied in the range 10 - 25 A and 5-10 μ s before the main current pulse to pre-ionize the argon gas filled into the capillary in sub-mbar pressure range (0.1 - 0.7 mbar). The pre-ionized argon gas was then subjected to a discharge current of \sim 26 kA with quarter period \sim 75 ns. The initial argon gas pressure in the capillary was changed from 0.1 - 1.0 mbar to explore the lasing conditions. Typical profiles of the erected voltage at the output of Marx bank and current flowing through the argon plasma can be seen in Fig. 3.20. The profile shows that the voltage falls sharply as

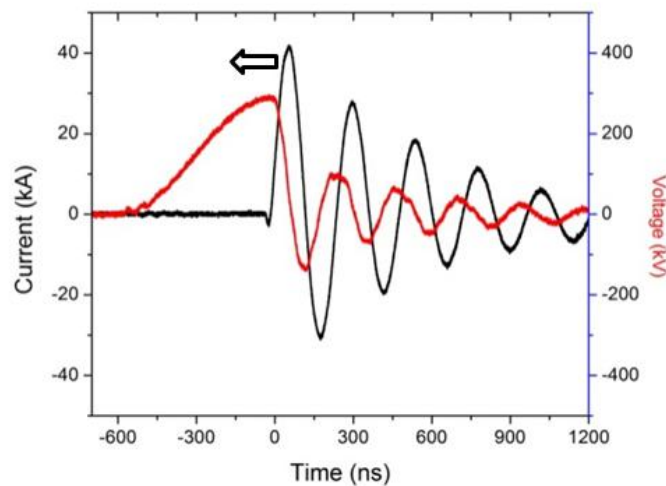


Fig.3.20: Typical voltage and current signal from capillary discharge system

the main spark-gap breaks down and soon after, the discharge current begins to rise rapidly. As the discharge is under-damped, both the voltage and the current waveforms

have under-damped oscillations. It is worth mentioning here that it is only the first quarter period of the current profile that matters for the lasing phenomena in the argon discharge plasma. Initially, these voltage and current profiles were found to be quite noisy due to EMI coupling to the signals. Later on, these signals were improved significantly as shown in Fig. 3.20 by the use of doubly shielded cables carrying them from the system up to the oscilloscope placed inside the Faraday cage.

3.2.1 Temporal study of capillary discharge emission

An indigenously developed vacuum photodiode having large sensor area (diameter \sim 30 mm) was used to study the temporal profile of the emission from capillary discharge plasma. This is a bi-planar diode with two electrodes, the cathode made of copper disc and anode made of stainless steel mesh placed at a separation of 1 mm from cathode. The incoming radiation enters the diode through the mesh and impinges on the cathode generating photo-electrons. A negative voltage of 0.7 kV is applied to the cathode and the mesh (anode) along with the body of the diode is grounded. Hence, the photo-electrons generated from the cathode are collected by the anode mesh leading to a current signal which is carried out through doubly shielded cable up to a fast oscilloscope for measurement. Figure 4a shows a typical signal recorded with vacuum diode placed at a distance of \sim 83 cm from the source after optimizing the experimental parameters like gas pressure and pre-pulse conditions. The temporal profile of the emission from plasma during the first half cycle of the current shows the existence of two distinct types of X-ray emissions. One is a relatively long duration radiation pulse (FWHM \sim 50 ns) which starts \sim 10 ns after the initiation of the discharge current and reaches its peak value at 80 - 90 ns after the initiation. This broad pulse is a result of Bremsstrahlung emission from the hot

plasma column and is highly diverging in nature. Therefore, this pulse dies out rapidly as the distance of the diode increases from the source. There exists a short duration X-ray pulse superimposed over the aforesaid broad pulse and appears before the current reaches its peak value. This pulse corresponds to the emission from the plasma when the pinch is formed and therefore it lasts for a very short duration i.e. for few ns. Interestingly, it was noticed that the slope of the rising edge of this short duration pulse is quite sensitive to the argon gas pressure in the capillary. When the argon gas pressure was optimized in fine steps, a very steep rise of the slope was observed as shown in Fig. 3.21a. The rise-time (10% to 90% of the amplitude) of this fast signal was measured to be ~ 1.2 ns. When the diode was placed closer to the source, the falling edge of this fast signal was not visible clearly due to the long lasting bremsstrahlung radiation from plasma. Hence, the vacuum diode was taken far away from the source. Figure 3.21b shows a typical signal recorded at a distance of ~ 1.7 m from the source. It was seen that the long duration pulse due to Bremsstrahlung radiation from plasma is selectively reduced in comparison to the fast rise signal when the vacuum photodiode detector is moved away from the source. This confirms that the fast signal has good directionality over the other plasma emissions. Please note that the amplitude of fast rising signal increases as one moves away from the source. This is due to the space-charge effect of the diode. Another interesting feature of this fast pulse was that it appears only in the presence of the pre-pulse. In the experiments done later, it was shown that this pulse indeed corresponds to the soft X-ray lasing in argon plasma. Efforts were made to increase the amplitude of this fast pulse. For this, the discharge current was increased in stages and at each stage, the experimental parameters like gas pressures and pre-pulse conditions were optimized. It was found that the signal is

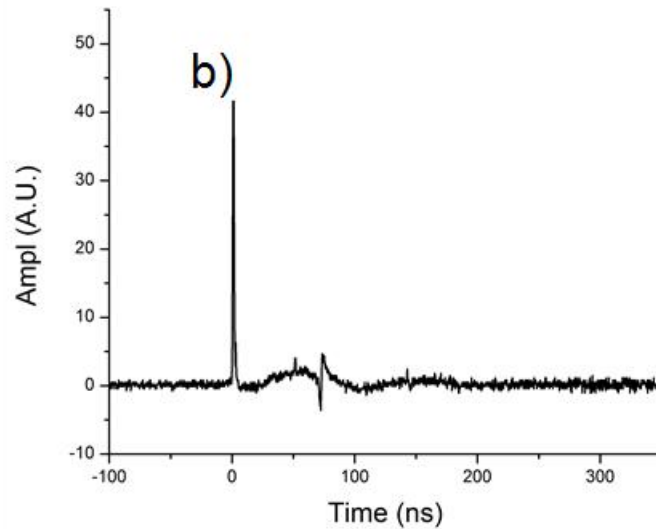
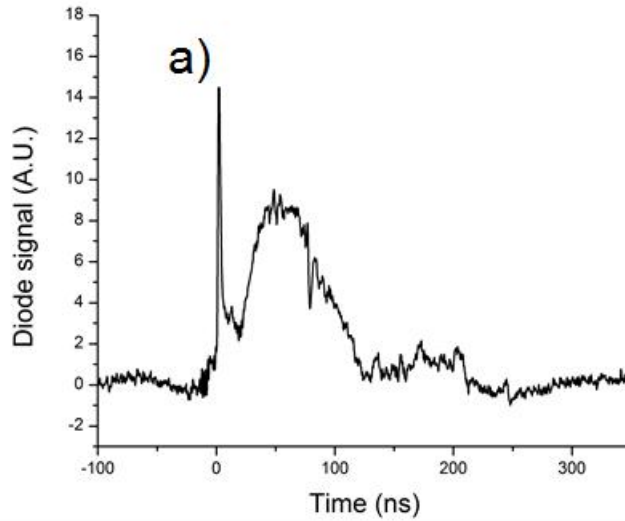


Fig.3.21: Vacuum diode signals a) showing the two types of X-ray emissions at a distance of 83 cm from the source, and b) same signal at a larger distance (1.7m) , showing the dominance of the lasing signal

enhanced significantly compared to the background plasma emissions at discharge current of 40 kA with rise time of 50 - 60 ns, Ar gas pressure of 0.35 mbar, pre-pulse current of ~ 20 A applying ~ 5 μ s before the main pulse. Also, it was important to keep the distance of vacuum diode away from the source (at ~ 1.7 m) for recording emission in

the fast pulse.

3.2.2 Study of the divergence

In order to confirm the lasing action, it was necessary to study the divergence of the radiation emitted from the argon pinch plasma. For this, the spatial profile of the beam was recorded at a large distance of ~ 1.7 m from source using micro-channel plate detector followed by phosphor screen. The latter was then imaged on to a CCD camera. The recorded profile shown in Fig. 3.22a clearly indicates the existence of an intense low divergence beam filling an area of few millimeters superimposed over the highly divergent plasma emission which fills the entire MCP screen. The size of the beam was used to estimate the divergence which turned out to be < 3.5 mrad. This low divergence beam disappears in the absence of pre-pulse and only the bremsstrahlung (incoherent) emission is seen on the MCP as shown in Fig. 3.22b. This trend clearly correlates the low divergence beam with the fast signal pulse recorded by the vacuum diode. The observed small bright spots on the MCP edge in the Fig. 3.22a and 3.22b are nothing but the artifacts occurring due to unwanted discharge on the MCP edge during the shot.

3.2.3 Spectral measurement of capillary discharge emission

The spectral study was also carried out to determine the lasing wavelength emitted from the argon pinch plasma under aforesaid optimized conditions. This was done by setting a transmission grating spectrograph in the path of the emitted radiation. The spectrograph uses a free-standing transmission grating having groove density 700 lines/mm (lpm) to disperse the incoming light. The spectrum was recorded on the

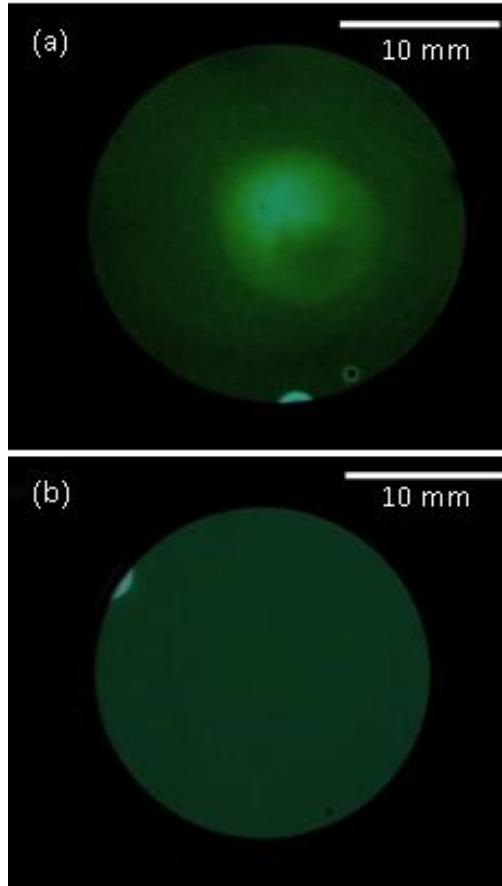


Fig.3.22: Spatial profile recorded on MCP a) with pre-pulse and b) without pre-pulse

MCP-phosphor assembly coupled to a CCD camera. It is important to align the slit of the grating at the center of the incident soft X-ray laser beam in order to get maximum intensity in the spectrum. A quadrant vacuum diode has been developed in-house and used to precisely locate the center of the X-ray laser beam. The quadrant vacuum photodiode is similar to the vacuum photodiode already discussed above except that the cathode is now divided into four quadrants and each quadrant record the part of the incoming light independently. The four quadrants provide four separate signals corresponding to the parts of the X-ray laser beam falling on them. The position of the quadrant diode was aligned with the center of the laser beam by equalizing the amplitude

of the signals recorded from all the four quadrants. A typical quadrant diode signal is shown in Fig. 3.23 when the amplitude of the laser signal recorded in all quadrants is almost same. Once the center of the X-ray laser beam is identified, it was very easy to

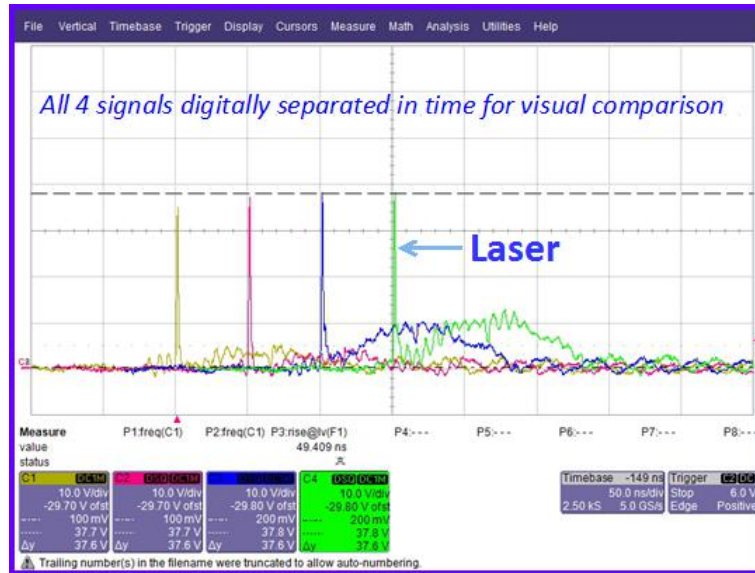


Fig.3.23: Laser pulse recorded in equal amplitude in all four quadrants of Quadrant vacuum photodiode

precisely keep the slit of the grating at this position. The grating is placed in a specifically designed holder with cross holes (light-tight) for evacuation purpose. The incoming light from the plasma is dispersed by the transmission grating and recorded on the MCP-CCD detection system. Figure 3.24a shows the recorded transmission grating spectrum and its intensity profile (binned) taken across the center of the spectrum under the optimized conditions of lasing. The spectrum clearly revealed intense soft X-ray laser line emission at 46.9 nm superimposed over the continuum emission spectrum of the plasma and its higher orders. The first emission line on either side of the zeroth order corresponds to the

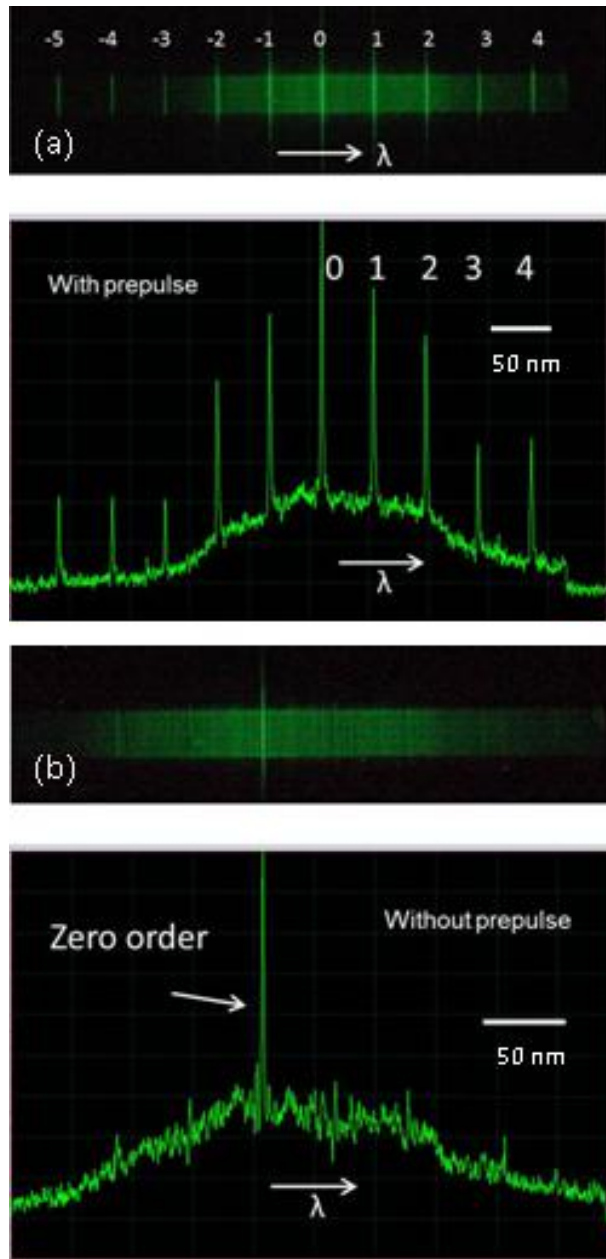


Fig.3.24: Transmission grating spectrum along with its binned intensity profile a) with pre-pulse and b) without pre-pulse; showing lasing line at 46.9 nm along with its various diffraction orders

spectral position of 1st order of lasing line at 46.9 nm. The separation between the second emission line and the first emission line was found to be same as that between first

emission line and the zeroth order. In the similar way, all the emission lines were found to be equally spaced. Their separations were quite consistent with those of the estimated higher diffraction orders of lasing line indicating that even higher diffraction orders (up to 5th order) of the lasing line are seen in the spectrum with prominent intensities. In absence of pre-pulse, the lasing line disappears along with its diffraction orders and only the zeroth order is recorded as shown in Fig. 3.24b. It was found that the highest diffraction order observed was limited by the MCP size and the distance between the grating and MCP. This distance was reduced further and the diffraction orders as high as up to 10th could be recorded with the X-ray laser as shown in Fig. 3.25. The detection of such high diffraction orders points towards the fact that the intensity of the soft X-ray laser beam is very high and it is monochromatic. The importance of the pre-pulse was once again noticed in the spectrum of the laser. As the pre-pulse was switched off, the intense lasing line along with its all diffraction orders disappeared from the spectrum. This observation was quite in line with the observation made in the case of spatial and temporal profiles of the laser as discussed earlier.

In all these experiments, the detectors whether it is MCP or vacuum diode, were placed at a large distance (~ 1 to 2 m) from the plasma source in order to enhance the signal to noise ratio for the soft X-ray laser. Any radiation, other than laser, will be much more diverging in nature and will be sufficiently suppressed with respect to the laser before being recorded at a far detector plane. Also, emissions in the higher wavelengths e.g. in the UV or visible region, are dispersed by the grating (700 lpm) at large angles compared to the 46.9 nm laser and will not be seen in the spectrum recorded by MCP placed at sufficiently higher distance from the grating. Due to this, only the

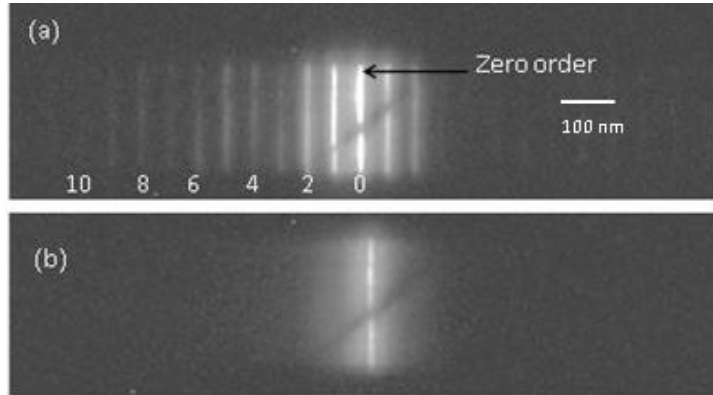


Fig.3.25: Diffraction orders recorded up to (a) 10th order in the spectrum and disappear (b) in absence of pre-pulse

bremsstrahlung emission in the XUV region will be visible as background in the spectrum, as shown in Fig. 3.24. In the temporal profile recorded by the vacuum diode, the incoherent radiation is seen as long pulse (few tens of nanoseconds) with laser pulse riding over it (see Fig. 3.21). Similar contribution of incoherent radiation is seen in the spatial profile also as low intensity background light filling the entire MCP screen (~ 25 mm) over which the laser beam can be distinctly observed as bright spot of few mm size. In the absence of pre-pulse, only the laser contribution disappears from the detectors. Hence, contribution from the incoherent radiation can be easily subtracted to retrieve the clean footprint of the soft X-ray laser at 46.9 nm.

3.2.4 Coherence measurement of the soft X-ray laser

A Young's double slit experiment was setup on the soft X-ray laser beam to measure its coherence in addition to its temporal, spatial and spectral studies. Fig. 3.26 depicts a schematic diagram of the experimental setup. A double slit (30 μm wide slits separated by

120 μm) was placed in the path of the soft X-ray laser beam at a distance of 88 cm from the capillary exit. With the help of the quadrant diode, it was ensured that the double slit is placed at the center of the laser beam. The double slit divides the wavefront of the laser beam equally into two parts which then mutually interfere to form interference

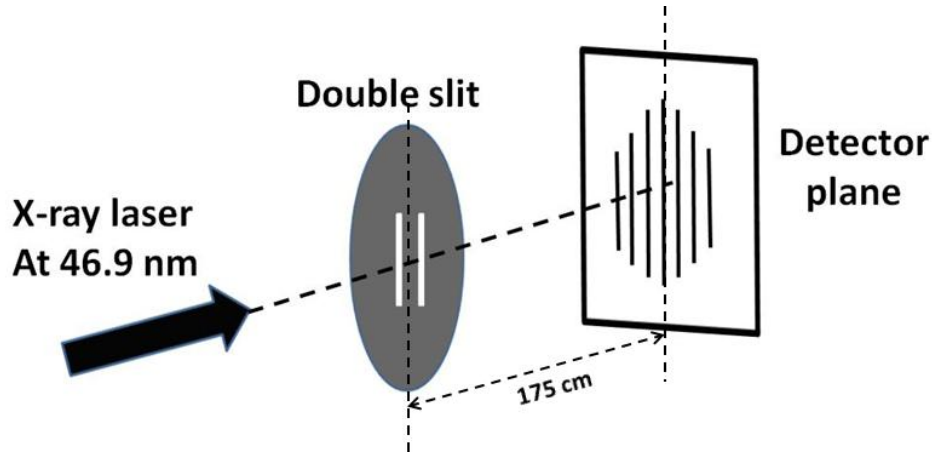


Fig.3.26: Schematic diagram of experimental layout for Young's double slit experiment

fringe pattern as shown in Fig. 3.27a. The visibility of the fringe pattern is a measure of the spatial coherence of the incident laser beam. The fringes were recorded on MCP kept at a large distance (~ 175 cm) from the double slit. The contrast of these interference fringes was very good as can be seen from the Figure 3.27b where a line out of the recorded fringe pattern is drawn in a direction normal to the fringe direction. The fringe separation was measured to be ~ 682 μm which is in good agreement with the laser wavelength of ~ 46.9 nm. However, it was necessary to minimize the contribution from background light in the recorded image before estimating the fringe visibility. For this, images of fringe pattern were recorded with and without prepulse in successive shots under similar conditions. The image without pre-pulse contains only the incoherent

plasma emission as the background signal and no fringe pattern is seen as the lasing does not take place without pre-pulse. The image without pre-pulse is subtracted from the image with pre-pulse in order to remove the background contribution arising due to incoherent plasma emission. As a result, the fringe pattern appearing in this resultant

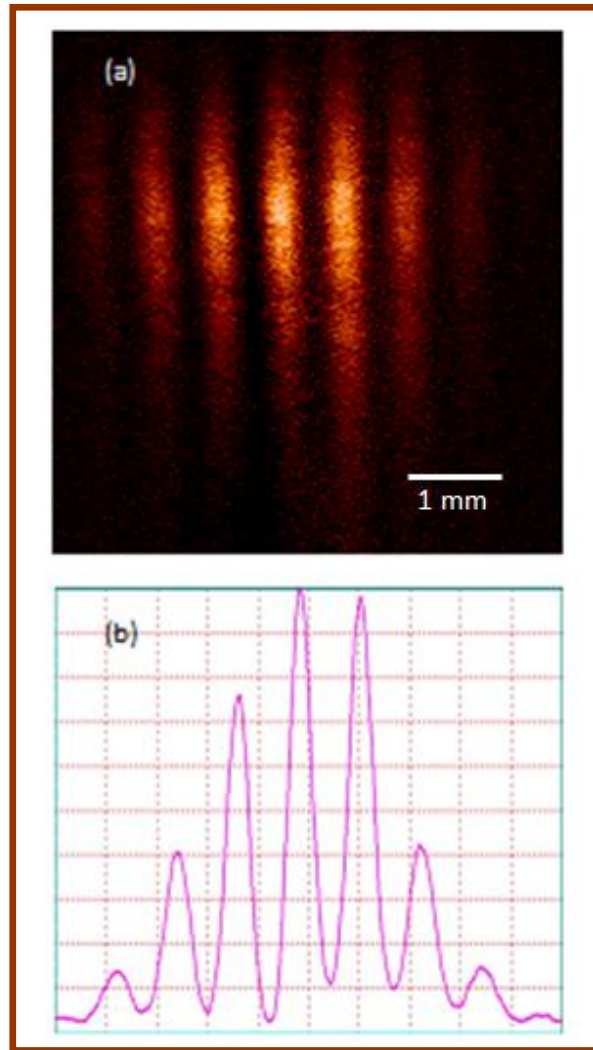


Fig.3.27: Good contrast Interference fringe pattern shown in (a). Also, shown is the transverse line-out (b) of these fringes

image contains contribution from laser beam only. The visibility of these interference

fringes {defined as $V = (I_{\max} - I_{\min})/(I_{\max} + I_{\min})$ } were measured to be $\sim 85\%$. If the incoming light is assumed to be Gaussian, the fringe visibility depends on the slit separation ' d ' and the spatial coherence radius ' L_c ' through relation, $V = \exp\left(-\frac{d^2}{2L_c^2}\right)$.

Using this relation, the transverse spatial coherence length was estimated to be $\sim 225 \mu\text{m}$ at a distance of 88 cm from the capillary, where the double slit was placed. This measured value of the spatial coherence length is modest if compared to what has been reported earlier for such soft X-ray lasers^{52,152} with relatively longer length of capillary. This is due to the fact that the spatial coherence of such a discharge laser has a strong dependence on the length of the column^{52, 152}. It is worth mentioning here that Y. Liu et al.¹⁵² have demonstrated full spatial coherence for a plasma column of length 36 cm.

To summarize, conditions suitable for soft X-ray lasing at 46.9 nm were explored by varying the experimental parameters of the capillary discharge excitation of argon plasma. The lasing was successfully achieved after the conditions were optimized. Pre-pulse, creating pre-plasma before the main discharge, was seen as essential requirement for lasing. The pulse width of the soft X-ray laser was measured to be ~ 1.2 ns (FWHM). From the spatial extent of the laser beam at fixed distance from the source, the divergence was estimated to be smaller than ~ 3.5 mrad. The spectral studies done using transmission grating spectrograph revealed intense lasing line emission at 46.9 nm. This was evident from the recorded higher diffraction orders which were as high as 10th order of the lasing line. Young's double slit experiment provided high contrast interference fringes indicating the good coherent nature of the soft X-ray laser beam. The spatial coherence length was estimated to be $\sim 225 \mu\text{m}$ at a distance of ~ 88 cm from the source.

3.3 Studies towards development of compact and repetitive soft X-ray laser at 46.9 nm

The capillary discharge soft X-ray laser at 46.9 nm described till now operated in single shot mode. It can not run at repetitive mode due to the involvement of much higher voltages (few hundreds of kV) and higher discharge currents (few tens of kA). Hence, studies were conducted with an aim to explore lasing conditions at lower voltages and currents. In this context, experiments were carried out on capillary discharge system ‘version 1’ to find out the minimum discharge current at which the laser at 46.9 nm can be obtained. The discharge current was reduced in step from ~ 45 kA to ~ 14 kA and the argon pressure in the capillary was optimized for each discharge current value in order to get enhanced laser amplitude. Interestingly, the laser pulse could be recorded with detectable intensity even at a discharge current as low as ~ 16 kA with proper optimization of parameters. The voltages required for such current amplitude were much below ~ 100 kV which indicated a good possibility to substitute the present pulse power driver as well as various sub-systems with those having very compact sizes. These information were quite helpful in designing and building of a very compact table-top capillary discharge X-ray laser which is termed as ‘Version 4’. This system was successfully tested at voltage of ~ 60 kV and was able to deliver ~ 18 kA discharge current. A photograph of the system is shown in Fig. 3.28. The laser pulse along with the discharge current obtained from this system is shown in Fig. 3.29. The system occupies a very small area of 0.4 m × 0.4 m on a small trolley in which all the sub-systems can be placed making the entire system as easily portable. However, the major advantage of this system was demonstrated recently when it was shown to deliver soft X-ray pulses at a

repetition rate of 0.1 Hz.

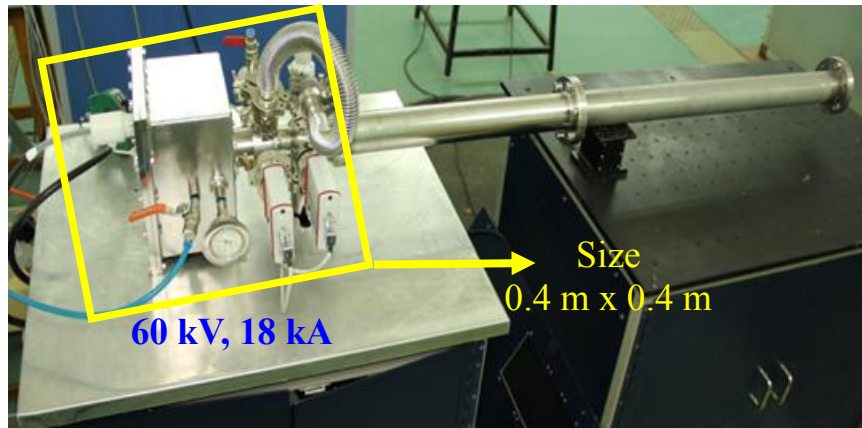


Fig.3.28: A very compact capillary discharge X-ray laser operating at repetition rate of 0.1 Hz

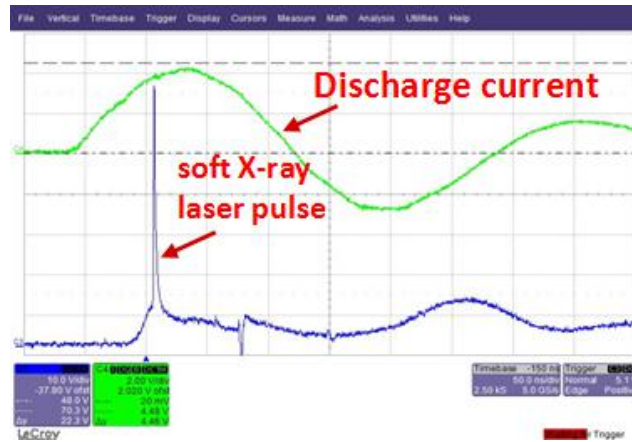


Fig.3.29: Discharge current and the laser pulse from compact capillary discharge X-ray laser operating at repetition rate of 0.1 Hz

CHAPTER 4: ROLE OF DISCHARGE CURRENT PROFILE ON THE ENERGY AND GAIN OF SOFT X-RAY LASER AT 46.9 NANOMETER

4.1 Introduction

Generation of soft X-ray laser at 46.9 nm requires formation of highly ionized argon ions i.e. Ar^{8+} (Ne-like) as lasing species. Under suitable conditions of density and temperature of plasma, these ions undergo electron collisional excitations which subsequently create population inversion between the $3p\ ^1S_0$ and $3s\ ^1P_1$ energy levels of Ar^{8+} ion leading to soft X-ray lasing at 46.9 nm. For this, a high discharge current of few tens of kA is required to pass rapidly (in few tens of ns time) through pre-ionized argon column inside a ceramic capillary tube. The azimuthal magnetic field generated from the current itself exerts strong Lorentz force on the plasma column in radially inward direction to form a hot and dense pinch plasma suitable for the required X-ray lasing at 46.9 nm. The X-ray lasing is dependent on wide range of experimental parameters and all these parameters have their own impact on the lasing action. These parameters include discharge current profile i.e. its amplitude and duration, capillary diameter, capillary length, capillary material, initial gas pressure and pre-pulse conditions i.e. its amplitude and delay with respect to the main discharge current. Role of some of these parameters have been studied previously in the literature^{125-127,153}. Among these various parameters, discharge current profile is one of the most important parameter to affect the X-ray lasing conditions. It depends on the amplitude as well as the duration of the current pulse. A discharge current with higher rate of rise (dI/dt) helps in achieving higher ionization states through faster pumping of plasma. It also helps in faster detachment of plasma

from the wall of the capillary in the early phase of magnetic compression. This restricts the impurities coming into the plasma from the capillary wall which otherwise may lead to loss of significant pump energy. So, if impurities are present in large number in plasma, the lasing species may not be heated to the temperature required for lasing thus decreasing the laser output. Beside this, the reduced wall ablation due to faster current also has a positive influence on the longer life of the capillary. Keeping these effects in mind, the role of dI/dt on the X-ray laser energy needs to be investigated experimentally. However, in order to change the value of dI/dt significantly, it is required to change both the amplitude and the pulse duration of the discharge current. A significant change in the current requires significantly higher voltage which in turn exerts higher stress on the pulse power systems. Also, the insulators used in various components of the capillary discharge system limit the maximum applied voltage due to the breakdown issues which finally limits the discharge current delivered. On the other hand, the pulse duration of the discharge current depends on the inductance (L) and capacitance (C) of the discharge circuit which in turn depends on the configuration of the pulse power driver as well as the geometry of the capillary discharge system. Thus, any change in the pulse duration requires modification in the geometry of the capillary discharge system which is not an easy task. Therefore, dI/dt becomes the most difficult parameter to be changed in a capillary discharge X-ray laser system. It is because of this reason that there are not enough experimental studies reported based on the variation of this parameter. This aspect has been investigated in the present chapter. The chapter also emphasizes the experimental studies carried out for the first time to understand the effect of current profile on the efficiency of the soft X-ray laser by measuring its gain-coefficient. The

study is important in view of maximizing the gain of the soft X-ray laser.

4.2 Experiments for changing the rate of rise (dI/dt) of the discharge current

Since the rate of rise of the discharge current i.e. dI/dt seems to have favourable effect on the laser output, it was decided to increase the dI/dt value and study its effect on the energy of the soft X-ray laser pulse. dI/dt can be increased either by increasing the current amplitude or by decreasing the pulse duration. It was planned to adopt the later one first. The pulse duration of the discharge current has dependence on the 'L' and 'C' value of the discharge circuit which is decided by the geometry of the various components like waterline capacitor, the spark gap chamber and the capillary chamber. After taking input from series of electrical simulation studies, the geometries were optimized and the sizes of the various components were tailored. This was done with an aim to significantly reduce the overall inductance of the discharge path. As a result, the capillary discharge X-ray laser system was upgraded from older version 1 to an upgraded version 2 (shown in Fig. 4.30) where the discharge current was much faster than earlier. Another advantage came out naturally with this kind of up-gradation was that the new system became very compact also. The quarter period of the current in the new version was measured to be ~ 42 ns compared to the earlier value of ~ 75 ns. This was measured with 15 cm long capillary. The rise-time (10% to 90%) of the current in the new system was found to be ~ 27 ns at a discharge current of ~ 26 kA. The dI/dt value was further enhanced in the new system by increasing the discharge current amplitude in steps from 26 kA to 44 kA keeping the quarter period fixed and only increasing the applied voltage.

Now experiments were carried out to measure the energy in the soft X-ray laser pulse in the version 1 and version 2 of the system. A comparative study of the laser energy was carried out with respect to the different values of dI/dt of discharge current. However, it

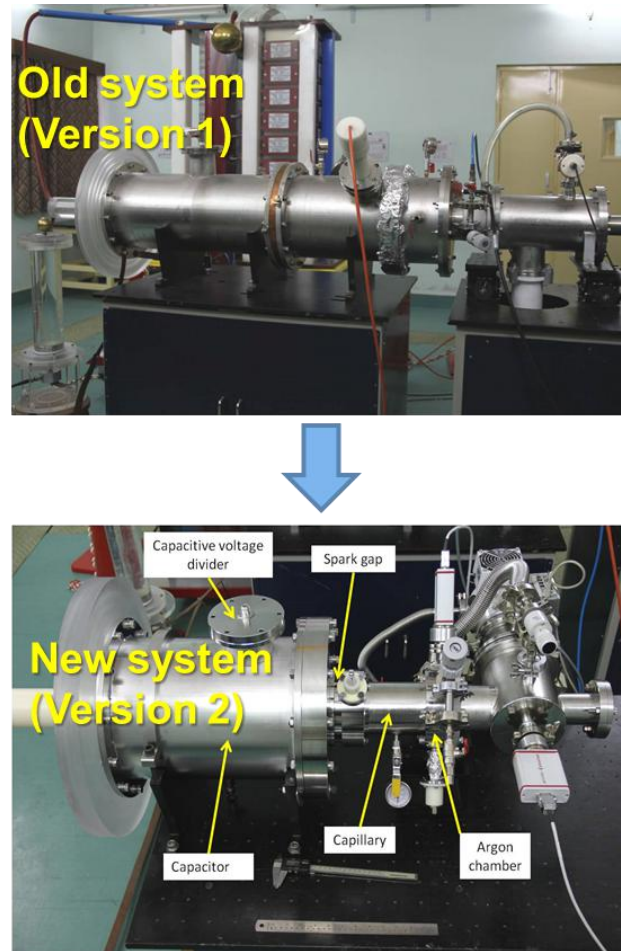


Fig.4.30: Photograph of the upgraded system (Version 2) in comparison to the old system (Version 1)

was required to measure the energy content in a single soft X-ray laser pulse before proceeding further. The procedure to measure the laser energy is described in the following section.

4.3 X-ray laser pulse energy measurement

Soft X-ray lasing was first achieved in version 1 of the capillary discharge system by optimizing the various experimental parameters for a discharge current of ~ 40 kA passing through pre-ionized argon gas filled inside an alumina capillary having a length 15 cm and inner diameter 2.8 mm. A pre-pulse current of 25 A was applied 5 μ s before the main discharge current in order to pre-ionize the argon gas. The initial argon pressure in the capillary was optimized to 0.31 mbar for achieving maximum lasing signal at the above current parameters. The temporal profile of the lasing signal was recorded using an in-house developed bi-planar vacuum diode. In order to facilitate the measurement of soft X-ray laser energy with good precision, it is required to record the clean laser pulse with minimum contribution from background plasma emission. This is possible by recording the laser pulse at a larger distance (few meters) from the source where the contribution from incoherent plasma emission is highly suppressed due to its larger divergence in comparison to the X-ray laser pulse. However, at such a larger distance, the size of the X-ray laser beam also increases due to its own divergence (few mrad). Hence, a large sized sensor is required to record the entire laser beam for energy measurement. The in-house developed vacuum diode fulfills this requirement quite satisfactorily as it has a large size sensor of 30 mm diameter made of copper. The diode was placed sufficiently far from the source i.e. at a distance of ~ 2.6 m from the source. A clean laser pulse with minimum contribution from the background plasma light is shown in Fig. 4.31. The energy in the laser pulse was measured in two steps. In the first step the total charge generated in the vacuum diode by the X-ray laser pulse estimated. In the second step, the quantum efficiency of the vacuum diode was obtained and this information was used to

estimate the energy. The diode was required to be well calibrated to estimate its quantum efficiency. The calibration was done using a commercial X-ray diode (AXUV IRD 20HS1). The procedure adopted for calibration is described as below. Firstly, the vacuum diode was reverse-biased with a negative voltage of 700 V applied to its copper cathode.

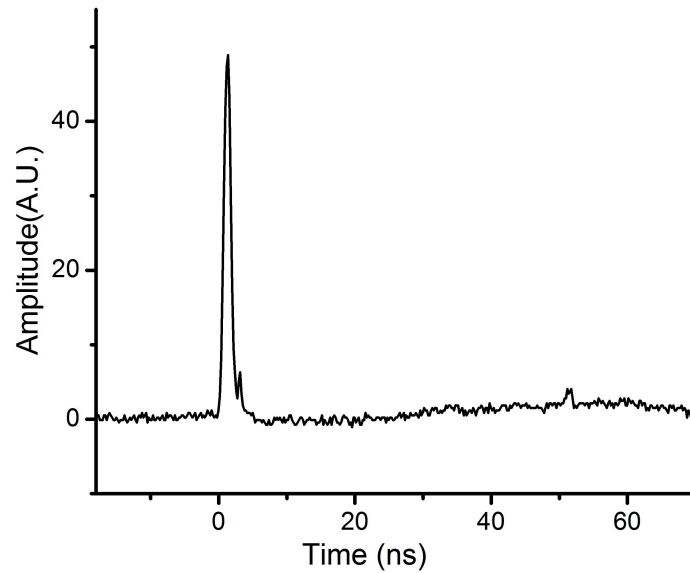


Fig.4.31: Clean X-ray laser pulse recorded with vacuum diode placed at 2.6 m from the source

The anode mesh of the diode was grounded. At 40 kA discharge current and 0.31 mbar gas pressure, the incoming soft X-ray laser light (46.9 nm) was allowed to enter the vacuum diode through the mesh electrode and incident on the cathode. The incoming photons generate photo-electrons from the cathode which are then collected by the anode. The resultant signal was then measured using a Lecroy (WR104MXi), 1 GHz, 10 GS/s oscilloscope (50 Ω termination) connected using a doubly shielded cable. The laser pulse was recorded on the oscilloscope with a signal amplitude of \sim 200 V. The recorded laser pulse was integrated over time to estimate the area (V-s) under the pulse. Although, the contribution of unwanted background plasma emission was minimized by keeping the

diode at large distance from the source, there was a small contribution still present in the laser pulse. In order to remove this contribution, the diode signal was recorded with and without pre-pulse in two successive shots under similar conditions. In the shot without pre-pulse, the lasing pulse is absent and the background contribution remains same. Therefore, the time-integrated area without pre-pulse was subtracted from that with pre-pulse to eliminate contribution of plasma background emission. The resultant integrated area corresponds to clean laser pulse and was divided by the 50Ω termination resistance to get the total charge generated in the vacuum diode by the incident laser pulse. This was estimated to be 8 nC.

Now, the quantum efficiency of the vacuum diode need to be estimated by calibrating it with commercial X-ray diode AXUV IRD 20 HS1. Firstly, X-ray laser pulse was recorded using this X-ray diode which has a sensor diameter of 5 mm, quantum efficiency 7.16 and responsivity 0.274 A/W for 46.9 nm lasing wavelength (photon energy ~ 26.5 eV). It was necessary to reduce the laser energy significantly in order to prevent the diode from going into saturation. This was achieved by placing an Al filter of thickness $1.5 \mu\text{m}$ in front of the diode. The charge generated from the laser pulse was estimated from the time-integrated area under the laser pulse. The same procedure was adopted again by replacing the X-ray diode with vacuum diode and keeping the other conditions same. Same filter was used this time also and an aperture of diameter 5 mm was placed in front of the vacuum diode in order to keep the exposed area same as that with commercial X-ray diode. The time-integrated area was compared with the previous case and it was found to be 70 times less as compared to that with X-ray diode. From this, the quantum efficiency of the vacuum diode was estimated to be 0.102.

Using this value of quantum efficiency estimated, the total charge 8 nC generated by the soft X-ray laser pulse on vacuum diode was found to be equivalent to $\sim 2 \mu\text{J}$ energy in the laser pulse. This was obtained with 40 kA discharge current, 0.31 mbar argon gas pressure in a capillary of length 15 cm and diameter 2.8 mm. The quarter period of the discharge current was ~ 75 ns and the rise-time (10% to 90% of peak value) of the discharge current was measured to be ~ 46 ns. This corresponds to a dI/dt value of 7.1×10^{11} A/s.

4.4 Effect of dI/dt on the X-ray laser pulse energy

The discharge current profiles obtained from old system (version 1) and new system (version 2) is shown in Fig. 4.32 for comparison with a peak current of 40 kA. The black solid curve corresponds to version 1 and red dashed curve corresponds to the version 2. The change in the slope of the current can be clearly observed in the two cases. The new system had a significant increase in the dI/dt value which was measured to be $\sim 1.2 \times 10^{12}$ A/s against $\sim 7.1 \times 10^{11}$ A/s in the old system. In the new system, the discharge current was increased in steps starting from comparatively much smaller peak value. However, at every step of the discharge current amplitude, the energy in the laser pulse needs to be maximized by optimizing the argon gas pressure. This is because the discharge current profile and the argon gas pressure are strongly correlated to each other as far as the lasing action is concerned. This is further supported from the fact that the population inversion for X-ray lasing requires optimum density and temperature of plasma. After this optimization, $2 \mu\text{J}$ of energy in the laser pulse could be achieved at a much smaller discharge current of 26 kA in the new system. It is interesting to note here that the similar laser energy was earlier obtained in the old system for a higher discharge current of 40

kA. In the new system, the dI/dt value of the current was further enhanced by increasing its amplitude with an aim to increase the laser energy as much as possible. Significant gain in the laser energy could be obtained as a result of this exercise. The obtained results

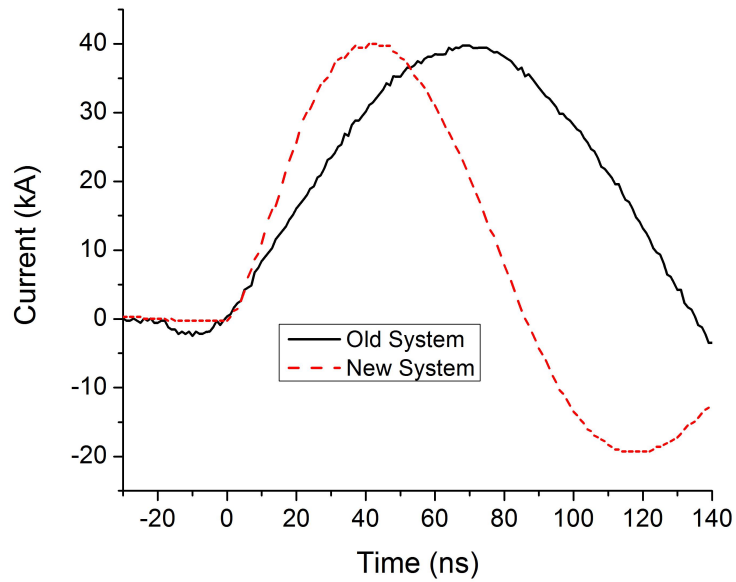


Fig.4.32: Discharge current profiles from old system (black solid curve) and the new system (red dashed curve) showing different rate of rise

have been summarized in Table 4.1. A careful observation of the results indicate that the dI/dt value for 26 kA discharge current in the new system is very close to that for 40 kA discharge current in the old system and the laser energy measured in the two cases are same. This reflects the important role played by the rate of rise of discharge current in increasing the laser output. The laser energy increased to 2.9 μJ when the peak discharge current was increased to 29 kA. Similarly, the discharge current was increased to 35 kA and the pressure-optimized laser energy in the new system could be enhanced to 3.4 μJ . It was found that the optimum gas pressure had also been increased from 0.30 mbar (at 26 kA) to 0.39 mbar (at 35 kA). Finally, when the capillary current was increased to 44 kA,

the laser energy was measured to be 4.0 μJ . This was certainly a significant increase in the laser energy in the new system as compared to what was achieved in the old system at 40 kA. As mentioned earlier also, the reason behind the increase in the laser energy at higher dI/dt can be attributed to the following facts. Discharge current with higher dI/dt

	Peak current (kA)	Quarter period of the current (ns)	Rate of rise [dI/dt] (A/s)	Laser Energy (μJ)	Optimum gas pressure (mbar)
Old System	40	75	7.11×10^{11}	2.0	0.31
New System	26	42	6.93×10^{11}	2.0	0.30
	29	42	8.92×10^{11}	2.9	0.35
	35	42	1.08×10^{12}	3.4	0.39
	44	42	1.30×10^{12}	4.0	0.50
	56	57	1.30×10^{12}	3.9	0.51

Table 4.1: Increase in laser energy as the dI/dt value of discharge current increases

causes faster detachment of plasma from the capillary wall when the compression just starts from the outer boundary. This leads to limited wall ablation and minimizes the impurity in the argon pinch plasma. As a result, the larger part of the pumping energy is coupled to the lasing species which in turn enhances the laser output. Beside this, higher dI/dt also leads to faster pumping of energy in the gain medium which can suppress the various relaxation processes competing with the ionization. This helps to obtain higher amount of highly ionized lasing species (Ar^{8+}) which has a favorable effect on the lasing action.

The importance of dI/dt over the peak value of the current for laser output was further investigated. For this, the discharge current was further increased at the cost of dI/dt in the new system. This was achieved by modifying the cylindrical waterline capacitor so as to increase the outer diameter of its inner electrode. It increases the capacitance value of the capacitor from 3.2 nF to 6.4 nF. Such a modification led to an increase in the discharge current amplitude up to ~ 56 kA with the new system. However, such a rise in the capacitance made the discharge current slower and the quarter period of the current was measured to be ~ 57 ns. The dI/dt value of this current profile was estimated to be $\sim 1.3 \times 10^{12}$ A/s which is similar to what was earlier measured for discharge current of ~ 44 kA. The energy of the soft X-ray laser pulse was measured with this new discharge current excitation after carrying out the optimization of gas pressure. Interestingly, the laser energy did not increase beyond ~ 4.0 μ J. This exercise signifies an important fact that increasing only the peak discharge current and keeping the dI/dt value unchanged is not favourable for the laser output. Figure 4.33 shows a plot of the measured energy in the X-ray laser pulse against different dI/dt values of the current. The solid curve connecting the data points is there just to guide the eye. The hollow circles indicate those special data points which have higher current amplitude but comparable dI/dt value with respect to the closest data point. However, these data points show no increase in the laser energy with respect to the neighbouring point. The study confirms that it is dI/dt rather than the peak value of the discharge current which has greater role to play in the generation of soft X-ray laser through fast capillary discharge scheme. In fact, it calls for a need to enhance the dI/dt value of the discharge current in order to relax the requirement of higher peak current. This can be achieved by making major modifications

in the pulsed power driver as well as spark gap switch and capillary chambers such that the discharge path is minimized. Another advantage of such modification will be reflected

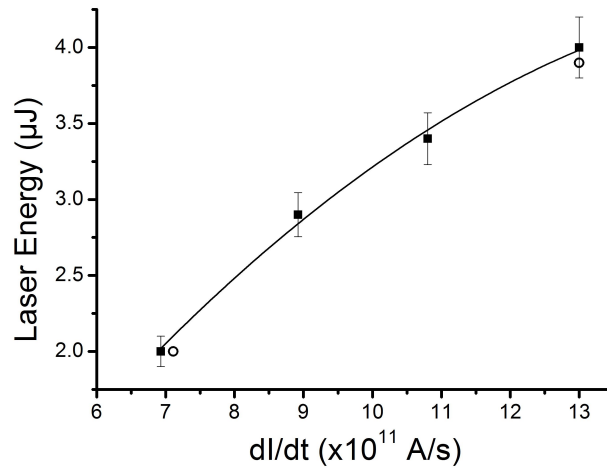


Fig.4.33: Graph showing the dependence of X-ray laser energy on dI/dt value of the current

in making the capillary discharge system more compact. The study will be quite helpful in the experiments aimed at achieving X-ray lasing at shorter wavelengths e.g. 13.4 nm in nitrogen where the simulations have predicted the requirement of much higher discharge current. Such stringent requirement can be relaxed up to the convenient level by making the rise of the current faster enough.

4.5 Gain-coefficient measurement of the X-ray laser

Experiments were performed to carry out the gain-measurement studies of 46.9 nm soft X-ray laser. The laser was generated from argon pinch plasma inside the capillary of 30 cm length and 2.8 mm diameter. The plasma was formed when the pre-ionized argon gas was subjected to main discharge current of 41 kA with quarter period ~ 72 ns. The long capillary was initially chosen in order to find out the plasma length beyond which

the soft X-ray laser starts saturating. The dI/dt value of the current was measured to be 7.5×10^{11} A/s. The argon gas pressure in the capillary was optimized for maximum amplitude of the laser pulse as recorded by the vacuum diode. In order to measure the gain-coefficient of this soft X-ray laser, it was required to vary the length of the gain medium (plasma) and see its effect on the laser output. However, one can not just change the capillary length for changing the plasma column length as it will alter the discharge circuit length also which will affect the current profile (dI/dt) due to change in the inductance of discharge circuit. It is mandatory here that while changing the length of the plasma column, the other parameters, which affects the laser output, must remain fixed. This condition was strictly adhered during the experiments. In order to vary the plasma length, metallic rods of different lengths were inserted in the capillary from high voltage electrode side. The rod was kept in direct contact with the high voltage electrode. Such an arrangement did not alter the inductance of the discharge path and hence there was no change in the discharge current parameters which was confirmed from the observed current profile. Using this technique, the length of plasma column (30 cm) was reduced to 24cm, 18.6 cm, 12.4 cm, 9.2 cm and 6 cm successively. At each length of the plasma column, the gas pressure was optimized to maximize and record the laser amplitude using the vacuum diode. These experimental findings have been shown in the form of a semi-log plot by triangular data points in Fig. 4.34 which shows how the gain of this laser behaves with different plasma lengths in a 30 cm long capillary. It is quite clear from the graph that the gain of the laser rises exponentially up to a plasma length of ~ 12 cm and then starts showing saturation behaviour. The saturation behaviour has been indicated in the graph by dotted line which is just to guide the eye. The initial part of the graph

showing exponential increase was fitted with Linford's formula¹⁵⁴ to estimate the gain-coefficient of the soft X-ray laser. The fitting is shown by the black solid curve in the graph. The gain coefficient was estimated from this fitting to be 0.69 cm^{-1} .

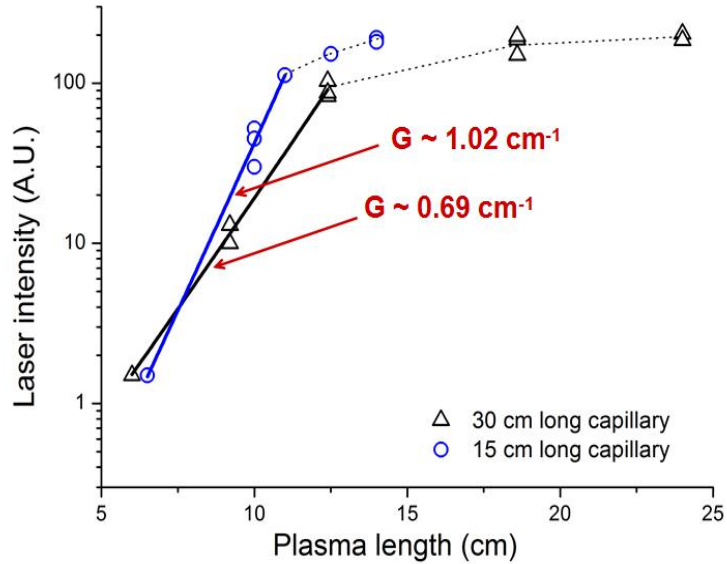


Fig.4.34: Semi-log plot of gain vs plasma length for slower (30 cm long capillary; triangular datapoints) and faster currents (15 cm long capillary; circular datapoints). Solid curves are the curve fitting of the initial exponentially varying part with Linford's formula¹⁵⁴

4.6 Effect of current pulse duration on the gain-coefficient

The gain-coefficient is a direct measure of the amplification efficiency of soft X-ray plasma amplifier. It indicates how efficiently a soft X-ray radiation of suitable wavelength can be amplified during its passage through the plasma acting as the gain medium. It is always desirable to have gain coefficient as high as possible to get high energy in the X-ray laser pulse. Experiments were conducted to investigate the effect of current pulse duration on the gain-coefficient of 46.9 nm soft X-ray laser with an aim to get higher gain-coefficient. The discharge current pulse duration depends on the inductance of the

discharge path which needs to be varied for the study. A close observation reveals that the capillary length has a major contribution in the overall inductance of the discharge path. Hence, it was decided to change the capillary length in order to change the inductance which in turn changes the pulse duration of the current. In view of this, 30 cm long capillary was reduced to a length of 15 cm and the necessary changes in the system were made to accommodate this smaller length of the capillary. As a result of this, the discharge current became faster with its quarter period reduced to ~ 60 ns from earlier value of ~ 72 ns. The discharge current amplitude was maintained at same as previous i.e. ~ 41 kA. A comparison of the two current profiles with capillary lengths 30 cm and 15 cm is shown in Fig. 4.35. This also led to an increase in the dI/dt value from 7.5×10^{11} A/s to 9.2×10^{11} A/s. With this faster current pulse, the plasma length was again varied and the

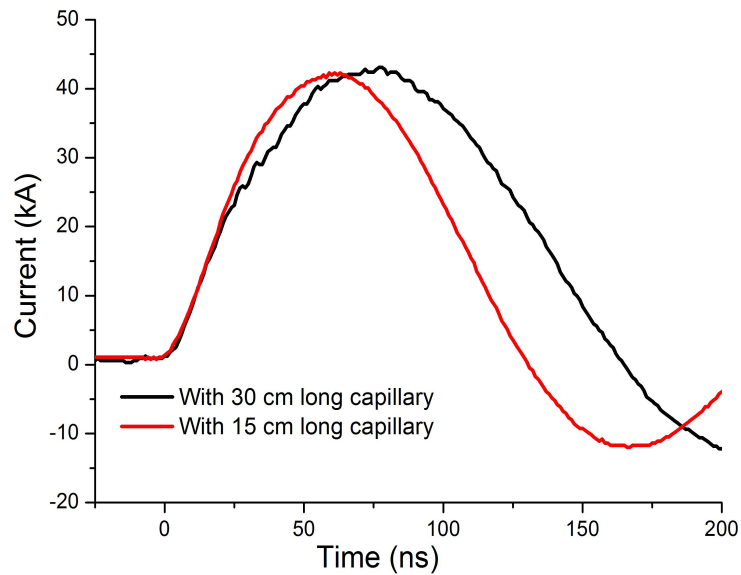


Fig.4.35: Discharge current profiles for 30 cm long capillary (black curve) and 15 cm long capillary (red curve)

pressure-optimized gain of the laser pulse was plotted against the plasma length on a semi-log plot as described in the previous section. The experimental curve is shown as

circular data points in Fig. 4.34. It is quite evident from the comparison of the initial slopes of the two experimental curves that gain increases at a much faster rate with 15 cm long capillary where the discharge current is faster. The exponential part of the circular data points was fitted with Linford's formula¹⁵⁴ and the fitted curve is shown by blue solid line. From the curve fitting, the gain-coefficient was estimated to be 1.02 cm^{-1} which is significantly higher ($\sim 48\%$) than earlier value of 0.69 cm^{-1} obtained with comparatively slower discharge current. The study provides a strong experimental confirmation that the soft X-ray amplification from the plasma is more efficient with a faster discharge current.

4.7 Effect of current amplitude on the gain-coefficient

The effect of discharge current amplitude on the gain-coefficient of 46.9 soft X-ray laser was studied experimentally. This experiment was performed with 15 cm long capillary rather than 30 cm to get higher gain. Here, the gain-coefficient measurement were performed at different current amplitudes viz. 41 kA, 36 kA, 31 kA and 26 kA with quarter period of current fixed at 60 ns. At each of these current amplitude, the graph of gain vs plasma length was obtained and the same has been shown in Fig. 4.36. The exponentially varying portion of these graphs were fitted as explained earlier and the gain coefficient was estimated to be 0.76 cm^{-1} , 1.33 cm^{-1} , 1.1 cm^{-1} and 1.02 cm^{-1} for discharge currents of 26 kA, 31 kA, 36 kA and 41 kA respectively. Fig. 4.37 shows the obtained variation in the gain-coefficient at different discharge current amplitude for easier visualization. The nature of the curve clearly reveals an interesting but important fact that there exists optimum value of current amplitude for gain to be at maximum. The highest gain coefficient of 1.33 cm^{-1} could be obtained as a result of this optimization of

current amplitude. This gain-coefficient was much higher ($\sim 93\%$) than what was obtained with a slower discharge current. Also, the measured gain-coefficient seems to be significant when compared to the values reported in other studies^{49,112,116,119,120,124} with this soft X-ray laser which are of course measured under different experimental conditions.

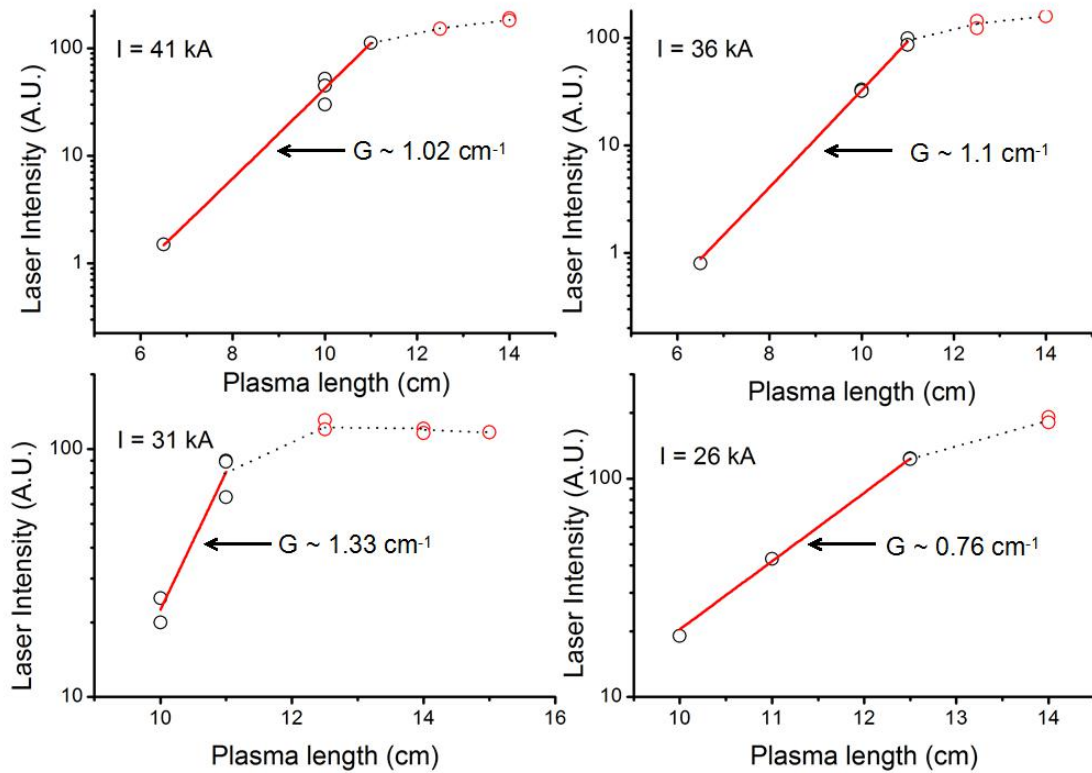


Fig.4.36: Semi-log plots of laser-gain vs plasma length for different discharge current amplitudes 41 kA, 36 kA, 31 kA and 26 kA. Exponentially varying portion of each plot has been fitted (shown as solid curve) with Linford's formula¹⁵⁴ to estimate gain-coefficient

The decrease in the gain of the laser at smaller discharge current can be attributed to the fact that the current is not sufficient enough to create required Ne-like ionization level (Ar^{8+}) in abundance. On the other side, a much higher current can lead to over-ionization

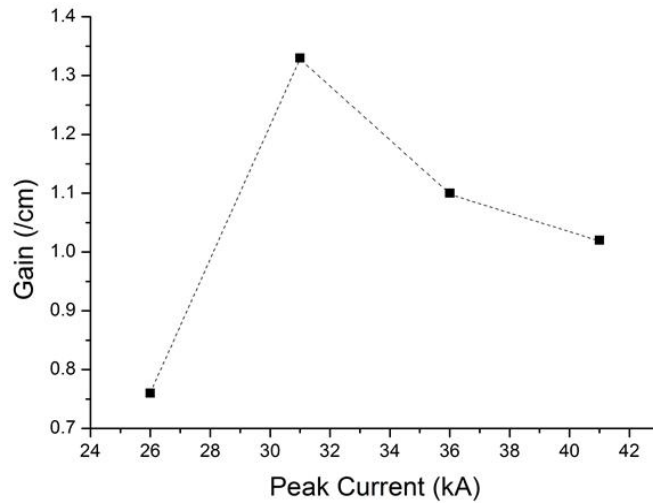


Fig.4.37: Dependence of gain-coefficient on the discharge current amplitude showing optimum behaviour

of argon ion above the Ar^{8+} and hence it is not favourable to lasing.

In summary, the first version of capillary discharge system was optimized at ~ 40 kA peak current which delivered $2.0 \mu\text{J}$ energy in the 46.9 nm X-ray laser pulse. The system was upgraded to ‘version 2’ to provide faster current pulse. As a result, the same energy could now be achieved at relatively smaller peak current of ~ 25 kA with dI/dt remaining almost same. Then, the current amplitude was further increased in steps up to ~ 44 kA in the upgraded system with current duration remaining constant. As a result, significant increase in the laser pulse energy was achieved up to $\sim 4.0 \mu\text{J}$. However, when the current amplitude was increased to 56 kA and at the same time, its duration was also increased keeping dI/dt almost same, no increase in laser pulse energy was observed. This indicated that dI/dt value of discharge current has more dominant effect on the laser output rather than its peak value and a constant increase in dI/dt leads to higher laser output.

Role of pulse duration and amplitude of discharge current on the gain-coefficient of

the X-ray laser was also studied. When the quarter period of the current was reduced from ~ 72 ns to ~ 60 ns making the current faster keeping its amplitude constant at ~ 41 kA, the gain-coefficient of the X-ray laser was found to be increased from 0.69 cm^{-1} to 1.02 cm^{-1} . Also, when the gain-coefficient was measured at different current amplitudes varying from 26 kA to 41 kA keeping the quarter period constant at ~ 60 ns, it showed an optimum behaviour i.e. gain-coefficient first increases and then decreases after a maximum value. Using this optimization of current amplitude, the maximum gain-coefficient was estimated to be $\sim 1.33 \text{ cm}^{-1}$ which is significantly higher than what was achieved earlier ($\sim 0.69 \text{ cm}^{-1}$).

CHAPTER 5: EXPLORING X-RAY LASING AT SHORTER WAVELENGTH

5.1 Introduction

Achieving capillary discharge X-ray laser to much shorter wavelengths than 46.9 nm has significant importance due to the numerous potential applications of such X-ray lasers as described in chapter 1. Most likely, these short wavelength X-ray lasers will be based on generating population inversion through recombination pumping scheme in H-like ions or through electron collisional excitation pumping in Ni-like ions. The pump power requirements for such lasing is undoubtedly much higher than what is required for the soft X-ray lasing realized at 46.9 nm in Ne-like Ar. Balmer- α transition at 13.4 nm in H-like N (N^{6+}) ion is one of the most promising lasing transition based on recombination pumping scheme¹³³. An energy level diagram of H-like N is given in Fig. 5.38 . This lasing scheme requires generation of fully ionized Nitrogen ions (N^{7+}) in abundance in high temperature plasma as a first requirement. Then, the temperature of the plasma at high density needs to be cooled very fast in few nanosecond time-scale so that an electron

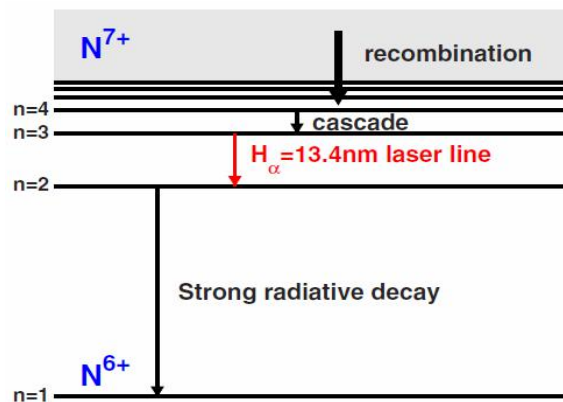


Fig.5.38: Energy level diagram of H-like N ion for recombination pumping

from continuum is allowed to enter the outer energy level by 3-body recombination. As

this electron cascades down to lower energy levels, population inversion naturally builds up between energy levels 3 and 2 leading to lasing at Balmer- α transition. In fast capillary discharge scheme, the fully stripped nitrogen ions can be formed by rapid ionization at pinch formation if a sufficiently powerful electrical driver is used to drive the plasma. The required rapid cooling can take place during subsequent expansion of pinched plasma which can lead to dominant 3-body recombination of N^{7+} ion to N^{6+} . The feasibility of this method of lasing was proposed for the first time by Vrba et al¹³³ and efforts were made by various groups later on for its experimental demonstration under different conditions¹³⁴⁻¹³⁷. Although, success has not been met as yet, these efforts have strongly suggested further investigations with much higher pulse power driver. Recently, the capillary discharge system in our laboratory was upgraded to deliver high pulse power with discharge current more than 100 kA with a quarter period of ~ 46 ns for this purpose. The experiments were carried out to explore the aforesaid recombination X-ray lasing in nitrogen Z-pinch plasma. These studies have been described in detail in this chapter. Studies done at such a high and fast discharge current excitations were not earlier available with nitrogen Z-pinch plasma and hence provide important inputs for future endeavour in this direction. The studies have also shown for the first time the experimental evidence of role of pre-pulse in formation of highly charged ions. Apart from nitrogen, initial experiments have been performed with some other gases e.g. C_2H_2 gas to explore 18.2 nm lasing in H-like C ion and Krypton gas to explore 32.8 nm lasing in Ni-like Kr ion. These experiments and their outcomes have been discussed briefly in the later sections of this chapter.

5.2 Up-gradation of capillary discharge system

As predicted by simulations, the proposed X-ray lasing in nitrogen requires highly stringent conditions in terms of fast and high current excitations as well as high gas pressures in the capillary¹³³. In order to meet these requirements, the capillary discharge system in our laboratory was upgraded to ‘Version 3’, a schematic diagram of the same is shown in Fig. 5.39. The high voltage generator had undergone major changes. The earlier used Marx-bank based charging unit was now substituted by an in-house fabricated Tesla-transformer based charging unit. It charges the waterline capacitor ($C \sim 6$ nF) up to a voltage of 400 - 500 kV connected in series with a self-triggered spark-gap switch and nitrogen-filled capillary. When the voltage at waterline capacitor is increased beyond a certain threshold value set by the breakdown level of spark-gap, the capacitor rapidly discharges in a few tens of nanoseconds through gas filled capillary and generates

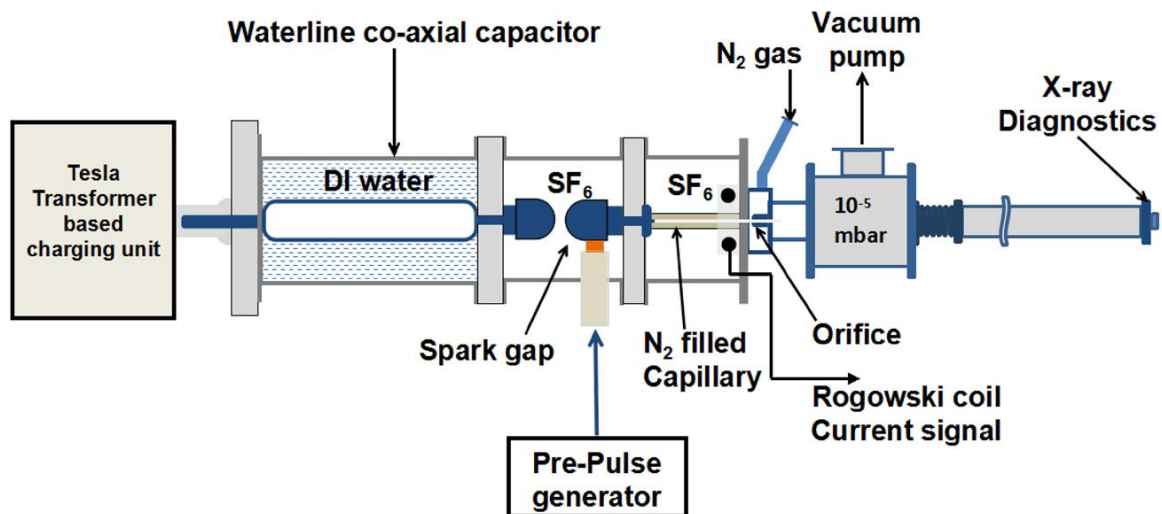


Fig.5.39: Schematic diagram of upgraded capillary discharge system ‘Version 3’

Z-pinch nitrogen plasma. Keeping the inner diameter same (2.8 mm), the length of alumina capillary was reduced to 96 mm from earlier value of 150 mm. This played

crucial role in lowering the inductance of the discharge circuit and hence making the current faster. Necessary changes were also made to increase the pre-pulse current beyond 100 A. The recombination pumping scheme for X-ray lasing requires higher plasma density and hence higher initial gas filling pressure in the capillary. Keeping higher gas pressure in the capillary severely affects the vacuum condition on the detector side and makes it difficult to use MCP like detector which needs high vacuum conditions. This difficulty was resolved by the use of an orifice of smaller diameter i.e. 0.6 mm instead of 1 mm used earlier to provide more effective differential pumping. It was kept at a distance of ~ 3 mm from the capillary exit. This orifice was made of copper-tungsten alloy to enjoy the dual benefits of good conductivity as well as ability to withstand hot plasma in close proximity with minimum ablation. The use of a small orifice makes its alignment more critical as it was now only slightly larger than the diameter of the pinch plasma column. Any slight misalignment is likely to obstruct the lasing signal significantly. To address this issue, the orifice was designed in such a way that it is locked in a position which is guided by the outer diameter of the capillary in tight tolerances. In this way, it was self-aligned with respect to the exit end of the capillary. While designing the orifice, special care had to be taken to keep provision for entry of the gas into the capillary as well as its vacuum sealing from the surroundings. On the measurement part, the voltage at the waterline capacitor was measured using a capacitive voltage divider whereas the discharge current was measured using a calibrated Rogowski coil. Figure 5.40 shows typical waveforms of waterline voltage and discharge current delivered by the system. System was able to deliver a peak discharge current of ~ 105 kA as shown in Fig. 5.40. However, it was operated at slightly lower discharge current for the present

experiments discussed here keeping in mind of the safety precaution for various insulators used as integral part of the system. Figure 5.40 also indicates a recorded soft X-ray laser pulse from argon discharge plasma under the identical experimental conditions.

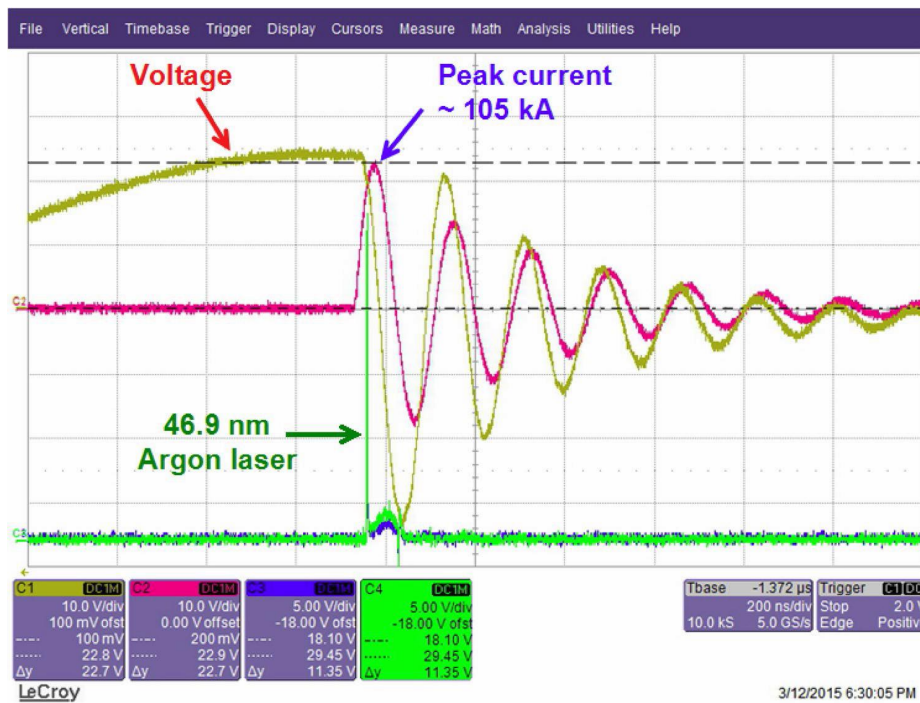


Fig.5.40: Typical voltage and current waveforms delivered by upgraded capillary discharge system ‘Version 3’ with peak current at 105 kA. Also, shown is the simultaneously obtained argon X-ray laser pulse at 46.9 nm

5.3 Exploring X-ray lasing in Nitrogen Z-pinch plasma

5.3.1 Experimental details

Using the capillary discharge system version 3, experiments were conducted in nitrogen gas-filled alumina capillary of length 96 mm and inner diameter 2.8 mm at discharge currents in the range from 60 to 95 kA. The quarter period of the discharge current in the present geometry was ~ 46 ns. The temporal profile of the emission from nitrogen Z-pinch plasma was recorded using a quadrant vacuum diode and a fast oscilloscope (1 GHz, 10GS/s, LeCroy - WR104MXi). Beside this, the spectrographic study of emission from nitrogen Z-pinch plasma was also carried out. A transmission grating spectrograph was setup for this purpose as shown in Fig.5.41. The spectrograph

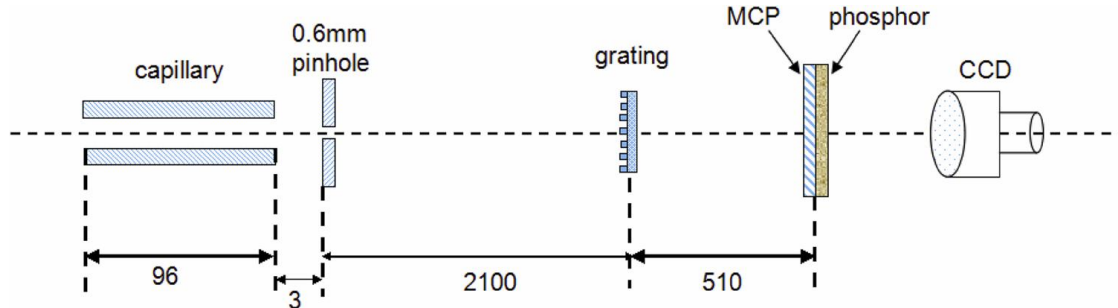


Fig.5.41: Schematic diagram of experimental setup for transmission grating spectrograph

consists of a free-standing transmission grating (700 lines/mm) to disperse the incoming radiation from nitrogen plasma which falls on an MCP detector having phosphor screen on the other end. The phosphor screen is then imaged on to a CCD camera to record the time-integrated spectrum. Time-integrated spectrum has an advantage that it can show a broad picture of the various emission lines formed at different moments in plasma in a single shot. Also, it was relatively easier in the time-integrated mode rather than the

time-resolved mode to search for a lasing line at 13.4 nm whose intensity and time of occurrence is not known in advance accurately. The spectrum was recorded with the spectral resolution ~ 0.2 nm when the MCP was kept at 51 cm from the grating. Also, it was important to identify the exact axial position in line with the capillary axis where the grating can be placed. This was done by taking reference of the 46.9 nm soft X-ray laser beam generated with argon filled capillary and recorded with quadrant diode which was aligned with the laser beam.

5.3.2 Results and discussion

In the temporal profile recorded using the quadrant vacuum diode, a fast pulse with a rise time of 5-8 ns was observed along with a long duration Bremsstrahlung emission from nitrogen plasma. The amplitude of this fast pulse was found to be quite sensitive with the gas pressure. Therefore, gas pressure in the capillary was varied from 2.5 mbar to 11.0 mbar in order to optimize the amplitude of the fast pulse. This optimization is depicted in Fig. 5.42a, 5.42b and 5.42c in which signals recorded at different gas pressures have been shown. In each figure, the three profiles shown in different colours are from three quadrants of the quadrant diode which ideally should be identical in amplitude. However, there exists small variation which may be attributed to small misalignment of the orifice with respect to the capillary axis even though precautions were taken to avoid it. It is quite clear from the recorded signals in Fig. 5.42 that the fast pulse has a larger amplitude as compared to the background plasma emission over a narrow pressure range. The enhanced fast pulse dominates in the gas pressure ranging from 4 to 8 mbar for a peak discharge current of ~ 85 kA. This fast pulse is seen at an

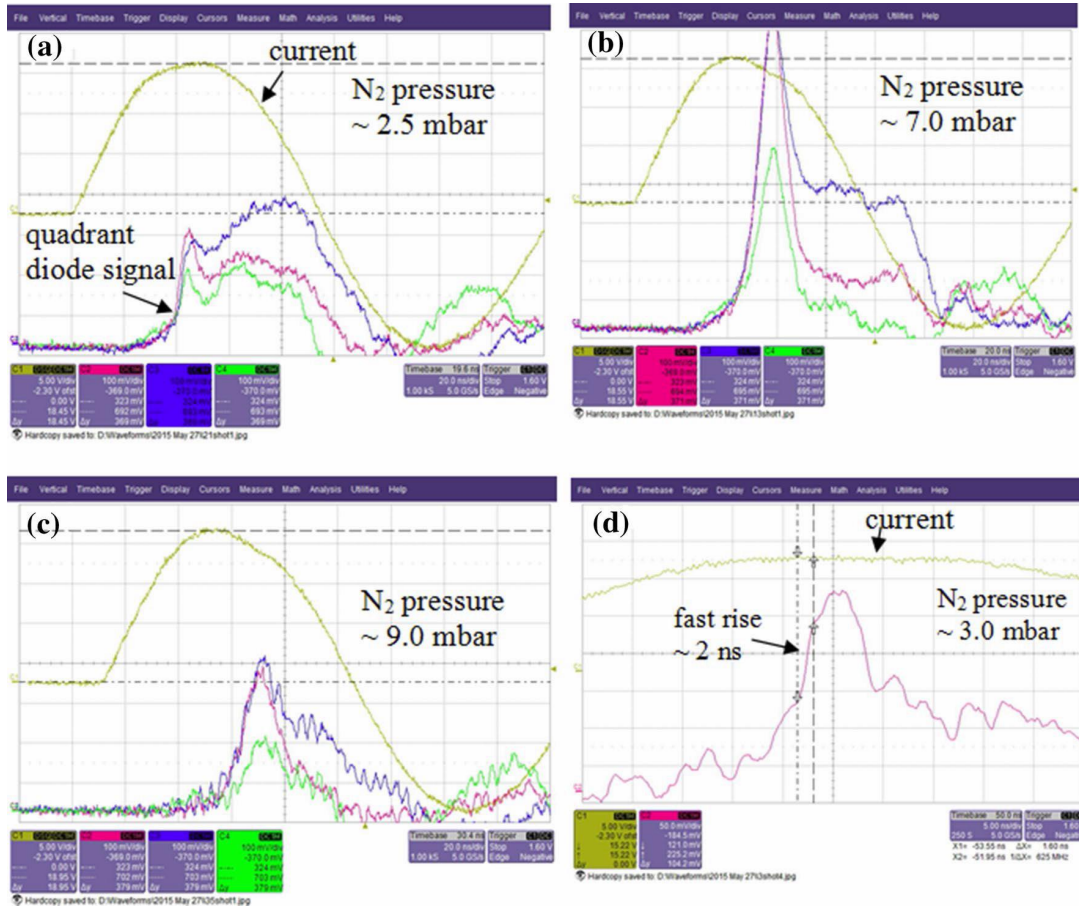


Fig.5.42: Temporal profile of the emission from nitrogen Z-pinch plasma as recorded by quadrant diode at different gas pressure: a) 2.5 mbar, b) 7.0 mbar, c) 9.0 mbar and d) 3.0 mbar (on expanded time-scale). Also, shown is the discharge current profile at each gas pressure.

instant when there is an abrupt change in the slope of the current waveform which is visible when the current profile is carefully observed. The abrupt change in the slope is the result of sudden increase in the plasma inductance when it is pinched to a minimum diameter¹¹⁵. This is a clear indication that the fast pulse is generated at the instant of pinch formation. In fact, significant and fast heating of the plasma at pinch time leads to the emission in the form of this fast pulse. The abrupt slope change in the current profile indicating the instant of pinch formation changes with the gas pressure. This behaviour is

readily reflected in the recorded profiles at different gas pressures as shown in Fig. 5.42. However, the instant of pinch formation should not be much before the peak of the discharge current otherwise the discharge will not be efficient¹⁵⁵. Furthermore, it is important for recombination pumping that the compressed plasma column should be expanded rapidly in order to facilitate cooling of the hot and dense plasma in a very fast time scale (few ns). The rapid expansion of plasma column will not be possible if the discharge current continues to increase after the plasma implosion at the axis. Keeping these facts in mind, the gas pressure has been kept beyond ~ 5 mbar to obtain pinch formation after the current peak, also shown in Fig. 5.42. It was found that the amplitude of fast pulse enhances when it occurs close to the peak of the current pulse and falls down rapidly if shifted away from the peak on either direction. Interestingly, a steep rise of ~ 2 ns has been observed at the rising edge of the fast pulse as shown in Fig. 5.42d in some specific conditions, especially at lower gas pressures. The temporal response of the detector was fast enough here to record the steep rise. There is a possibility that plasma is heated to higher temperatures if the gas pressure is small. Therefore, the recorded steep rise can be seen as very fast emission from short-lived higher charge states of nitrogen which can be achieved at small gas pressures. This had a strong dependence on the discharge current amplitude and the gas pressure. Hence, observation of such a fast edge (~ 2 ns) is very encouraging for further investigations.

Spectrographic studies were also carried out to investigate the spectrum of the emission from nitrogen Z-pinch plasma under different experimental conditions. The transmission grating spectrum was recorded by varying the gas pressures in capillary at a high discharge current of ~ 95 kA. Such a spectrum is shown in Fig. 5.43 at an optimized

gas pressure of 8.5 mbar. For better clarity, one side of the zeroth order is shown in the spectrum without loss of any information. The zeroth order recorded in the spectrum was taken as reference for zero dispersion. The binned intensity profile of the spectrum shown in Fig. 5.43 exhibits the presence of various X-ray emission lines from nitrogen Z-pinch plasma. The spectral lines have been identified from NIST atomic spectra database¹⁵⁶.

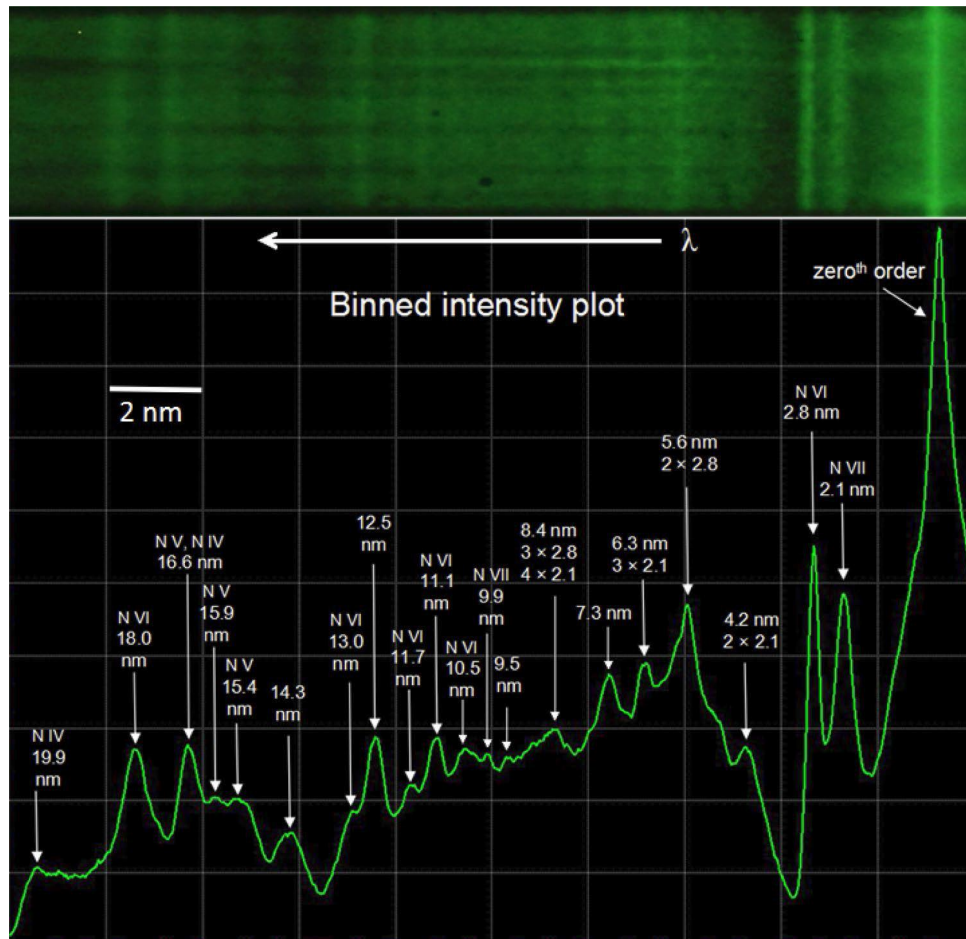


Fig.5.43: Transmission grating spectrum recorded with 95 kA peak current and 8.5 mbar gas pressure in presence of prepulse. The intensity profile of spectrum is shown in the lower portion

The presence of higher charge states of nitrogen have been revealed by the identification

of various spectral lines, especially those towards the shorter wavelength side. A closer look at the spectrum shows the presence of two dominant spectral lines, one at 2.8 nm and the other at 2.1 nm which were observed along with their several diffraction orders. Beside these, there exists various comparatively weaker lines at higher wavelengths also which corresponds to emission lines from different charge states of nitrogen. By looking at the intensity of the 2.8 nm and 2.1 nm lines, gas pressure was optimized. The emission at 2.8 nm was identified to be He- α emission from N^{5+} ion beyond doubt. However, emission at 2.1 nm was found to be little puzzling. This emission at 2.1 nm resembles with the Ly- β line of N^{6+} ion. But, interestingly there was no Ly- α emission of N^{6+} seen at 2.4 nm which is supposed to be stronger than Ly- β emission. In such a case, it was difficult to treat 2.1 nm line as Ly- β emission. The other possible match for this line was He- α emission from O^{6+} charge state of oxygen. Oxygen may enter the plasma in the form of impurity either coming from the gas itself or from the wall ablation of alumina (Al_2O_3) capillary. In order to have better understanding of the source of 2.1 nm line, different experiments were performed. Intensities of both lines (2.8 nm and 2.1 nm) were found varying with the gas pressure in the capillary. Also, when the nitrogen was replaced with argon gas under similar discharge current excitations, both lines disappeared. These experimental facts indicated that the oxygen impurity in the nitrogen gas can be a cause of 2.1 nm emission rather than the wall ablation. In order to confirm it, experiments were repeated with high purity (99.999%) nitrogen gas. But, there was no change in the intensity of the 2.1 nm line emission. Interestingly, the intensity remains same even when experiments were repeated with air having 21% oxygen and also with pure oxygen gas. This shows that the origin of this line is not linked to oxygen content in any way. In fact,

considering all the above observations carefully, it appears that the origin of 2.1 nm line emission must be linked to nitrogen only and to be more specific, Ly- β is the only possibility. However, a final confirmation requires extensive spectroscopic simulations of hot and highly dense plasma which must include all the excitation, de-excitation, ionization and recombination processes and must take into account the opacity effects also.

Role of pre-ionization on the spectrum of nitrogen Z-pinch plasma was also studied. Experiments revealed that the spectral lines at 2.8 and 2.1 nm get disappeared if there is no pre-pulse. Such a spectrum is shown in Fig. 5.44. This shows that pre-pulse is essential to achieve higher charge states of nitrogen ions. However, when the pre-pulse

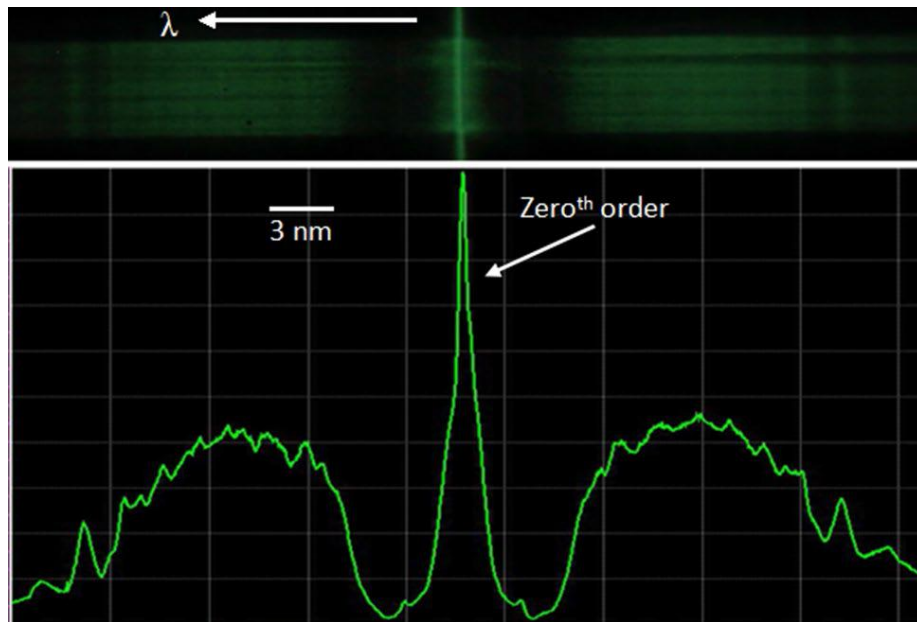


Fig.5.44: Transmission grating spectrum at 95 kA peak current and 8.5 mbar gas pressure in absence of pre-pulse. The intensity profile of spectrum is shown in the lower portion

was increased from 20 A to 120 A, no significant change was observed in the spectrum. The pre-pulse amplitude could not be increased further due to some limitations imposed

on the pre-pulse electrode geometry in our capillary discharge system. However, it is planned to explore further with a stronger pre-pulse in future. It was also found during the study that the two emission lines re-appear even without the pre-pulse at gas pressures below 3.0 mbar. This is because if the electrical driver remains the same, plasma attains a higher temperature at lower gas pressure. This higher temperature seems to be sufficient enough to produce nitrogen ions of higher charge states even in the absence of pre-pulse. It is worth to mention here that when the gas pressure was varied during the experiments, no appreciable change was observed in either the amplitude or duration of the discharge current. Below 3.0 mbar gas pressure, the most interesting observation was the faint appearance of Ly- α line of N⁶⁺ ion at 2.47 nm as shown in [Fig. 5.45](#). This points out that higher temperature of plasma is achieved at these conditions which is sufficient enough to form N⁶⁺ charge state of nitrogen.

An estimation of plasma density requires here precise measurement of diameter of pinch plasma using time-resolved X-ray pin-hole imaging. Such experiments will be done in near future. However, an estimate of density can be obtained from the compression ratio of the plasma taking to be 1:100 as is observed in various studies^{135,136,157}. This value, however, is an underestimation as the discharge current amplitude is much higher in the present experiments. Filling gas pressure of 3.0 mbar corresponds to a nitrogen density of $1.4 \times 10^{17} \text{ cm}^{-3}$. Assuming the average charge state of nitrogen to be $z \sim 5$ (under-estimated), the electron density is approximately estimated to be $7.2 \times 10^{19} \text{ cm}^{-3}$ at the compressed condition. In the similar fashion, the gas pressure of 8.5 mbar corresponds to an approximate electron density of $2.0 \times 10^{20} \text{ cm}^{-3}$. The actual electron density may be higher than what is estimated here. It is worth to mention here that

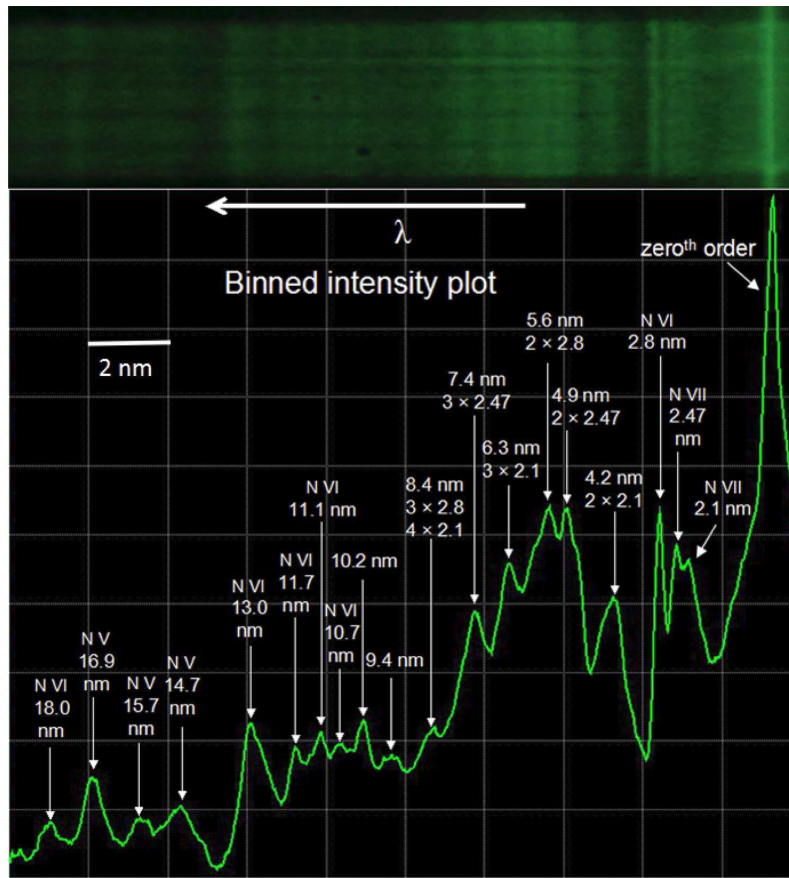


Fig.5.45: Transmission grating spectrum at 95 kA peak current and 2.0 mbar gas pressure in presence of pre-pulse. The intensity profile of spectrum is shown in the lower figure.

Nevrkla et al¹⁵⁷ measured a temperature of ~ 90 eV from spectroscopic simulation with a comparatively larger gain-volume and smaller peak current. Same is the case in report by Gissis et al¹³⁶ where electron temperature of $\sim 75 - 85$ eV was estimated. Since, the experiments described here have utilized comparatively higher and faster electrical driver to pump energy in a smaller gain volume, it is expected that the plasma temperature reached in these experiments are higher than what was achieved in those reports. Nevertheless, a detailed spectroscopic simulation will be required in future to estimate the plasma conditions more precisely.

Observation of Ly- α emission at smaller gas pressure is also well supported by the

appearance of a fast signal (~ 2 ns rise-time) in the temporal profile recorded by vacuum diode as described earlier. It is highly desirable to look for the experimental conditions where the intensity of Ly- α emission becomes stronger because this will point towards achieving fully ionized state of nitrogen (N^{7+}). However, it is not possible to reduce the gas pressure below a certain limit as ion density will become insufficient to produce any detectable intensity in Ly- α emission. Also, lowering the gas pressure decreases the pinch time for a fixed current profile as shown in Fig. 5.42 and if the pinch time becomes substantially smaller than the quarter period of the current, the discharge will not be seen as efficient¹⁵⁵. An efficient discharge demands pinch formation to be close to the peak of the current. In principle, this condition can still be fulfilled with lower gas pressure if one uses a capillary with larger inner diameter as it will compensate for the decrease in pinch time. However, this arrangement will have another issue. It would be difficult to maintain the uniformity of such larger diameter plasma column during the axial compression. However, there exists another option. Instead of using higher ID capillary, one can use a smaller ID capillary and the discharge current can be made faster such that its quarter period (few ns) would become comparable to the pinch time making the discharge still efficient. In this context, it would be worth mentioning recent results by Avaria et al¹⁵⁸ in which an experimental confirmation is provided for achieving homogeneous plasma columns with ionization levels typical of mega-ampere discharges. Such ionization levels were obtained by rapidly heating gas-filled channels of small diameter i.e. ~ 520 μm utilizing current pulses of nanosecond rise time and moderate amplitude of ~ 40 kA.

5.4 Exploring X-ray lasing in Carbon Z-pinch plasma

Since carbon is a low Z element as compared to nitrogen, its higher ionization is relatively easier to obtain. Therefore, an effort has been made here to investigate the possible X-ray lasing at 18.2 nm in C^{5+} ion utilizing the upgraded capillary discharge system 'Version 3'. The lasing transition at 18.2 nm in carbon corresponds to Balmer- α transition in H-like carbon ion i.e. C^{5+} ion and is based on recombination pumping scheme which demands creation of fully ionized carbon ion i.e. C^{6+} in abundance followed by 3-body recombination of one electron to the outer shell of C^{6+} ion to form C^{5+} ion leading to required population inversion. This lasing was demonstrated in very early stages of development of capillary discharge systems for X-ray lasing. However, it was not very successful due to very small gain-length¹¹¹. That was a kind of ablative discharge where the carbon as gain medium was obtained with ablation from capillary inner wall which was made of carbon containing material. Such discharges were suffered from serious problem of in-homogeneity of plasma column and poor control on the plasma density leading to small gain-length. Keeping these developments in mind, experiments were performed here using C_2H_2 gas in the capillary to provide the required carbon atoms with a good control over the gas density. The experimental details and their outcomes are explained in the next section.

5.4.1 Initial experiments in C_2H_2 filled capillary and results

Alumina capillary of 2.8 mm inner diameter and 96 mm length was filled with acetylene gas and subjected to the fast and high discharge current ~ 90 kA with quarter period ~ 46 ns delivered by the upgraded capillary discharge system (version 3). The temporal profile of the emission from carbon Z-pinch plasma was recorded with vacuum

diode. Keeping the amplitude of the discharge current fixed, the gas pressure was varied from 0.1 mbar to 6.0 mbar. A prepulse current in the range from 50 - 130 A was used few microseconds before the main discharge current in order to pre-ionize the gas. There was no significant change observed in the diode signal while varying the prepulse amplitude. A typical diode signal is shown in Fig. 5.46. However, very interesting observation was made in the diode signal when the prepulse was switched off. In absence of prepulse, a fast pulse of few ns was observed in the diode signal even at higher gas pressures. This is shown in Fig. 5.47. In order to further investigate the carbon discharge plasma, experiments were carried out to record its spectrum using transmission grating spectrograph in a similar way as was done with nitrogen plasma. Effect of gas pressure and the pre-pulse on the carbon spectrum was studied. Gas pressure in the capillary was

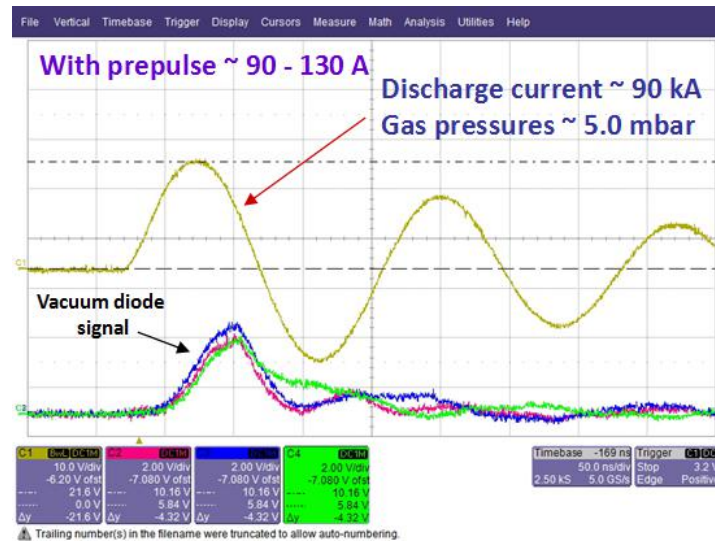


Fig.5.46: Temporal profile of emission from carbon Z-pinch plasma in presence of prepulse

varied in presence of pre-pulse having amplitude in the range from 50 to 130 A. No appreciable change in the spectrum was seen as a result of this variation in gas pressure.

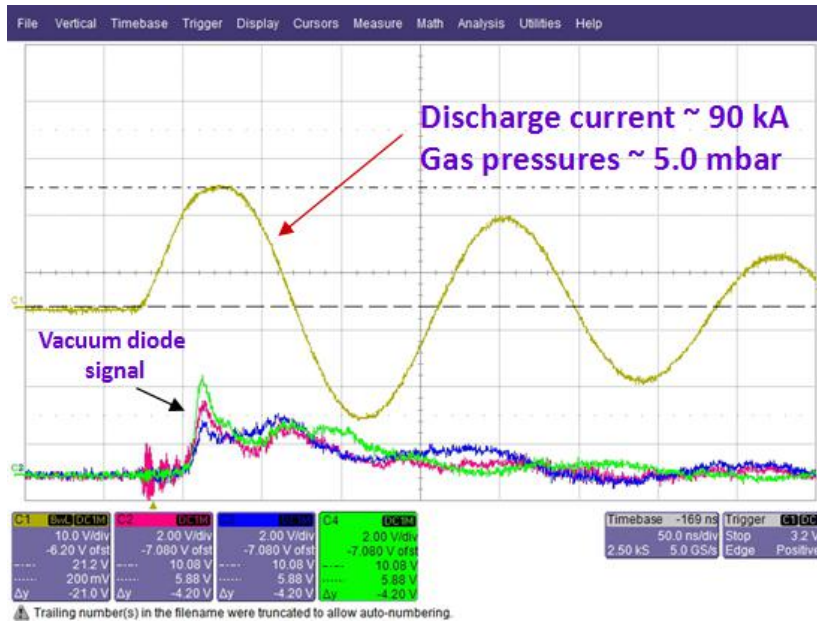


Fig.5.47: Temporal profile of emission from carbon Z-pinch plasma in absence of prepulse

A band of emission in the wavelength range from 5 to 8 nm was observed, as shown in Fig. 5.48a. However, when the pre-pulse was switched off, two strong line emissions were observed in the spectrum as shown in Fig. 5.48b. These line emissions were identified to be He- α and Ly- α emission of carbon at 4.0 nm and 3.4 nm respectively. These emissions confirm the presence of He-like C i.e. C^{4+} ion and H-like C i.e. C^{5+} ion in the plasma. Unlike nitrogen plasma, here the presence of Ly- α emission was observed even at higher gas pressures e.g. 5 - 6 mbar. The repeatability of these observations were confirmed by taking several number of shots. The occurrence of these two line emissions can be easily correlated to the previous observation of fast pulse of few ns in the diode signal when the prepulse was switched off. Further experiments are required to understand the dynamics of carbon discharge plasma.

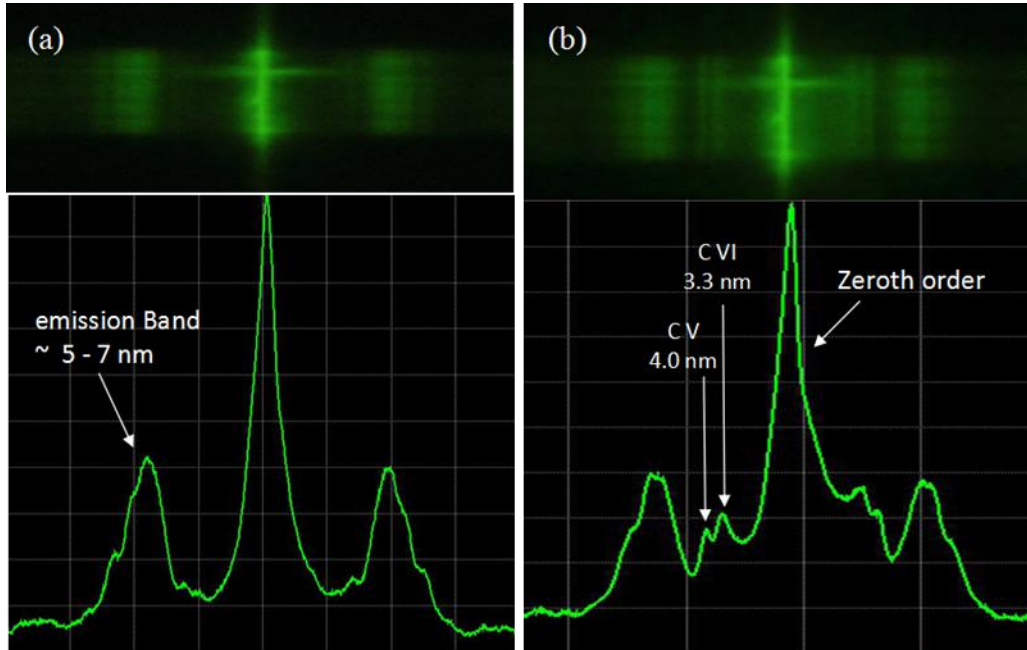


Fig.5.48: Transmission grating spectrum of carbon Z-pinch plasma at ~ 90 kA peak discharge current and gas pressure of 5.0 mbar (a) in presence of prepulse and, (b) in absence of prepulse

5.5 Exploring X-ray lasing in Krypton Z-pinch plasma

Krypton has a possible lasing transition at 32.8 nm in Ni-like ionization state i.e. in Ni^{8+} based on electron collisional excitation pumping. The mechanism of lasing is quite similar to that of Ne-like Ar. The only difference lies in the fact that here Ni-like closed shell is the ground state instead of Ne-like state. Since, ionization energy required to create Kr^{8+} state is comparable to that required for Ar^{8+} , it seems that the formation of lasing species Kr^{8+} is quite possible with our capillary discharge system. Hence, experiments were also planned to explore lasing in Ni-like Kr ion.

5.5.1 Initial experiments in Kr filled capillary and results

Experiments were performed to explore the possibility of X-ray lasing in Ni-like

Kr ions using fast capillary discharge scheme. Temporal as well as spectroscopic study of Kr plasma were carried out at different discharge currents of ~ 85 kA, 65 kA and 53 kA with ~ 46 ns as quarter period. Gas pressure in the capillary was varied from 0.05 mbar to 0.5 mbar and prepulse current was varied from 20 A to 100 A. In the temporal profile, fast pulse of ~ 3.5 ns rise-time was detected at smaller gas pressures ~ 0.1 to 0.18 mbar apart from the pinch signal as shown in Fig. 5.49. At higher pressures, this fast emission gets disappeared and the amplitude of pinch signal continue to increase. In the spectroscopic study, identification of different line emissions from Kr plasma revealed the formation of different charge states of Kr like Kr^{7+} , Kr^{8+} and Kr^{9+} . However, no emission at 32.8 nm was observed. The presence of Kr^{9+} indicated that the plasma is over-ionized as Kr^{8+} is

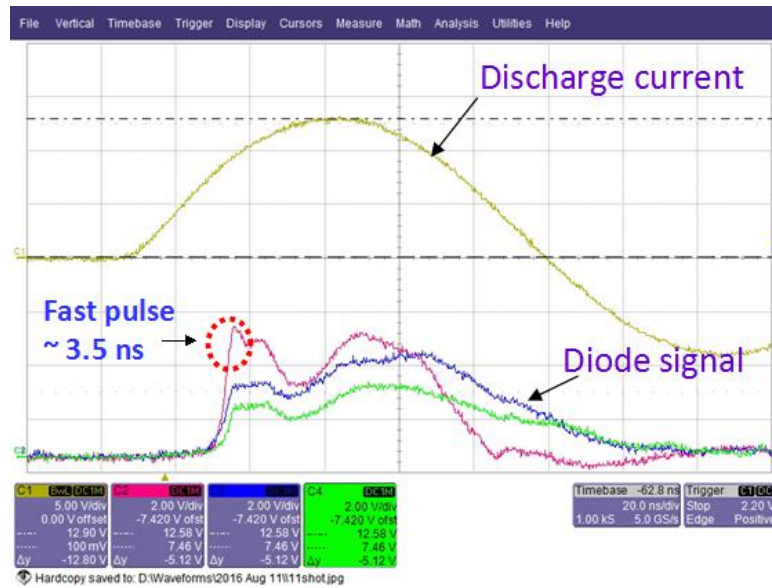


Fig.5.49: Temporal profile of Krypton Z-pinch plasma at ~ 53 kA peak current and gas pressure of 0.13 mbar

the lasing species. For this, the discharge current was successively reduced from 85 kA to 65 kA and then to ~ 53 kA to reduce the temperature of plasma. A spectrum of krypton

Z-pinch plasma recorded at ~ 53 kA is shown in Fig. 5.50. The existence of 9.2 nm emission line still confirms the presence of Kr^{9+} ion. In order to further suppress the formation of Kr^{9+} , the gas pressure was kept at maximum possible gas pressure of 0.4

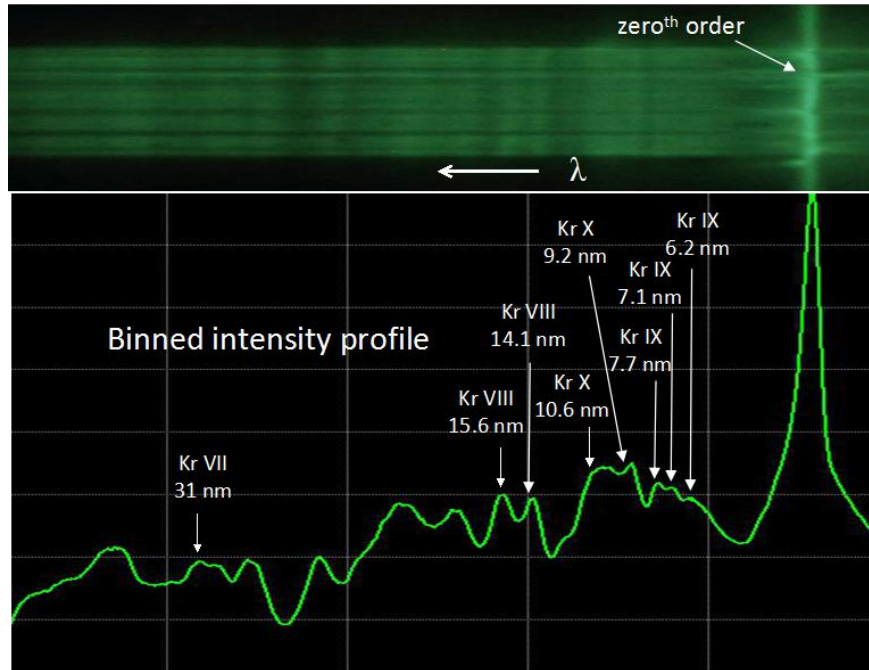


Fig.5.50: Spectrum of Krypton Z-pinch plasma at ~ 53 kA peak current and gas pressure of 0.13 mbar

mbar and the discharge current was reduced to 25 kA. Even in these conditions, plasma line corresponding to Kr^{9+} ion is still present indicating that current should go further down. Such studies are first of its kind with discharge created Kr plasma where Kr atoms were found to be over-ionized than required for lasing. However, practical difficulties were felt in reducing the discharge current below 25 kA from the existing capillary discharge system which was designed for higher current. Hence, experiment could not be performed at such lower currents. However, experiments with such low current will be performed in future to explore the lasing in Ni-like Kr ion.

In summary, the experiments described in this chapter have shown that although the capillary discharge system was upgraded to provide a powerful electrical driver (peak current ~ 95 kA, $T_{1/4} \sim 46$ ns) to pump nitrogen plasma, it was not sufficient enough to produce the fully ionized nitrogen ion. Even H-like N state was not found to be present in the plasma at higher gas pressures (above 5 mbar). It formed only when the gas pressures was reduced below 3.0 mbar. These facts point out that plasma temperature needs to be raised still higher to get fully ionized nitrogen ions and it must be achieved at higher gas pressures to get sufficient density required for recombination pumping of H-like N ion. Experiments revealed that H-like state were formed in carbon even at higher gas pressure unlike nitrogen. This is because carbon is a low Z element than nitrogen and hence requires relatively smaller energy for ionization. However, the electrical driver used here seems to be still insufficient to get the lasing species in abundance. Conditions for lasing in Ni-like Kr are likely to be in reach of the electrical driver as seen from the experiments. It requires further optimization of experimental parameters at smaller current.

CHAPTER 6: SUMMARY AND FUTURE OUTLOOK

In the present thesis work, experimental investigations have been carried out in the area of coherent soft X-ray generation from highly ionized plasmas driven by fast capillary discharge. Using the indigenously developed capillary discharge system, soft X-ray laser at 46.9 nm was successfully realized in argon discharge plasma and characterized for its various properties. The output energy and the gain-coefficient of this laser were significantly enhanced by studying the effect of discharge current profile which is normally seen as the parameter difficult to be changed in capillary discharge system. The studies with 46.9 nm soft X-ray laser have provided inputs which were culminated into the development of a very compact and easily portable version of this laser operating in repetitive mode. Significant experimental efforts were also put in to explore X-ray lasing in comparatively shorter wavelength using different gas media. Such X-ray lasing has not been realized so far anywhere in the world using discharge produced plasmas. The studies conducted in this thesis work towards shorter wavelength X-ray lasing led to some important conclusions and provided greater insights in the area which will certainly help in future endeavour in this direction.

6.1 Summary of the important results

Soft X-ray lasing in argon plasma at 46.9 nm was achieved with fast capillary discharge system. In-depth studies of temporal, spectral and spatial characteristics of this laser were performed using various diagnostic tools and detectors. The temporal profile recorded with a vacuum diode measured a distinct laser peak with a pulse width of ~ 1.2 ns (FWHM). The spatial profile measurement indicated that the soft X-ray laser beam has

good directionality with a divergence smaller than 3.5 mrad. The spectral studies of the laser beam confirmed the intense lasing line emission at 46.9 nm with its diffraction orders as high as upto 10th orders were recorded. Young's double slit interference experiments were conducted to test and measure the coherence of the soft X-ray laser beam. Spatial coherence length was estimated from the high contrast interference fringes obtained with these experiments. This capillary discharge soft X-ray laser is running in single shot mode. Due to involvement of high voltage (few hundreds of kV) and high current (few tens of kA), it was not possible to operate it into repetitive mode. Therefore, experiments were made to reduce the voltage and current as low as possible and obtain laser at the same time. This study played crucial role in the development of a very compact and portable version of this laser presently running at 0.1 Hz repetition rate which requires very small voltage of ~ 60 kV and current ~ 18 kA to obtain the lasing.

The important role of rate of rise of discharge current (dI/dt) on the output of this soft X-ray laser at 46.9 nm was experimentally established. Through experiments, it was shown that the requirement of high peak current can be relaxed significantly if dI/dt is sufficiently high. In fact, the study shows that dI/dt has a much important role to play rather than the peak value of the current to get higher energy laser pulses. By increasing the value of the dI/dt , the laser energy was enhanced from 2.0 to 4.0 μ J. Another interesting fact was revealed that mere increase in the peak current will not be sufficient to increase the laser pulse energy, unless the dI/dt value is also increased.

Experimentally, it has been shown for the first time in the soft x-ray laser based on fast capillary discharge that faster current excitation of pinch plasma can significantly enhance the efficiency of the laser. It was found that the gain-coefficient of the 46.9 nm

X-ray laser increases from 0.69 cm^{-1} to 1.02 cm^{-1} , i.e. an increase of $\sim 48\%$, if the current is made faster i.e. the quarter period of the current pulse is reduced from $\sim 72 \text{ ns}$ to $\sim 60 \text{ ns}$ keeping the amplitude fixed. Also, through a series of experiments, it was revealed that the higher gain-coefficient requires optimum discharge current amplitude and can be further enhanced to 1.33 cm^{-1} by such optimization. This gain-coefficient is $\sim 93\%$ higher than 0.69 cm^{-1} which was obtained with a slower discharge current with quarter period of $\sim 72 \text{ ns}$.

Experimental studies were conducted in depth with an aim to extend the soft X-ray lasing towards much shorter wavelength than 46.9 nm . In this direction, high and fast discharge current having $\sim 95 \text{ kA}$ amplitude and 46 ns quarter period was used to excite nitrogen plasma for exploring X-ray lasing at 13.4 nm using three-body recombination scheme. As signature of pinch emission, a dominant fast pulse ($5\text{--}8 \text{ ns}$ rise time) was recorded with vacuum diode after optimization of nitrogen gas pressure in the capillary. Much faster pulses with rise time ($\sim 2 \text{ ns}$) were also observed at smaller gas pressures. The spectroscopic study undertaken at these fast and large current excitations clearly revealed strong emission of He- α line at 2.8 nm and another spectral line at 2.1 nm , along with various plasma emission lines of different ionization states of nitrogen. The potential Ly- α spectral line of N^{6+} at 2.4 nm could not be observed at higher gas pressures. However, its faint signature was visible when the gas pressure was decreased significantly, stressing on the need of further heating of nitrogen plasma for generation of higher charge states, i.e. N^{6+} and N^{7+} in abundance. The role of the pre-pulse was also studied and found to be very important in achieving higher ionization states. This indicated the requirement of a stronger pre-pulse. A higher and faster current pulse at smaller gas pressures with

smaller diameter capillary seems to have large potential towards demonstration of recombination X-ray lasing at 13.4 nm in nitrogen Z-pinch plasma.

Experiments with acetylene gas were carried out to investigate carbon Z-pinch plasma to explore soft X-ray lasing at 18.2 nm. As carbon is a low Z element than nitrogen, it requires relatively smaller pump energy to achieve the required H-like C ion (C^{5+}). Experiments done with large and fast current, similar to nitrogen, revealed the formation of H-like C ion even at higher gas pressure regime but still found to be insufficient to produce intense Ly- α emission which is a step forward towards achieving fully ionized state of carbon.

Experiments were also performed with Krypton gas which have shown encouraging results. Krypton has a soft X-ray lasing transition at 32.8 nm in Ni-like Kr ion just as 46.9 nm in Ne-like Ar ion. In the experiments, it was seen that Kr ions are over-ionized to Kr^{9+} even with a very small discharge current of 25 kA with ~ 46 ns quarter period. Since, the conditions required to form the lasing species (Kr^{8+}) seems to be quite within reach, parameters can be optimized at smaller discharge current to facilitate formation of lasing species in abundance.

6.2 Future outlook

In the area of 46.9 nm soft X-ray laser, a compact and portable version running at 0.1 Hz repetition rate has already been demonstrated. There is a good possibility to improve its repetition rate to few Hz with few μJ energy per pulse. The size of the system on a small trolley is not more than 0.4 m \times 0.4 m with all its required components and sub-systems placed inside the trolley. Such a compact and repetitive soft X-ray laser has potential applications in laboratory scale setup in very wide range of areas which have

been described under chapter 1. Experiments will be made in future to use the system in nano-patterning and interferometric lithography applications. Another potential application in future is to use the laser to probe high density plasma generated in ultra-short and ultra-intense laser plasma interaction experiments.

In the area of generation of shorter wavelength X-ray laser from capillary discharge plasmas, experiments are planned to be conducted with nitrogen and carbon (using carbon-containing gases) Z-pinch plasmas using capillaries of different ID. These experiments will bring greater insights on the further road-map as to which path will be more beneficial out of two potential available options to get intense Ly- α emission. One option is using higher ID capillary with present current pulse duration and the other is smaller ID capillary with very fast (few ns) current pulse, with both options satisfying the condition of efficient discharge. Considering the recent result reported by Avaria et al¹⁵⁸, the later option seems to be more promising towards achieving very high ionization state required for shorter wavelength X-ray lasing. The use of smaller ID capillary in the later option will have additional advantage of faster cooling of plasma for recombination pumping due to close proximity of capillary wall with the pinch plasma.

In the experiments done with krypton gas to explore 32.8 nm lasing, encouraging results have been obtained. Experiments have revealed the presence of over-ionized krypton ion i.e. Kr⁹⁺ in the krypton plasma excited by moderate amplitude of discharge current. Therefore, it will be exciting to explore the lasing conditions in krypton at much smaller discharge current with optimization of various experimental parameters in future.

REFERENCES

- ¹ C.A. Brewer, F. Brizuela, P. Wachulak, D.H. Martz, W. Chao, E.H. Anderson, D.T. Attwood, A.V. Vinogradov, I.A. Artyukov, A.G. Ponomareko, V.V. Kondratenko, M.C. Marconi, J.J. Rocca, C.S. Menoni, *Opt. Lett.* **33**, 518 (2008)
- ² I. Kuznetsov, J. Filevich, F. Dong, M. Woolston, W. Chao, E.H. Anderson, E.R. Bernstein, D.C. Crick, J.J. Rocca, C.S. Menoni, *Nat. Commun.* **6**, 6944 (2015)
- ³ M. Purvis, J. Grava, J. Filevich, M.C. Marconi, J. Dunn, S.J. Moon, V.N. Shlyaptsev, E. Jankowska, J.J. Rocca, *Phys. Rev. E* **76**, 046402 (2007)
- ⁴ L. Urbanski, A. Isoyan, A. Stein, J.J. Rocca, C.S. Menoni, M.C. Marconi, *Opt. Lett.* **37**, 3633 (2012)
- ⁵ M.C. Marconi, P.W. Wachulak, *Prog. Quant. Elect.* **34**, 173 (2010)
- ⁶ P.W. Wachulak, M.C. Marconi, R.A. Bartels, C.S. Menoni, J.J. Rocca, *J. Opt. Soc. Am. B* **25**, 1811 (2008)
- ⁷ E. Novakova, L. Vysin, T. Burian, L. Juha, M. Davidkova, V. Mucka, V. Cuba, M.E. Grisham, S. Heinbuch, J.J. Rocca, *Phys. Rev. E* **91**, 042718 (2015)
- ⁸ M. Wieland, C. Spielmann, U. Kleineberg, T. Westerwalbesloh, U. Heinzmann, and T. Wilhein, *Ultramicroscopy* **102**, 93 (2005)
- ⁹ R. L. Sandberg, A. Paul, D. A. Raymondson, S. Hädrich, D. M. Gaudiosi, J. Holtsnider, R. I. Tobey, O. Cohen, M. M. Murnane, H. C. Kapteyn, C. Song, J. Miao, Y. Liu, and F. Salmassi, *Phys. Rev. Lett.* **99**, 098103 (2007)
- ¹⁰ P. A. C. Takman, H. Stollberg, G. A. Johansson, A. Holmberg, M. Lindblom, and H. M. Hertz, *J. Microsc.* **226**, 175 (2007)
- ¹¹ M. Kishimoto, M. Tanaka, R. Tai, K. Sukegawa, M. Kado, N. Hasegawa, H. Tang, T. Kawachi, P. Lu, K. Nagashima, H. Daido, Y. Kato, K. Nagai, and H. Takenaka, *J. Phys. IV* **104**, 141 (2003)
- ¹² G. Vaschenko, F. Brizuela, C. Brewer, M. Grisham, H. Mancini, C. S. Menoni, M. C. Marconi, J. J. Rocca, W. Chao, J. A. Liddle, E. H. Anderson, D. T. Attwood, A. V. Vinogradov, I. A. Artioukov, Y. P. Pershyn, and V. V. Kondratenko, *Opt. Lett.* **30**, 2095 (2005)
- ¹³ F. Brizuela, G. Vaschenko, C. Brewer, M. Grisham, C. S. Menoni, M. C. Marconi, J. J. Rocca, W. Chao, J. A. Liddle, E. H. Anderson, D. T. Attwood, A. V. Vinogradov, I. A. Artioukov, Y. P. Pershyn, and V. V. Kondratenko, *Opt. Express* **13**, 3983 (2005)
- ¹⁴ G. Vaschenko, C. Brewer, E. Brizuela, Y. Wang, M. A. Larotonda, B. M. Luther, M. C. Marconi, J. J. Rocca, and C. S. Menoni, *Opt. Lett.* **31**, 1214 (2006)
- ¹⁵ Takashi Kimura, Yasumasa Joti, Akemi Shibuya, Changyong Song, Sangsoo Kim, Kensuke Tono, Makina Yabashi, Masatada Tamakoshi, Toshiyuki Moriya, Tairo Oshima, Tetsuya Ishikawa, Yoshitaka Bessho and Yoshinori Nishino, *Nat. Commun.* **5**, 3052 (2014)
- ¹⁶ V. Pelletier, K. Asakawa, M.S. Wu, D. H. Adamson, R. A. Register and P. M. Chaikin, *Applied Physics*

-
- Letters **88**, 211114 (2006)
- ¹⁷ E.E. Scime, E.H. Anderson, D.J. McComas and M. L. Schattenburg, *Applied Optics* **34**, 648 (1995)
- ¹⁸ G.A. Baker and D.S. Moore, *Analytical and Bioanalytical Chemistry* **382**, 1751 (2005)
- ¹⁹ R. Zia, J.A. Schuller, A. Chandran and M. L. Brongersma, *Materials Today* **9**, 20 (2006)
- ²⁰ J.J. Baumberg, T.A. Kelf, Y. Sugawara, S. Cintra, M. E. Abdelsalam, P. N. Barlett and A. E. Russell, *Nano Letters* **5**, 2262 (2005)
- ²¹ M. Campbell, D.N. Sharp, M.T. Harrison, R. G. Denning and A. J. Tuberfield, *Nature* **404**, 53 (2000)
- ²² W.J. Fan, S. Zhang, K.J. Malloy and S. R. J. Brueck, *Journal of Vacuum Science & Technology B* **23**, 2700 (2005)
- ²³ L.J. Heyderman, H.H. Solak, C. David, D. Atkinson, R. P. Cowburn and F. Nolting, *Applied Physics Letters* **85**, 4989 (2004)
- ²⁴ S.Y. Chou and P.R. Krauss, *Journal of Applied Physics* **79**, 5066 (1996)
- ²⁵ F.B. Mancoff, N.D. Rizzo, B.N. Engel and S. Tehrani, *Nature* **437**, 393 (2005)
- ²⁶ M. G. Capeluto, G. Vaschenko, M. Grisham, M. C. Marconi, S. Luduena, L. Pietrasanta, Y. F. Lu, B. Parkinson, C. S. Menoni and J. J. Rocca, *IEEE Trans. Nanotechnol.* **5**, 3 (2006)
- ²⁷ P. W. Wachulak, M. G. Capeluto, M. C. Marconi, C. S. Menoni, and J. J. Rocca, "Patterning of nano-scale arrays by table-top extreme ultraviolet laser interferometric lithography," *Opt. Express* **15**, 3465 (2007)
- ²⁸ P.W. Wachulak, M. Grisham, S. Heinbuch, D. Martz, W. Rockward, D. Hill, J. J. Rocca, C. S. Menoni, E. Anderson and M. Marconi, *J. Opt. Soc. Am. B* **25**, B104 (2008)
- ²⁹ C. Jacobsen and M. Howells, *Journal of Vacuum Science & Technology B* **10**, 3177 (1992)
- ³⁰ C. Jacobsen and M.R. Howells, *Journal of Applied Physics* **71**, 2993 (1992)
- ³¹ A. Isoyan, Y.C. Cheng, F. Jiang, J. Wallace, F. Cerrina and S. Bollepalli, *Journal of Vacuum Science & Technology B* **25**, 2145 (2007)
- ³² M.R. Howells and C. Jacobsen, *Applied Optics* **30**, 1580 (1991)
- ³³ A. Isoyan, F. Jiang, Y.C. Cheng, P. Wachulak, L. Urbanski, J.J. Rocca, C.S. Menoni, M.C. Marconi and F. Cerrina, *SPIE Proceedings* **7271**, 72713O (2009)
- ³⁴ L. B. Da Silva, T. W. Barbee, Jr., R. Cauble, P. Celliers, D. Ciarlo, S. Libby, R. A. London, D. Matthews, S. Mrowka, J. C. Moreno, D. Ress, J. E. Trebes, A. S. Wan and F. Weber, *Phys. Rev. Lett.* **74**, 3991 (1995)
- ³⁵ A. S. Wan, T. W. Barbee, Jr., R. Cauble, P. Celliers, L. B. Da Silva, J. C. Moreno, P. W. Rambo, G. F. Stone, J. E. Trebes, and F. Weber, *Phys. Rev. E* **55**, 6293 (1997)
- ³⁶ Jorge Filevich, Jorge J. Rocca, Mario C. Marconi, Raymond F. Smith, James Dunn, Roisin Keenan, James R. Hunter, Stephen J. Moon, Joseph Nilsen, Andrew Ng and Vyacheslav N. Shlyaptsev, *Applied Optics*, **43**, 3938 (2004)
- ³⁷ P. Celliers, F. Weber, L. B. Da Silva, T. W. Barbee, Jr., R. Cauble, A. S. Wan and J. C. Moreno, *Opt. Lett.* **20**, 1907 (1995)

-
- ³⁸ J. J. Rocca, C. H. Moreno, M. C. Marconi and K. Kanizay, *Opt. Lett.* **24**, 420 (1999)
- ³⁹ C. H. Moreno, M. C. Marconi, K. Kanizay, J. J. Rocca, Y. A. Uspenskii, A. V. Vinogradov and Y. A. Pershin, *Phys. Rev. E* **60**, 911 (1999)
- ⁴⁰ J. Filevich, K. Kanizay, M. C. Marconi, J. L. A. Chilla and J. J. Rocca, *Opt. Lett.* **25**, 356 (2000)
- ⁴¹ S. M. Vinko, et al., *Nature* **482**, 59 (2012)
- ⁴² J. Feldhaus, J. Arthur and J.B. Hastings, *J. Phys. B* **38**, S799 (2005)
- ⁴³ C. Winterfeldt, C. Spielmann and G. Gerber, *Rev. Mod. Phys.* **80**, 117 (2008)
- ⁴⁴ D.H. Martz, D. Alessi, B.M. Luther, Y. Wang, D. Kemp, M. Berrill and J.J. Rocca, *Opt. Lett.* **35**, 1632 (2010)
- ⁴⁵ J. Dunn, Y. Li, A.L. Osterheld, J. Nilsen, J.R. Hunter and V.N. Shlyaptsev, *Phys. Rev. Lett.* **84**, 4834 (2000)
- ⁴⁶ T. Kawachi, M. Kado, M. Tanaka, A. Sasaki, N. Hasegawa, A.V. Kilpio, S. Namba, K. Nagashima, P. Lu, K. Takahashi, H. Tang, R. Tai, M. Kishimoto, M. Koike, H. Daido and Y. Kato, *Phys. Rev. A* **66**, 033815 (2002)
- ⁴⁷ Y. Wang, M.A. Larotonda, B.M. Luther, D. Alessi, M. Berrill, V.N. Shlyaptsev and J.J. Rocca, *Phys. Rev. A* **72**, 053807 (2005)
- ⁴⁸ H.T. Kim, I.W. Choi, N. Hafz, J.H. Sung, T.J. Yu, K.H. Hong, T.M. Jeong, Y.C. Noh, D.K. Ko, K.A. Janulewicz, J. Tummler, P.V. Nickles, W. Sandner and J. Lee, *Phys. Rev. A* **77**, 023807 (2008)
- ⁴⁹ J.J. Rocca, V. Shlyaptsev, F.G. Tomasel, O.D. Cortazar, D. Hartshorn and J.L.A. Chilla, *Phys. Rev. Lett.* **73**, 2192 (1994)
- ⁵⁰ J.J. Rocca, *Rev. Sci. Instrum.* **70**, 3799 (1999)
- ⁵¹ G. Tomassetti, A. Ritucci, A. Reale, L. Palladino, L. Reale, S.V. Kukhlevsky, F. Flora, L. Mezi, A. Faenov, T. Pikuz and A. Gaudieri, *Opt. Commun.* **231**, 403 (2004)
- ⁵² Y. Liu, M. Seminario, F.G. Tomasel, C. Chang, J.J. Rocca and D.T. Attwood, *Phys. Rev. A* **63**, 033802 (2001)
- ⁵³ H. Tanaka, et al., *Nat. Photonics* **6**, 540 (2012)
- ⁵⁴ B. W. J. McNeil and N. R. Thompson, *Nat. Photonics* **4**, 814 (2010)
- ⁵⁵ J. M. J. Madey, *J. Appl. Phys.* **42**, 1906 (1971)
- ⁵⁶ L. R. Elias, W. M. Fairbank, J. M. J. Madey, H. A. Schwettman and T. I. Smith, *Phys. Rev. Lett.* **36**, 717 (1976)
- ⁵⁷ D. A. G. Deacon, L. R. Elias, J. M. J. Madey, G. J. Ramian, H. A. Schwettman, and T. I. Smith, *Phys. Rev. Lett.* **38**, 892 (1977)
- ⁵⁸ P. Emma, et al., *Nature Photon.* **4**, 641 (2010)
- ⁵⁹ M. Altarelli, *Nucl. Instrum. Methods* **B269**, 2845 (2011)
- ⁶⁰ T. Ishikawa, et al., *Nat. Photonics* **6**, 540 (2012)
- ⁶¹ W. Ackermann, et al., *Nat. Photonics* **1**, 336 (2007)
- ⁶² E. Allaria, et al., *Nat. Photonics* **6**, 699 (2012)

-
- ⁶³ J. N. Galayda, Proceedings of the 2014 International Particle Accelerator Conference, Dresden, Germany, p. 935 (2014) [<http://accelconf.web.cern.ch/AccelConf/IPAC2014/papers/tuoca01.pdf>]
- ⁶⁴ M. Bellini, C. Lynga, A. Tozzi, M. Gaarde, T. Hänsch, A. L’Huillier and C. G. Wahlström, Phys. Rev. Lett. **81**, 297 (1998)
- ⁶⁵ C. Lyna, M. Gaarde, C. Delfin, M. Bellini, T. Hänsch, A. L’Huillier and C. G. Wahlström, Phys. Rev. A **60**, 4823 (1999)
- ⁶⁶ P. Salières, A. L’Huillier, P. Antoine and M. Lewenstein, Adv. At. Mol. Opt. Phys. **41**, 83 (1999)
- ⁶⁷ J. Terschläsen, M. Asgaker, M. Svanqvist, S. Plogmaker, J. Nordgren, J. E. Rubensson, H. Siegbahn and J. Söderström, Nucl. Instrum. Methods Phys. Res. A **768**, 84 (2014)
- ⁶⁸ C. Benko, T. Allison, A. Cingöz, L. Hua, F. Labaye, D. Yost and J. Ye, Nat. Photon. **8**, 530 (2014)
- ⁶⁹ T. Popmintchev et al, Science **336**, 1287 (2012)
- ⁷⁰ F. Silva, M. S. Teichmann, S. L. Cousin, M. Hemmer and J. Biegert, Nat. Commun. **6**, 6611 (2015)
- ⁷¹ F. Calegari, G. Sansone, S. Stagira, C. Vozzi and M. Nisoli, J. Phys. B: At. Mol. Opt. Phys. **49**, 062001 (2016)
- ⁷² A. McPherson, G. Gibson, H. Jara, U. Johann, T. S. Luk, I. A. McIntyre, K. Boyer and C. K. Rhodes, J. Opt. Soc. Am. B **4**, 595 (1987)
- ⁷³ M. Ferray, A. L’Huillier, X. F. Li, L. A. Lompré, G. Mainfray and C. Manus, J. Phys. B **21**, L31 (1988)
- ⁷⁴ G. Farkas and C. Tóth, Phys. Lett. A **168**, 447 (1992)
- ⁷⁵ S. Harris, J. Macklin and T. Hänsch, Opt. Commun. **100**, 487 (1993)
- ⁷⁶ P. Paul, E. Toma, P. Breger, G. Mullot, F. Audebert, P. Balcou, H. Muller and P. Agostini, Science **292**, 1689 (2001)
- ⁷⁷ M. Hentschel, R. Kienberger, C. Spielmann, G. Reider, N. Milosevic, T. Brabec, P. Corkum, U. Heinzmann, M. Drescher and F. Krausz, Nature **414**, 509 (2001)
- ⁷⁸ J. Seres, E. Seres, A. Verhoef, G. Tempea, C. Strelči, P. Wobrauschek, V. Yakovlev, A. Scrinzi, C. Spielmann and F. Krausz, Nature **433**, 7026 (2005)
- ⁷⁹ R. Jones, K. Moll, M. Thorpe and J. Ye, Phys. Rev. Lett. **94**, 193201 (2005)
- ⁸⁰ C. Gohle, T. Udem, M. Herrmann, J. Rauschenberger, R. Holzwarth, H. Schuessler, F. Krausz and T. Hänsch, Nature **436**, 234 (2005)
- ⁸¹ A. Rundquist, C. G. Durfee III, Z. Chang, C. Herne, S. Backus, M. M. Murnane and H. C. Kapteyn, Science **280**, 1412 (1998)
- ⁸² G. Tsakiris, K. Eidmann, J. Meyer-ter Vehn and F. Krausz, New J. Phys. **8**, 19 (2006)
- ⁸³ S. Ghimire, A. Dichiara, E. Sistrunk, P. Agostini, L. Dimauro and D. Reis, Nat. Phys. **7**, 138 (2011)
- ⁸⁴ D. L. Mathews, et al., Phys. Rev. Lett. **54**, 110 (1985)
- ⁸⁵ S. Suckewer, C. H. Skinner, H. Milchberg, C. Keane, and D. Voorhees, Phys. Rev. Lett. **55**, 1753 (1985)
- ⁸⁶ S. Suckewer and P. Jaegle, Laser Phys. Lett. **6**, 411 (2009)
- ⁸⁷ G.A. Gudzenko and L.A. Shelepin, Soviet Physics Doklady **10**, 147 (1965)
- ⁸⁸ E.Ya. Kononov and K.N. Koshelev, Sov. J. Quantum Electron. **4**, 1340 (1975)

-
- ⁸⁹ R.C. Elton, *Appl. Opt.* **14**, 97 (1975)
- ⁹⁰ P. Jaeger, G. Jamelot, A. Carillon and C. Wehenkel, *Jpn. J. Appl. Phys. Suppl.* **17-2**, 483 (1978)
- ⁹¹ D. Jacoby, G.J. Pert, S.A. Ramsden, L.D. Shorrock and G.J. Tallents, *Opt. Commun.* **37**, 193 (1981)
- ⁹² D. Jacoby, G.J. Pert, L.D. Shorrock and G.J. Tallents, *J. Phys. B* **15**, 3557 (1982)
- ⁹³ A.N. Zherikhin, K.N. Koshelev and V.S. Letokhov, *Sov. J. Quantum Electron.* **6**, 82 (1976)
- ⁹⁴ A.V. Vinogradov, I.I. Sobel'man and E.A. Yukov, *Sov. J. Quantum Electron.* **7**, 32 (1977)
- ⁹⁵ L.A. Vainshtein, A.V. Vinogradov, U.I. Safronova and I.Yu. Skobelev, *Sov. J. Quantum Electron.* **8**, 239 (1978)
- ⁹⁶ A.V. Vinogradov and V.N. Shlyaptsev, *Sov. J. Quantum Electron.* **10**, 754 (1980)
- ⁹⁷ Y. Nagata, K. Midorikawa, S. Kubodera, M. Obara, H. Tashiro and K. Toyoda, *Phys. Rev. Lett.* **71**, 3774 (1993)
- ⁹⁸ K.M. Krushelnick, W. Tighe and S. Suckewer, *J. Opt. Soc. Am. B* **13**, 306 (1996)
- ⁹⁹ D.V. Korobkin, C.H. Nam, S. Suckewer and A. Goltsov, *Phys. Rev. Lett.* **77**, 5206 (1996)
- ¹⁰⁰ B.E. Lemoff, G.Y. Yin, C.L. Gordon, III, C.P.J. Barty and S.E. Harris, *Phys. Rev. Lett.* **74**, 1574 (1995)
- ¹⁰¹ Y.L. Li, G. Pretzler, P.X. Lu and E.E. Fill, *Phys. Rev. A* **53**, R652 (1996)
- ¹⁰² Y.L. Li, P.X. Lu, G. Pretzler and E.E. Fill, *Opt. Commun.* **133**, 196 (1997)
- ¹⁰³ J. Zhang, A.G. MacPhee, J.Y. Lin, E. Wolfrum, J. Nilsen, T.W. Barbee, Jr., C.N. Danson, M.H. Key, C.L.S. Lewis, D. Neely, R.M.N. O'Rourke, G.J. Pert, R.F. Smith, G.J. Tallents and J.S. Wark, *Proc. SPIE* **3156**, 53 (1997)
- ¹⁰⁴ V.N. Shlyaptsev, J. Dunn, S. Moon, R. Smith, R. Keenan, J. Nilsen, K.B. Fournier, J. Kuba, A.L. Osterheld, J.J.G. Rocca, B.M. Luther, Y. Wang and M.C. Marconi, *Proc. SPIE* **5197**, 221 (2003)
- ¹⁰⁵ R. Keenan, J. Dunn, P.K. Patel, D.F. Price, R.F. Smith and V.N. Shlyaptsev, *Phys. Rev. Lett.* **94**, 103901 (2005)
- ¹⁰⁶ Y. Wang, M.A. Larotonda, B.M. Luther, D. Alessi, M. Berrill, V.N. Shlyaptsev and J.J. Rocca, *Phys. Rev. A* **72**, 053807 (2005)
- ¹⁰⁷ B.M. Luther, Y. Wang, M.A. Larotonda, D. Alessi, M. Berrill, M.C. Marconi, J.J. Rocca and V.N. Shlyaptsev, *Opt. Lett.* **30**, 165 (2005)
- ¹⁰⁸ Ph. Zeitoun, G. Faivre, S. Sebban, T. Mocek, A. Hallou, M. Fajardo, D. Aubert, Ph. Balcou, F. Burgy, D. Douillet, S. Kazamias, G. de Lach`eze-Murel, T. Lefrou, S. le Pape, P. Merc`ere, H. Merdji, A.S. Morlens, J.P. Rousseau and C. Valentin, *Nature* **431**, 426 (2004)
- ¹⁰⁹ Y. Wang, E. Granados, M.A. Larotonda, M. Berrill, B.M. Luther, D. Patel, C.S. Menoni and J.J. Rocca, *Phys. Rev. Lett.* **97**, 123901 (2006)
- ¹¹⁰ Y. Wang, E. Granados, F. Pedaci, D. Alessi, B. Luther, M. Berrill and J.J. Rocca, *Nature Photonics* **2**, 94 (2008)
- ¹¹¹ C. Steden and H.J. Kunze, *Phys. Lett.* **151**, 534 (1990)
- ¹¹² J.J. Rocca, D.P. Clark, J.L.A. Chilla and V.N. Shlyaptsev, *Phys. Rev. Lett.* **77**, 1476 (1996)
- ¹¹³ B.R. Benware, C.H. Moreno, D.J. Burd and J.J. Rocca, *Opt. Lett.* **22**, 796 (1997)

-
- ¹¹⁴ C.D. Macchietto, B.R. Benware and J.J. Rocca, *Opt. Lett.* **24**, 1115 (1999)
- ¹¹⁵ S. Heinbuch, M. Grisham, D. Martz and J.J. Rocca, *Opt. Express* **13**, 4050 (2005)
- ¹¹⁶ A. Ben-Kish, M. Shuker, R.A. Nemirovsky, A. Fisher, A. Ron and J.L. Schwob, *Phys. Rev. Lett.* **87**, 015002 (2001)
- ¹¹⁷ G. Niimi, Y. Hayashi, M. Nakajima, M. Watanabe, A. Okino, K. Horioka and E. Hotta, *J. Phys. D Appl. Phys.* **34**, 2123 (2001)
- ¹¹⁸ N. Sakamoto, M. Masnavi, M. Nakajima, T. Kawamura and K. Horioka, *Jpn. J. Appl. Phys.* **47**, 2250 (2008)
- ¹¹⁹ Y. Hayashi, Y. Xiao, N. Sakamoto, H. Miyahara, G. Niimi, M. Watanabe, A. Okino, K. Horioka and E. Hotta, *Jpn. J. Appl. Phys.* **42**, 5285 (2003)
- ¹²⁰ G. Tomassetti, A. Ritucci, A. Reale, L. Palladino, L. Reale, S.V. Kukhlevsky, F. Flora, L. Mezi, A. Faenov, T. Pikuz and A. Gaudieri, *Opt. Commun.* **231**, 403 (2004)
- ¹²¹ G. Tomassetti, A. Ritucci, A. Reale, L. Palladino, L. Reale, S.V. Kukhlevsky, F. Flora, L. Mezi, J. Kaiser, A. Faenov and T. Pikuz, *Eur. Phys. J. D* **19**, 73 (2002)
- ¹²² A. Ritucci, G. Tomassetti, A. Reale, F. Flora, L. Mezi, *Phys. Rev. A* **70**, 023818 (2004)
- ¹²³ A. Ritucci, G. Tomassetti, A. Reale and L. Reale, *Appl. Phys. Lett.* **86**, 101106 (2005)
- ¹²⁴ C.A. Tan, K.H. Kwek, *J. Phys. D* **40**, 4787 (2007)
- ¹²⁵ C.A. Tan, K.H. Kwek, *Phys. Rev. A* **75**, 043808 (2007)
- ¹²⁶ Y. Zhao, Y. Cheng, B. Luan, Y. Wu and Q. Wang, *J. Phys. D* **39**, 342 (2006)
- ¹²⁷ Y.P. Zhao, S. Jiang, Y. Xie and Q. Wang, *Appl. Phys. B* **99**, 535 (2010)
- ¹²⁸ Y. Xie, Q. Wang, Y.P. Zhao, M.Z. Mo, S.T. Yang, T. Liu and D.W. Yang, *Laser Phys.* **20**, 226 (2010)
- ¹²⁹ Y.P. Zhao, S. Jiang, Y. Xie, D. Yang, S. Teng, D. Chen and Q. Wang, *Opt. Lett.* **36**, 3458 (2011)
- ¹³⁰ K. Kolacek, J. Schmidt, V. Bohacek, M. Ripa, O. Frolov, P. Vrba, J. Straus, V. Prukner, A.A. Rupasov and A.S. Shikanov, *Plasma Phys. Rep.* **34**, 162 (2008)
- ¹³¹ F.G. Tomasel, J.J. Rocca, V.N. Shlyaptsev and C.D. Macchietto, *Phys. Rev. A* **55**, 1437 (1997)
- ¹³² M. Frati, M. Seminario and J.J. Rocca, *Opt. Lett.* **14**, 1022 (2000)
- ¹³³ P. Vrba, M. Vrbova, N.A. Bobrova and P.V. Sasorov, *Cent. Eur. J. Phys.* **3**, 564 (2005)
- ¹³⁴ K. Kolacek, J. Schmidt, V. Prukner, O. Frolov and J. Straus, *Laser Part. Beams* **26**, 167 (2008)
- ¹³⁵ N.S. Kampel, A. Rikanati, I. Be'ery, A. Ben-Kish, A. Fisher and A. Ron, *Phys. Rev. E* **78**, 056404 (2008)
- ¹³⁶ I. Gissis, A. Rikanati, I. Be'ery, A. Fisher and E. Behar, *J. Quant. Spectrosc. Radiat. Transfer* **127**, 176 (2013)
- ¹³⁷ Y. Sakai, S. Takahashi, T. Hosokai, M. Watanabe, G.H. Kim and E. Hotta, *J. Appl. Phys.* **107**, 083303 (2010)
- ¹³⁸ S. Barnwal, Y.B.S.R. Prasad, S. Nigam, K. Aneesh, M.L. Sharma, R.P. Kushwaha, P.K. Tripathi, P.A. Naik, J.A. Chakera, C.P. Navathe, P.D. Gupta, *Appl. Phys. B: Lasers Opt.* **117**, 131 (2014)

-
- ¹³⁹ S. Barnwal, S. Nigam, K. Aneesh, Y.B.S.R. Prasad, A. S. Joshi and P.A. Naik, *Laser Phys.* **27**, 055003 (2016)
- ¹⁴⁰ S. Barnwal, S. Nigam, K. Aneesh, Y.B.S.R. Prasad, P.A. Naik, C.P. Navathe and P.D. Gupta, *Appl. Phys. B: Lasers Opt.* **122**, 169 (2016)
- ¹⁴¹ S. Barnwal, S. Nigam, K. Aneesh, Y.B.S.R. Prasad, M. L. Sharma, P. K. Tripathi, A.S. Joshi, P.A. Naik, H. S. Vora and P.D. Gupta, *Appl. Phys. B: Lasers Opt.* **123**, 178 (2017)
- ¹⁴² W.H. Bennett, *Phys. Rev.* **45**, 890 (1934)
- ¹⁴³ M.G. Haines, *Plasma Phys. Control. Fusion* **53**, 093001 (2011)
- ¹⁴⁴ D.D. Ryutov, M.S. Derzon and M.K. Matzen, *Rev. Mod. Phys.* **72**, 167 (2000)
- ¹⁴⁵ V.N. Shlyaptsev, J.J. Rocca and A.L. Osterheld, *Proc. SPIE Int. Soc. Opt. Eng.* **2520**, 365 (1995)
- ¹⁴⁶ D.E. Kim, D.S. Kim and A.L. Osterheld, *J. Appl. Phys.* **84**, 5862 (1998)
- ¹⁴⁷ E. Kuffel, W. S. Zaengle and J. Kuffel, “High Voltage Engineering Fundamentals”, Second edition (2000), published by Butterworth-Heinemann, UK
- ¹⁴⁸ S. T. Pai and Q. Zhang, “Introduction to High Power Pulse Technology”, (1995), published by World Scientific Publishing Co. Pte. Ltd., Singapore
- ¹⁴⁹ M. S. Naidu and V. Kamaraju, “High Voltage Engineering”, Second edition (1996), published by Tata McGraw-Hill, India
- ¹⁵⁰ H. Bluhm, “Pulsed Power Systems, Principles and applications”, 2006, published by Springer-Verlag Berlin Heidelberg, Germany
- ¹⁵¹ Y.B.S.R. Prasad, S. Nigam, K. Aneesh, S. Barnwal, P.K. Tripathi, P.A. Naik, C.P. Navathe and P.D. Gupta, *Sadhana* **36**, 349 (2011)
- ¹⁵² M.C. Marconi, J.L.A. Chilla, C.H. Moreno, B.R. Benware and J.J. Rocca, *Phys. Rev. Lett.* **79**, 2799 (1997)
- ¹⁵³ M. Shuker, A. Ben-Kish, R.A. Nemirovsky, A. Fisher and A. Ron, *Phys. Plasmas* **13**, 013102 (2006)
- ¹⁵⁴ G. J. Linford, E. R. Peressini, W. R. Sooy and M. L. Spaeth, *Appl. Opt.* **13**, 379 (1974)
- ¹⁵⁵ K. Lee, J.H. Kim and D. Kim, *Phys. Plasmas* **9**, 4749 (2002)
- ¹⁵⁶ A. Kramida, Y. Ralchenko, J. Reader, NIST ASD Team. NIST atomic spectra database (version 5.4)]. National Institute of Standards and Technology, Gaithersburg, MD, (2016). [http:// physics.nist.gov/asd](http://physics.nist.gov/asd) [10/14/2015. Accessed 19 Aug 2016
- ¹⁵⁷ M. Nevrkla, A. Jancarek, F. Nawaz, T. Parkman and M. Vrbova, *Proc. SPIE* **9510**, 951013-1 (2015)
- ¹⁵⁸ G. Avaria, M. Grisham, J. Li, F.G. Tomasel, V.N. Shlyaptsev, M. Busquet, M. Woolston and J.J. Rocca, *Phys. Rev. Lett.* **114**, 095001 (2015)